THESIS FOR THE DEGREE OF DOCTOR OF PHILOSOPHY

TRANSPORT AND CONTAINMENT CHEMISTRY OF RUTHENIUM UNDER SEVERE ACCIDENT CONDITIONS IN A NUCLEAR POWER PLANT

IVAN KAJAN

Nuclear chemistry
Department of Chemistry and Chemical Engineering

CHALMERS UNIVERSITY OF TECHNOLOGY

Gothenburg, Sweden 2016

Transport and Containment Chemistry of Ruthenium under Severe Accident Conditions in a Nuclear Power Plant
IVAN KAJAN
ISBN 978-91-7597-464-4

Ny Serie Nr. 4145
ISSN nr: 346-718X

Nuclear chemistry
Department of Chemistry and Chemical Engineering
Chalmers University of Technology
SE-412 96 Göteborg
Sweden
Telephone + 46 (0)31-772 1000

Cover:
SEM image of ruthenium dioxide aerosol particles at 30k magnification.
Image taken by Unto Tapper.

Printed by:
Chalmers Reproservice
Gothenburg, Sweden 2016

Transport and Containment Chemistry of Ruthenium under Severe Accident Conditions in a Nuclear Power Plant

IVAN KAJAN

Department of Chemistry and Chemical Engineering
Chalmers University of Technology

Abstract

During a severe nuclear accident volatile elements and elements readily forming volatile compounds are the main concern regarding the release of radioactive material to the environment. As ruthenium is prone to form volatile oxides under severe nuclear accident conditions as well as having radiotoxic isotopes, it is one of the more important elements during such an accident.

In this work the chemical behavior of ruthenium during the transport in the reactor cooling system and the chemistry of ruthenium within the containment was studied.

Studies on ruthenium transport included the effect of temperature, air-radiolysis products and aerosols on the quantity and chemical form of transported ruthenium during an accident. During the experiments the temperature had significant effect both release and transport of ruthenium. Different air radiolysis products affected both quantity and physical form of the transported ruthenium.

The other part of the studies was focused on the chemistry of ruthenium within the containment. These experiments aimed at the interaction of ruthenium tetroxide with metallic (Al, Cu, Zn) and epoxy paint covered surfaces within the containment. Ruthenium had great affinity towards these surfaces that led to the formation of ruthenium rich deposits and thus a clear retention. Chemical characterization as well as quantification of these deposits was obtained.

The effect of gamma radiation on the formed ruthenium deposits was shown and re-volatilized fractions of ruthenium under different atmospheres and received doses were determined decreasing the retention significantly.

Studies focused on interaction of ruthenium tetroxide with iodine-covered surfaces showed its ability to oxidize iodine deposit and re-volatilize iodine from the aluminum and zinc metals. Iodine covered surfaces were also proved to be an effective trap of ruthenium within the containment.

Data obtained from these studies can be utilized for the better understanding of severe accident phenomenology and behavior of radionuclides during an accident.

Keywords: ruthenium, ruthenium tetroxide, nuclear accident, containment, fission products, radiolysis

List of Publications

This thesis is based on the work contained in the following publications:

I. Kajan, I., Lassesson, H., Persson, I., Ekberg C.: Interaction of ruthenium tetroxide with surfaces of nuclear containment building. Journal of Nuclear Science and Technology, 53(9), 1397-1408, 2016

Contribution: Main author, all experimental work, part of processing and interpretation of data.*

II. Kajan, I., Glänneskog, H., Thorn, J., Ekberg, C.: Impact of gamma radiation on the ruthenium deposited materials in a nuclear power plant. Journal of Radioanalytical and Nuclear Chemistry, 309(2), 743-749, 2016

Contribution: Main author, all experimental work, processing and interpretation of data.*

III. Kajan, I., Tietze, S., Ekberg, C.: Interaction of ruthenium tetroxide with iodine-covered surfaces of materials in nuclear reactor containment building, Accepted for publication in Journal of Nuclear Science and Technology, 2016

Contribution: Main author, part of experimental work, processing and interpretation of data.

IV. Kajan, I., Kärkelä, T., Auvinen, A., Ekberg, C.: Ruthenium chemistry and transport in a RCS due to air radiolysis products. Submitted to Journal of Radioanalytical and Nuclear Chemistry

Contribution: Main author, part of experimental work, part of processing and interpretation of data.

V. Kärkelä, T., Kajan, I., Tapper, U., Auvinen, A., Ekberg, C.: Ruthenium transport in a RCS with airborne CsI. Submitted to Progress in Nuclear Energy

Contribution: Part of experimental work, part of processing and interpretation of data.

** Except preparation of paint coupons.*

TABLE OF CONTENTS

1. Introduction

Energy is the main driving force in the development of modern society. All advanced economies require access to energy sources for their further development and growth. Supply of electricity is one of the main pillars of modern society. However, electricity production is strongly connected to the generation of CO_2, one of the main identified reasons for global climate change[1]. Up to 40% of energy-related CO_2 release occurs from electricity production[2]. Thus increasing carbon-free sources of electricity into the electricity mix without jeopardizing electricity security is one of the current challenges in the energy sector.

Nuclear power reactors with low life cycle release of CO_2 emissions are one of the alternatives for low carbon density electricity production[3].There are currently (01/2016) about 440 nuclear power reactors operating in the world, with more than 380 000MWd capacity[4]. A further 65 nuclear power reactors are under construction[4, 5]. As of January 2016 around 11% of the electricity produced in the world was delivered by nuclear power plants[4]. In Sweden 9 nuclear power reactors were in operation as of 02/2016, situated within 3 nuclear power plant sites[5]. These deliver 40% of the overall electricity production in Sweden[6].

Although nuclear energy is a reliable and highly effective source of electricity, there are two main drawbacks associated with its use. These are i) the storage of the radioactive waste remaining after the use of the fuel, and ii) nuclear accidents connected with the release of artificial radioactivity into the environment. The importance of nuclear accidents was highlighted recently after the Fukushima-Daiichi accident in 2011. In the European Union all nuclear power plants were stress tested, investigating the possible weaknesses in accident scenario handling plans. To decrease radiological consequences in case of a nuclear accident a better understanding of the processes leading to release of radionuclides to the environment is necessary. Thus understanding the release, transport and chemical processes of radionuclides during an accident and consequent counter actions lead to increased safety in case of a nuclear accident.

Nuclear accidents management is nowadays focused mainly on the modeling of accident scenarios. However, models can be only as good as the experimental data they are based on. This leads to the need for correct and precise experimental data that will increase the accuracy of radionuclides behavior predictions during a potential accident. The evaluation of ruthenium behavior during a nuclear accident nowadays is based mainly on the experimental data obtained from VERCORS and PHÉBUS experiments[7-12]. However, in these experiments no effect of other fission products or radiation on ruthenium chemistry in the containment was taken into account. Therefore the evaluation of ruthenium chemistry in such cases was a focus of this work.

1.1. Objectives

The focus of this work is the behavior of ruthenium in a severe nuclear accident. The aim is to determine the processes affecting the transport and chemical speciation of ruthenium in RCS (Reactor Cooling System). Further, the focus is on the behavior of gaseous ruthenium tetroxide in the containment of the NPP (Nuclear Power Plant). The interaction with different surfaces within the containment, interaction with iodine-covered surfaces and the possibility of

gamma-radiation induced re-vaporization of ruthenium from these surfaces are also part of the work.

2. Background

2.1. Nuclear accidents

A nuclear accident can be defined as "Any accident involving facilities or activities from which a release of radioactive material occurs or is likely to occur and which has resulted or may result in an international transboundary release that could be of radiological safety significance for another State."[13][1] The severity of nuclear accident is classified according to the International Nuclear Events Scale (INES) introduced by the International Atomic Energy Agency (IAEA). The scale is presented in Figure 1. This scale provides information about the safety significance of nuclear accidents. The infamous Chernobyl (1986) and Fukushima-Daiichi (2011) accidents were the only two accidents to date classified as level 7[14, 15].

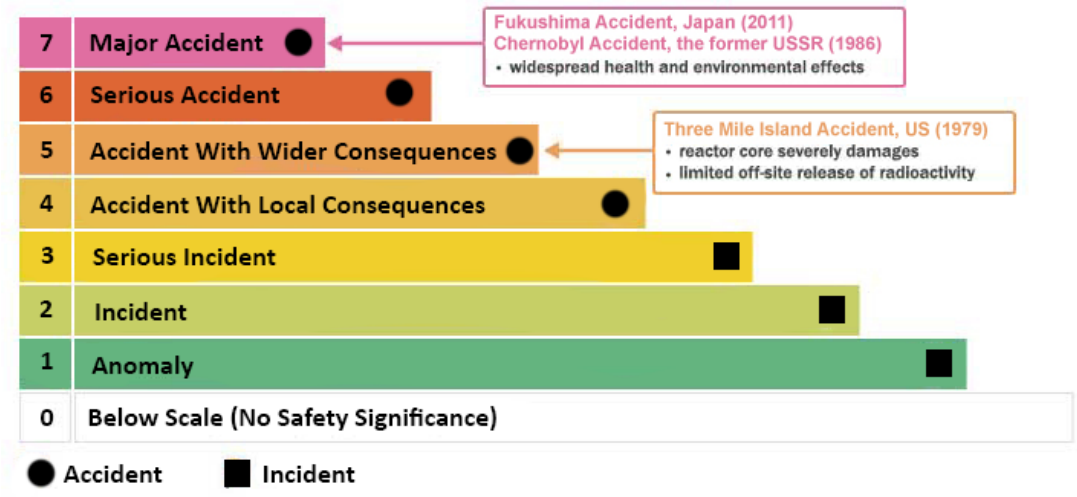

Figure 1. *INES scale of nuclear accidents classification*[16].

The two most general causes of a nuclear accident are inadequate cooling of the reactor core (also called Loss of Coolant Accident (LOCA)) and sudden increase of the core reactivity, known as Reactivity Initiated Accident (RIA). During the LOCA accidents in general the inadequate cooling of the fuel leads to insufficient transfer of the heat produced by the residual decay heat in the fuel, resulting in core damage and possible melting of the fuel[17]. During the Fukushima-Daiichi accident (2011) loss of power to the plant led to the subsequent insufficient cooling of the reactor core in units 1, 2 and 3, causing an accident[18]. The RIA type of accident involves unwanted increase of the fission rate in the reactor fuel. As a consequence a significant rise in the fuel power occurs, and therefore also results in an increase in the temperature of the fuel. This increase can lead to the failure of the nuclear fuel rods. Further progression of a RIA accident may lead to rapid steam evolution and possible damage to the reactor pressure vessel[19]. The Chernobyl accident (1986) was triggered by the RIA sequence when reactivity of the core was suddenly increased due to the ineffective handling of control rods during a safety test[20].

[1] This is not explicitly stated to be a definition of *nuclear accident*, but it is derived from the statement of the scope

2.1.1. Behavior of radionuclides in case of a nuclear accident

In nuclear reactors the most common fuel used consists of cylindrically shaped pellets made of UO_2 or a plutonium-uranium oxides (MOX) mixture[21]. During the operation of the reactor energy is produced due to the fission of uranium or plutonium. This occurs by absorption of neutron by fissile nucleus and consequent fission of the nucleus into two fragments and additional neutrons. The energy released through the fission process (ca. 200 MeV per fission) is released mainly in the form of the kinetic energy of the formed fragments. These fragments, which are also called fission products (FPs), are asymmetrically distributed in size, as can be seen in Figure 2. There are about 30 ways that the fission can occur, thus approximately 60 fission products can be formed during the operation of the nuclear reactor[22]. Some of the fission products are radioactive, which results in the production of a wide variety of elements in the burned nuclear fuel.

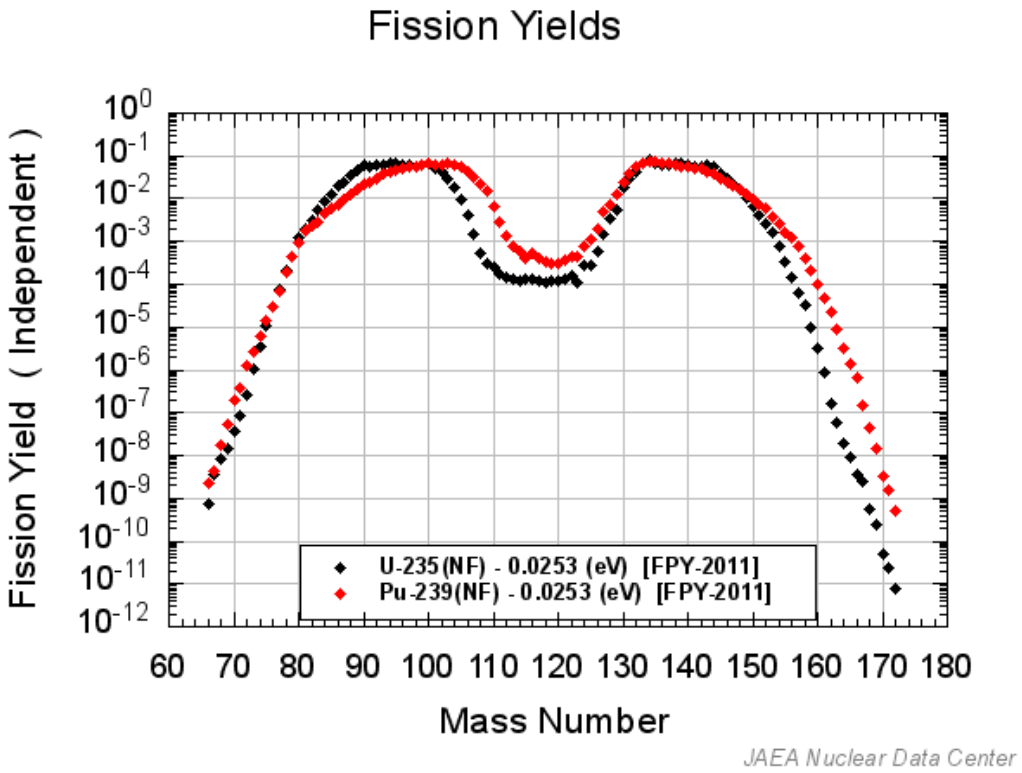

Figure 2. *Fission products yields by fission of ^{235}U (black) and ^{239}Pu (red) by thermal neutrons*[23].

It is clear from Figure 2 that the atomic mass distribution of the formed fission products is quite wide. Naturally, the more fissions per fuel mass (also called burn-up), the greater the accumulation of fission products. The average burn-up of the fuel in light water reactors (LWR) can be up to 6% of the initial uranium or plutonium content[24]. The relative amounts of fission products depend on the burn-up level of the fuel, where roughly 8% are noble gasses (Xe, Kr), 10% are noble metals from the platinum group (Ru, Pd, Pt, Rh), and roughly 25% of new formed elements belong to lanthanides and actinides series[24]. The release of

fission products, especially the radioactive ones, is one of the main concerns during a nuclear accident due to their impact on the environment and humans.
All modern nuclear power plants include a defense in-depth approach to the safety design. Apart from the other safety systems in the modern nuclear plants four important physical barriers leading to the decrease of fission products release into the environment are part of this approach. The first and second barriers are the fuel in which the fission products are generated and the cladding. The third is the reactor vessel that contains the fuel core. The fourth is the containment building that is supposed to keep the fission products from eventually escaping the reactor vessel inside, to lower the risk of escaping into the environment[25]. However if all four barriers are corrupted the fission products can be released into the environment. As fission products have to permeate all three barriers before being released into the environment different phenomena are involved at each consecutive step.
The release phases of fission products from the fuel are divided into 5 phases, as presented in Table 1.

Table 1. *Release phases and their duration for PWRs and BWRs*[26].

Release phase	**Duration PWR (hours)**	**Duration BWR (hours)**
Coolant activity	10-30s	30s
Gap Activity	0.5	0.5
Early In-Vessel	1.3	1.5
Ex-Vessel	2	3
Late In-Vessel	10	10

Release phases are defined based on the different phenomena occurring during an accident[26]. Coolant activity phase corresponds to the time between when the coolant pipe ruptures until the first fuel rod is assumed to fail. The gap activity phase starts with the cladding failure. During this phase a portion of the more-volatile fission products that were collected in the gap between the fuel pellet and cladding are released into the containment. The major portion of the fission products is still retained within the fuel. As the temperature of the fuel is raised to the level where less-volatile fission products are also released from the fuel the gap activity phase ends. Early In-Vessel phase is characterized by the change of reactor core geometrical properties due to the melting of the materials in the core. Significant amounts of fission products are released during this phase. Ex-Vessel phase is a continuation of Early In-vessel phase, when the reactor vessel is ruptured and melted core debris enters the cavity. Significant amounts of volatile as well as minor amounts of non-volatile fission products are released through this phase and corium-concrete reactions are taking place. Ex-Vessel phase terminates when the debris is cooled enough that no significant release of the fission products takes place[26, 27]. Simultaneously with the Ex-vessel phase a phase known as Late In-Vessel phase occurs. This phase is characterized by re-volatilization of fission products previously released from the fuel and deposited on the structures in the reactor coolant system (RCS)[27]. Simplified schematics of the release and transport of fission products is presented in Figure 3[28].

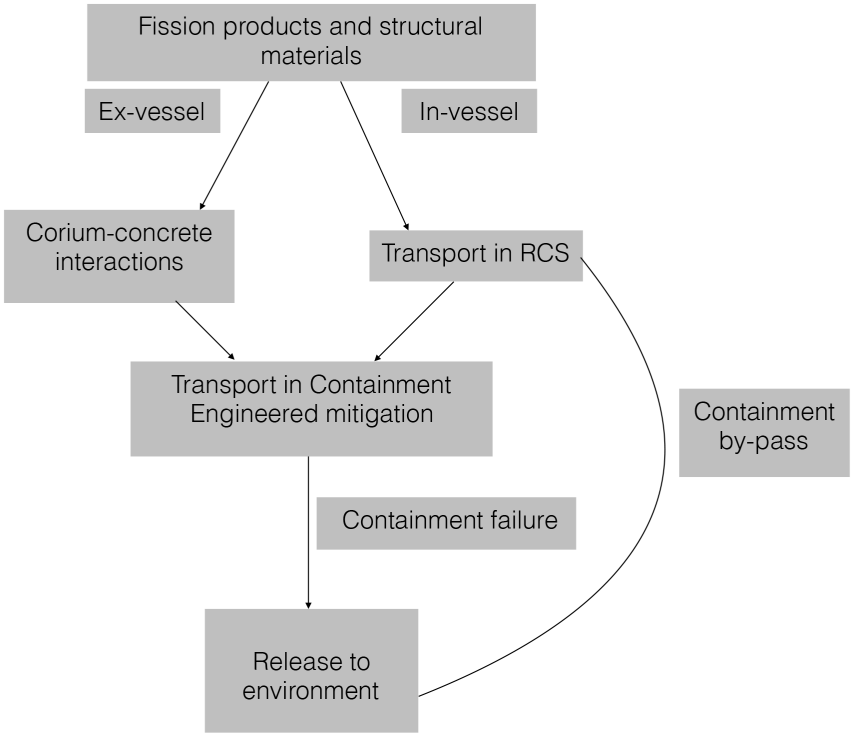

Figure 3. *Paths of fission products release and transport*

The amount of hazardous materials released into the environment from the facility during an accident is called the *source term*. More precisely *in containment-source term* is used when "the fission product inventory in the containment at any given time during an accident" is meant[26]. At this point it should be noted that radionuclides produced during the operation of the reactor are produced also by activation of the materials. These activation products will also contribute to the source term once released from the material. The source term quantification is one of the crucial steps during accident risk evaluation. In case of nuclear reactor accident when compared to an accident in the non-nuclear facility the main difference is release of radioactive substances into the environment and subsequent radiological consequences. The source term evaluation is one of the main problems within severe nuclear accidents research[28]. One of the most important assets during the source term evaluation is the quantification and determination of the chemical and physical form of nuclides released from the fuel matrix itself during an accident.

2.1.2. Fission products classification and release

Volatility of radionuclides produced during the reactor operation is the attribute determining the mobility of FP during a nuclear accident. Volatile FPs are easily released from the fuel and thus significantly contribute to the volatile source term during an accident. Degree of volatility also determines the phase through which particular FPs are released from the fuel matrix. One of the possible FP and activation products categorizations according to their volatility is presented in Table 2.

Table 2. *Fission and activation products volatility according to* [28] *and* [26]

Group	**Representative fission or activation products**
Noble gasses	Kr, Xe,
Volatile FP	I, Br, Cs, Te, Rb
Semi-volatile FP	Mo, Rh, Tc, Pd
Low-volatile FP	Ru, Eu, Sr, Nb, La, Ce
Non-volatile FP	Actinides, Zr, Nd

There are several parameters affecting the quantity of fission or activation products released from the fuel.

Temperature is the main driving force in the release process for the noble gases and volatile fission products[28, 29]. These are usually released easily in the very beginning of an accident through the gap period and release continues during all other release phases mentioned in Table 1. The process of the gaseous fission products release can be described in two steps. The first step is the diffusion of atoms or bubbles towards the grain boundaries[30]. At the grain boundaries the gas is accumulated into larger bubbles that can migrate further to the free volume of the fuel rods[28, 30]. If the consistency of the fuel rod is broken then accumulated gas can be released.

Oxidizing/reducing conditions strongly affect the release rates of semi-volatile and low volatile elements. For example, release of Ru or Mo can be very high under oxidizing conditions, whereas other elements (Ba, Sr, La, Eu, Rh) are more prone to be released under reducing conditions[10, 28, 31, 32]. This behavior was observed under the PHÉBUS integral experimental program, as well as VERCORS separate effect test series[8, 31].

In the case of semi and low volatile elements their chemical form within the fuel strongly affects the release process. Noble metals tend to form metallic precipitates known as white inclusions that consist of Ru, Mo, Tc, Pd, and Rh[24, 30, 33, 34]. Other elements, such as Ba or Zr were identified to be in higher oxidation states, as Ba^{2+} and Zr^{4+} respectively[35]. Rare earth elements (RE) were shown to be dissolved within the fuel matrix in the form of their oxides[30]. This occurs while forming RE rich and RE depleted regions within the fuel matrix[36]. Generally their chemical state can be described as UO_2-REO_2 and UO_2-RE_2O_3[30].

Burn up and physical state of the fuel also affects the release of fission products in terms of both kinetics and amplitude of the released nuclides. Moreover if UO_2 is oxidized into the form of U_3O_8 with consecutive increase of the volume (about 30%[37]) fragmentation of fuel can be observed. As a consequence of higher surface area uranium and fission products are further attacked by oxygen. Thus an increased release of the nuclides will be observed[38]. This is a crucial step for release of low-volatile elements such as ruthenium because of the better oxygen penetration under oxidizing conditions during an accident[37, 39, 40].

Interaction with cladding or structural materials can delay the release of some fission products due to chemical reactions. As an example Ba, Te, Sb can be retained in zirconium cladding materials and then re-released after the further oxidation of the cladding material[41, 42].

Fuel type different microstructure of UO_2 and MOX fuel affects the release of nuclides, with higher release rates observed in MOX fuels. This behavior takes place probably because of the more heterogenic composition of MOX fuels where the local burn-up of plutonium aggregates can be significantly higher when compared to the whole pellet[28].
As all these phenomena affect the behavior of fission and activation products a complex system is formed. To get a better understanding of the FP/AP behavior in a nuclear accident there is a need to understand the behavior of specific elements separately, as well as their behavior in the different conditions possibly occurring during a severe nuclear accident. In this thesis further focus was given to the behavior of ruthenium during severe nuclear accident conditions.

2.2. Production of ruthenium in the fuel

During the operation of a nuclear power plant (NPP) a significant amount of ruthenium is built up in the fuel as a product of nuclear fission. From Figure 2 it can be seen that mass numbers for ruthenium isotopes lie in the center of the first peaks for fission yields for fission of both ^{235}U and ^{239}Pu. Ruthenium is therefore one of the most abundant elements produced in nuclear fission during the operation of a nuclear reactor. The sums of fission yields for different masses are presented in Table 3. From the presented data it can be seen that fission yield for ruthenium decrease in the following order ^{238}U(fast neutrons)>^{239}Pu>^{235}U. As a consequence ruthenium production is higher in low enriched and MOX fuels. The importance of high fission yield of ruthenium for ^{238}U fission by fast neutrons will also be significant in generation IV fast reactors. Additionally fission yield increases with burn up of the conventional UO_2 fuel due to the production of ^{239}Pu in the fuel matrix during nuclear reactor operation.

Table 3. *Properties and fission yields of ruthenium isotopes[43, 44]*

Mass number	^{235}U yield (%)[43]	^{239}Pu yield (%)[43]	^{238}U yield with fast neutrons (%)[44]	Ruthenium isotope	Half life[43]	Decay mode[43]
100	6.249	6.840		^{100}Ru	stable	
101	5.167	6.176	6.14	^{101}Ru	stable	
102	4.287	6.081	6.4	^{102}Ru	stable	
103	3.103	6.948	5.7	^{103}Ru	39.35 d	β-
104	1.874	6.074	5.02	^{104}Ru	stable	
105	0.9469	5.765	3.75	^{105}Ru	4.44 h	β-
106	0.4108	4.193	2.48	^{106}Ru	373.6 d	β-
107	0.1396	3.177	1.25	^{107}Ru	3.8 min	β-
108	0.05727	2.056	0.6	^{108}Ru	4.5 min	β-
109	0.02886	1.673	0.75	^{109}Ru	34.5 s	β-
110	0.02542	0.6248		^{110}Ru	11.6 s	β-

The amount of ruthenium in the fuel is built up linearly following the burn up of fuel. The amounts calculated using the BURNUP code can be seen in Figure 4[45]. Approximately 30% of the ruthenium bulk consists of radioactive isotopes, mainly ^{103}Ru and ^{106}Ru. From Figure 4 it can be seen that after 1500 days of burn

up in a reactor with thermal neutron flux of 10E13 $n \cdot cm^{-2} \cdot s^{-1}$ enriched with 3.5% ^{235}U nearly 2kg of ruthenium is formed per one ton of IHM (Initial Heavy Metal).

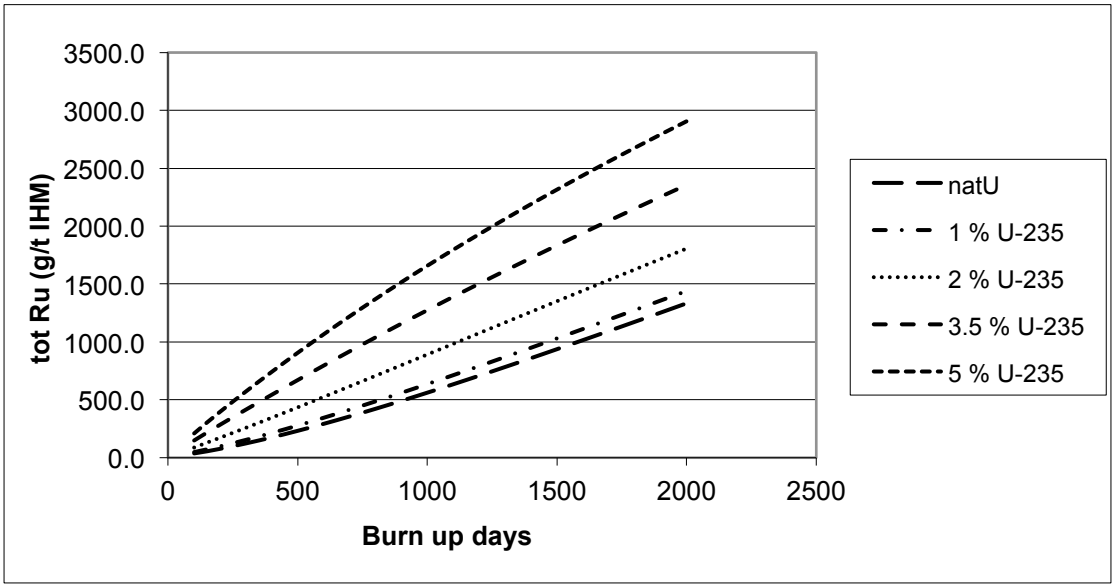

Figure 4. *The amount of ruthenium per ton of fuel with different burn up and enrichment.*

If 72.5 tons of the fuel in reactor are assumed to have a respective burn up of 10.5, 21, 31.5 and 42 GWd/t the mass of formed ruthenium (137kg) will be between the masses of iodine (12.7kg) and cesium (161kg)[28]. As a consequence the ruthenium isotopes will significantly contribute to the overall activity of the fuel after the shutdown of the reactor, as presented in Table 4[28].

Table 4. *The activity of ruthenium isotopes as % of total activity in the fuel*[28]

Time after shutdown	**Shutdown**	**1 h**	**1 week**	**1 month**
Activity of ruthenium (% of total activity)	1.85%	3.11%	3.67%	10.27%

The chemical speciation of the ruthenium produced in the fuel has previously been widely examined. Ruthenium tends to form metallic precipitates with other metals, mainly Mo, Tc, Rh and Pd in white inclusions where all the elements are in their metallic state[24, 30, 33, 46]. The composition of white inclusions shows great variations dependable on the burn up O/U/Pu ratio, temperature gradients in the fuel pins and the oxygen potential[47-49]. White inclusions have a tendency to coagulate outside of grain boundaries in the cooler parts of the fuel pins[30].

2.3. Release of ruthenium from the fuel

Along with iodine and cesium, ruthenium is considered to be one of the important elements released during a nuclear accident. This is due to the high radiological risk ruthenium possess as well as its semi-volatile properties. From the chemical point of view a semi-volatile element can be characterized by high vapor pressure in metal or oxide form but not in both[37]. Several ruthenium

oxides have a high vapor pressure, thus ruthenium needs to be first oxidized from its metallic state to become volatile.

In the case of a nuclear accident several factors will affect the behavior of ruthenium. The burn up, physical state of the fuel, reducing or oxidizing atmosphere and temperature will influence the amount and the kinetics of the released ruthenium. Effects of different conditions on the release of radionuclides were previously studied under several experimental programs[9, 12, 29, 31, 50-52]. As shown in various experiments, oxygen potential and temperature are the main driving forces for the vaporization of ruthenium from the fuel[11, 53]. However, it was demonstrated that under oxidizing conditions the cladding and fuel matrix itself need to be oxidized first for sufficient ruthenium release due to the oxygen affinity decreasing in the order Zr-UO_2-Ru[37, 53]. Thus degradation of the fuel matrix and cladding is an unnecessary step for the ruthenium release from the fuel.

During the PHÉBUS integral tests prototypic nuclear reactor accident conditions were studied. Based on the online and post-experimental measurements, release of the fission products could be evaluated[7, 32]. Experiments showed the release of ruthenium from the fuel pins to be up to 2.1% of initial inventory. The results were obtained in a steam-rich environment with a temperature of approximately 2000°C[32, 54]. In the case of a steam-poor atmosphere with boron injection into the coolant flow, the release of ruthenium decreased to 0.15% of the initial inventory[32, 54].

The VERCORS experimental program was focused on the PWR fuel rod degradation and behavior of fission products in case of an accident[10-12]. Tests conducted under the VERCORS experimental program determined the release of ruthenium to range from 0.36% up to 6% of the initial inventory[55]. In all experiments the maximum temperature of the fuel was kept at 2570 °C at the end of the experiment. The 6% release was detected in two out of six experiments with an atmosphere consisting of steam (VERCORS-5) and surprisingly also under a hydrogen atmosphere (VERCORS-4)[10]. However, during the VERCORS-4 experiment oxidizing conditions were kept for the part of the test when H_2O-H_2 mixture was injected into the gas stream[10]. The VERCORS tests included two additional experimental loops (RT and HT). The RT loop was focused on the transport of fission products in the PWR primary circuit and their interaction with elements composed of neutron absorbers. The HT loop was used with a focus on the release of low volatile FP and transuranium elements. All these tests were conducted by heating the fuel sample up to the melting point[10, 31]. In these test sets the fuel was heated to the melting point so that the entire volatility of fission products could be determined[31]. Release of ruthenium in VERCORS-RT tests ranged from 1.5% to 28.1% depending on the applied conditions, such as atmosphere and temperature[10, 31]. In the case of the VERCORS-HT tests the released ruthenium fraction was detected to be up to 65% under a steam atmosphere and temperature of 2150°C[10].

As a general conclusion from the experiments performed on fission products release, temperature, oxidizing/reducing conditions and burn up are the main factors affecting the release of ruthenium from the fuel. Oxidizing conditions and steam promote the release of ruthenium up to 65% of the initial inventory, presumably due to the production of its volatile oxides. Reducing conditions suppress the release and the maximum released fraction was always below 10% in the experiments[56]. High burn up of the fuel and high temperature both lead to the higher release of ruthenium [11]. The highest risk for a ruthenium release

from the fuel is therefore an accident sequence with air ingress following vessel melt-through[57].

2.4. Transport of ruthenium through the reactor cooling system

Once ruthenium is released from the fuel and consistency of reactor cooling system (RCS) is lost, it can be transported through the RCS into the containment. Such a scenario is shown in Figure 5[34].

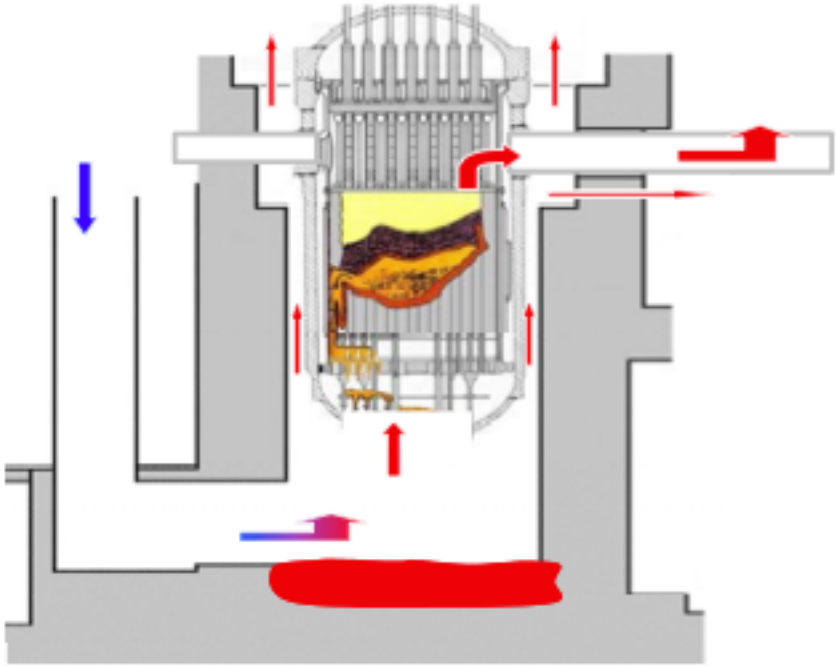

Figure 5. *The air ingress scenario following vessel failure during a severe accident*[34].

Few studies were done on ruthenium transport phenomena in the past. In the framework of the RUSET experimental program both release and transport of ruthenium under oxidizing conditions were examined. It was shown that ruthenium evaporation occurs mainly in the forms of RuO_3 and RuO_4[58, 59]. Partial pressure of RuO_4 at the outlet of the experimental facility was in the range of 10^{-6} bar, which is about 4 orders higher than thermodynamic calculations predict[60]. Further effects of other fission products on vaporization and transport of ruthenium were examined within the program. Decrease of the release rate of ruthenium from the Mo-Ru-Rh-Pd matrix to 45%-65% of that from pure ruthenium at temperatures of 1000°C-1100°C was detected[57-59]. Another fission product, cesium, delayed the transport of the ruthenium from the experimental facility. If cesium was present in the flow the partial pressure of ruthenium at the outlet of the facility was decreased. On the other hand the partial pressure of RuO_4 was increased if cesium was deposited on the surface of the tubes before introduction of ruthenium into the system[59, 61].
Other studies of ruthenium transport were conducted at VTT. In these experiments the effects of different oxidizing atmospheres and temperature on the transport of ruthenium species were determined. The fraction of ruthenium aerosols transported through the facility was shown to increase with temperature from about 1% at 1100 K up to 35% at 1700 K[57]. These aerosols originate mainly from the thermal decomposition of RuO_3 that takes place when

the temperature in the system drops under 1000 K[62]. Introduction of seed particles into the atmosphere additionally doubled the aerosol fraction. The opposite effect was detected in the case of the gaseous ruthenium fraction. Whereas about 40% of released ruthenium was transported in the form of RuO_4 at 1300 K in dry air, this fraction decreased to 0.11% at 1700 K[57, 63, 64]. The gaseous fraction of overall ruthenium transported through the facility increased to 89% if steam was introduced to the system, compared to 62% in a dry air atmosphere at 1300 K[65]. In all the experiments performed at VTT a significant deposition of solid ruthenium particles was observed at the outlet of the furnace, with very steep temperature gradient. These deposits were attributed to the thermal decomposition of RuO_3[63, 66].
From the experiments performed on the ruthenium transport a very strong effect of temperature can be seen on the transport of ruthenium and its chemical form. Increased temperature promotes overall ruthenium transport, whereas the gaseous fraction of ruthenium is decreased. Humidity in the atmosphere increases the ruthenium transport. Other fission products and seed particles seem to affect ruthenium transport in different ways..

2.5. Ruthenium chemistry in a containment of a nuclear power plant

Several studies were performed on the behavior of ruthenium in the containment[67-72]. Ruthenium behavior in the containment was shown to be strongly dependent on its chemical form. It was shown that RuO_4 is the main gaseous species of ruthenium under the conditions in containment[73]. Hence its behavior was a focus of the performed research studies. RuO_4 is not thermodynamically stable at containment conditions. The kinetics of its decomposition, however, seems not to be very fast. The half-life time of RuO_4 in the air was determined to be 5 h at 90°C and 9 h at 40°C in the presence of steam[68]. The decomposition rate was strongly affected by the steam content in the atmosphere, which accelerated the decomposition when compared to the dry air[68]. Determination of ruthenium tetroxide distribution between water and gas phase was investigated by Holm, showing complete absorption of RuO_4 into the water phase within 5 minutes after gas injection[72]. Investigation studies on the absorption of RuO_4 into water with addition of NO and NO_2 into the gas phase showed very strong sorption of ruthenium in the water due to the formation of ruthenium nitrosyl and nitroso complexes, thus decreasing the volatility of ruthenium[74].
Interaction of RuO_4 with surfaces in the containment building was studied with respect to epoxy paint, zinc, aluminum copper and steel. It was shown that ruthenium decomposes on the materials into the form of hydrated RuO_2 or ruthenium hydroxo-oxides [67, 71]. However as the XPS (X-ray photoelectron spectroscopy) technique was used in the studies, only chemical characterization of the upper surface layers (<10nm) was performed. In the work of Mun et.al., further investigations of the behavior of formed deposits were performed. It was shown that both gamma radiation and ozone are able to re-vaporize ruthenium from the deposits back into the gas phase as RuO_4 [69, 70]. Steel coupons painted with epoxy paint with ruthenium deposits were irradiated in the gamma source with dose rate of ≈4kGy/h. As a result a maximum 4.2% re-vaporized fraction of ruthenium was detected after 16 hours of irradiation in humid air at 90°C[69]. No further experiments at different temperatures or dose rates were performed. Therefore the impact of gamma radiation with higher dose rates typical for the early stage of accident is still unknown[75]. Similar coupons were used for the

experiments with ozone in the atmosphere, where re-vaporization of ruthenium was quite significant. Temperature and humidity and ozone concentration were the key factors affecting re-vaporization rates of the ruthenium from the samples[70].

2.6. Ruthenium in Nuclear accidents

As mentioned before, during decades of nuclear power production several nuclear accidents have occurred. In some of these significant ruthenium releases were detected. During the Chernobyl accident in 1986 the activity concentration of ruthenium isotopes in the air and on the ground was similar to ^{131}I and ^{137}Cs[76-78]. In the case of the Chernobyl accident the activity ratios of $^{103}Ru/^{137}Cs$ and $^{106}Ru/^{137}Cs$ were 1.98 and 0.86, respectively[15] The release of radioactive ruthenium isotopes was also detected in other minor accidents[79, 80]. In the case of the Fukushima-Daiichi accident the release of ^{106}Ru was detected in the water with the activity ratio of $^{106}Ru/^{137}Cs$ ranging between 0.07-0.2[81]. Ruthenium release was also observed in accidents within nuclear waste reprocessing and storage facilities. One of the most significant releases occurred at the Hanford reprocessing site, where a high release of the ^{103}Ru and ^{106}Ru isotopes was detected in 1950[82].

2.7. Health hazards of ruthenium released to the environment

The health hazards that ruthenium released from the fuel can possess consists of two factors; the chemical toxicity of the ruthenium itself and the radiological risk originating from the radioactive isotopes of ruthenium. Regarding the chemical toxicity of ruthenium the risk has not been broadly studied due to both the low occurrence of ruthenium in the Earth's crust (0.0001ppm)[83] and the minor industrial use of ruthenium. It is assumed that ruthenium in its metallic state behaves in the human body in a similar way to the other platinum group metals. In addition, some chemical forms of ruthenium represent a specific risk due to their chemical properties. Volatile forms of ruthenium (RuO_3, RuO_4) pose a risk due to their oxidizing properties in human tissues. Ruthenium in the form of RuO_4 is also toxic and explosive[84]. Additionally RuO_4 acts as an irritant to the human skin and its occurrence can lead to possible cornea damage in the eye[85].

The importance of the ruthenium from the radiological point of view is mainly due to the occurrence of ^{103}Ru and ^{106}Ru isotopes with half-lives of 39.5d and 373.5 days, respectively[43]. Ruthenium is therefore important from both short and medium term time scales from a radiological point of view. Radiological protection defines 4 groups of radionuclides, defining their radio-toxicity. ^{103}Ru belongs to the moderate toxicity group, whereas ^{106}Ru belongs to the high toxicity group, in the same group that also ^{131}I and ^{137}Cs are classified[86].

The chemical form of ruthenium predetermines the possibilities of ruthenium uptake into the body. In its volatile form (RuO_4, RuO_3) ruthenium can be inhaled and deposited into the lungs or throat. This will lead to internal contamination where ^{103}Ru and ^{106}Ru will cause a high internal dose to the respiratory system via energy released during beta decay. In cases of external sorption of ruthenium on the skin this will cause an external contamination, where the dose distribution will be more even.

A special case regarding contamination is ruthenium in the form of what are known as "hot particles", which were observed after the Chernobyl accident[87,

88]. These microscopic-sized particles with an aerodynamic diameter of 1-38 μm with an average diameter of 10 μm proved to be quite mobile in the environment by reaching trajectory lengths of up to 1400-1800 km[89]. A dose of 50 $mSv.cm^{-2}$ for the basal cell layer may be exceeded in one hour provided a ruthenium particle larger than 8 μm in diameter is deposited on the skin[90].

3. Theory

3.1. Ruthenium chemical properties

Ruthenium belongs to the platinum group metals in the periodic table. Ruthenium is a rare element with an estimated abundance in the Earth's crust of about 0.0001ppm[83]. Natural ruthenium consists of several stable isotopes, with the most abundant being ^{102}Ru (31%)[43]. The chemistry of ruthenium is highly complex, with oxidation states ranging from VIII to 0 and –II[73, 83, 84, 91]. In this work the focus is given to the ruthenium species most relevant in the case of a nuclear accident.

Regarding ruthenium the major concerns in the case of a nuclear accident are its volatile species, which can be easily released from the nuclear fuel. These are mainly ruthenium oxides that are volatile at elevated temperatures. Ruthenium forms several volatile oxides when heated in an oxygen-rich atmosphere; RuO, RuO_2, RuO_3 and RuO_4[92]. Besides these, in the case of humidity in the atmosphere different forms of volatile ruthenium oxo-hydroxides ($RuO_x(OH)_y$) can be formed[93]. Besides ruthenium oxygen species, ruthenium can form several other compounds with other important fission products. Among these $CsRuO_4$, Cs_2RuO_4 and RuI_3, RuI_2 are those of greatest interest[73, 84, 94].

Thermodynamic studies on the ruthenium oxides have been done to a high level in the past[62, 92, 95-98]. This allows predictions about the behavior and volatilization of ruthenium oxides during a severe nuclear accident to be made. Partial pressures of different ruthenium oxides as a function of temperature, calculated with FACTSAGE 7.0. software[99], are presented in Figure 6.

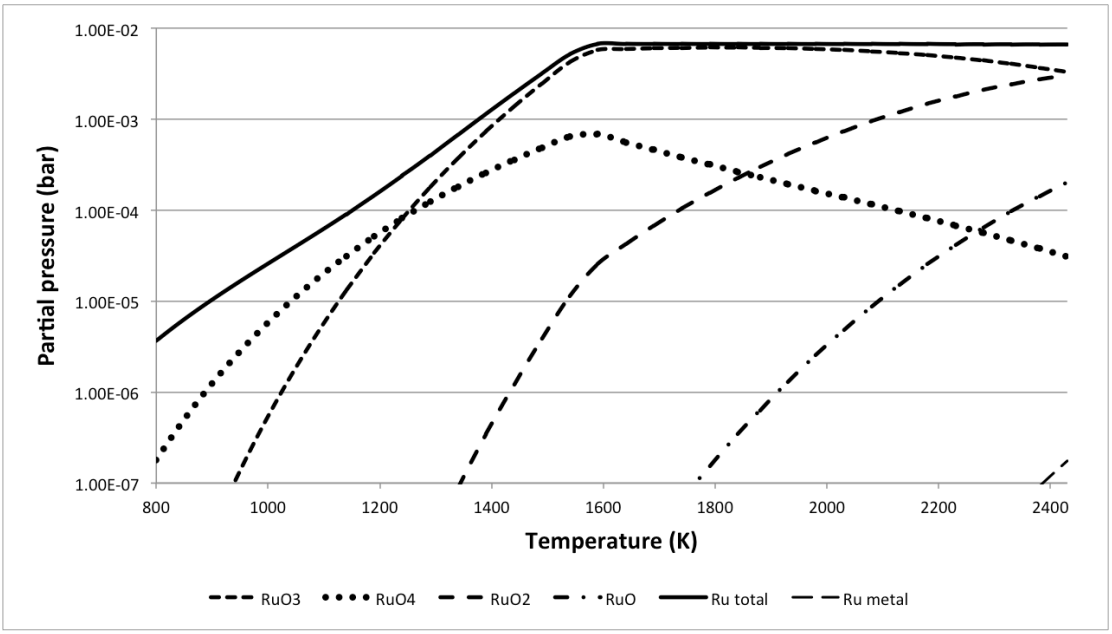

Figure 6. *Ruthenium oxide pressures as a function of temperature in an air atmosphere (pO_2 = 0.2095 atm).*

From the calculations presented it can be concluded that the oxides with the highest contribution to the volatile ruthenium source term will be $RuO_{3(g)}$ and $RuO_{4(g)}$ at temperatures below 1693 K. Further volatilization of ruthenium in the forms of $RuO_{(g)}$, $RuO_{2(g)}$ and $Ru_{(g)}$ also occurs at higher temperatures. It should be noted that the thermodynamic data regarding ruthenium volatile oxides are

subject to uncertainty due to the very few data points evaluated experimentally. Thus extrapolation of the values in the databases is inevitable.

3.2. Ruthenium oxides

As previously mentioned, RuO, RuO_2, RuO_3 and RuO_4 are ruthenium oxides that are volatile at mild or elevated temperatures. Their chemical and physical properties are summed up in following sections.

3.2.1. RuO

Ruthenium monoxide has previously only been detected in gaseous phase[62, 98]. However there are some doubts about its existence[97, 98, 100]. To the author's knowledge no proper chemical characterization of RuO, except its thermodynamic properties is available. This is mainly due the high temperature region of the existence of RuO and the lack of a viable way to separate it from the other ruthenium volatile compounds in the gas phase.

3.2.2. RuO_2

Ruthenium dioxide at room temperature is a black-blue solid with a rutile structure[83, 84, 101, 102]. Under oxygen atmosphere at elevated temperatures RuO_2 can be oxidized into higher ruthenium oxides with consequent volatilization. At temperatures over 1400 K RuO_2 volatilizes itself[95]. The anhydrous crystalline form of RuO_2 is insoluble, however amorphous forms of hydrated RuO_2 can be dissolved in concentrated HCl[103] or by using oxidizing agents in a basic media[67].

3.2.3. RuO_3

Ruthenium trioxide is a gaseous ruthenium oxide that is stable at temperatures over 1000 K[62, 100, 104]. In the past there was a discussion regarding its existence also in a solid form[105, 106] but the hypothesis regarding the existence of RuO_3 in a solid state is not widely accepted[62, 71]. From the thermodynamic equilibrium calculations presented in Figure 6, it can be seen that RuO_3 will be the predominant volatile species of ruthenium contributing to its release from the fuel at temperatures ranging from 1200 to 2200 K. As the temperature drops below 1000 K RuO_3 readily decomposes to solid RuO_2 and oxygen according to equation (1)[62, 64].

$$2RuO_{3(g)} \leftrightarrow 2RuO_{2(s)} + O_2 \quad (1)$$

3.2.4. RuO_4

Ruthenium tetroxide is volatile, toxic and a low temperature melting compound of ruthenium in oxidation state +VIII[84]. The yellow, needle shaped crystals melt at 25.4 °C and are reported to explosively decompose below the boiling point (130 °C[107])[84, 107, 108]. RuO_4 readily sublimes from its solid form at temperatures higher than 7 °C[109]. The volatility of RuO_4 is caused by the saturated covalent bonds in its symmetrical tetrahedral structure resulting in low binding energy between ruthenium atoms. Vapors of RuO_4 are yellow with an odor similar to ozone. Vapors are irritating to tissues and are toxic.

RuO_4 is sparingly soluble in water with a solubility of 17.1 g/l at 273 K and 19.6 g/l at 293 K[110]. Dissolved RuO_4 acts as a weak acid due to the reactions 2 and 3.

$$RuO_{4(g)} + H_2O \leftrightarrow H_2RuO_5 \quad (2)$$
$$H_2RuO_5 + H_2O \leftrightarrow HRuO_5^- + H_3O^+ \quad (3)$$

With pKa for the second reaction equal to 11.2 at 298 K[73].

The basic character of dissolved RuO_4 is due to reaction (4).

$$H_2RuO_5 \leftrightarrow HRuO_4^+ + OH^- \quad (4)$$

With pKa equal to 14.2 at 298 K[73].

In acidic or neutral water solutions RuO_4 is reduced to Ru +IV or Ru+III forms[111]. In basic solutions with pH higher than 8, ruthenium tetroxide is reduced to the perruthenate (Ru+VII) and the ruthenate (Ru+VI) form[112]. A Pourbaix diagram calculated with FACTsage 7.11. software[113] for the ruthenium/water system is shown in Figure 7.

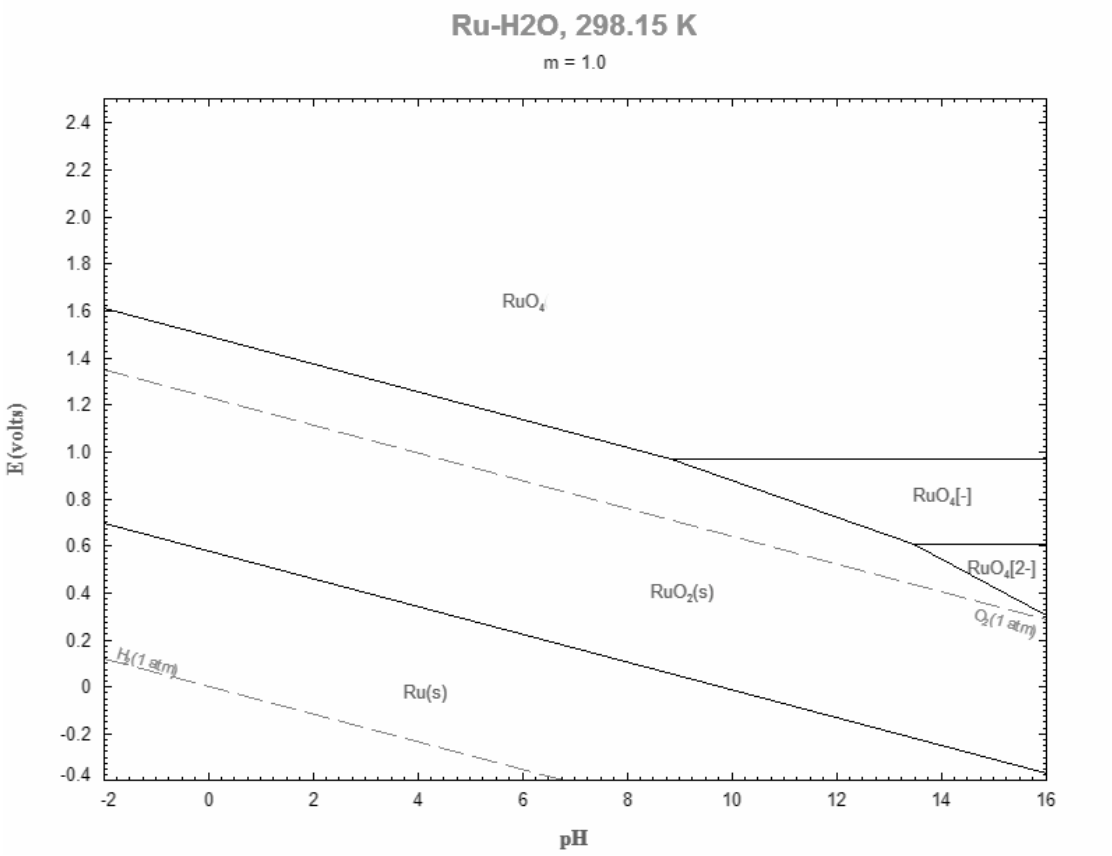

Figure 7. *Pourbaix diagram for Ru/water system[99].*

In the gaseous form RuO_4 is thermodynamically unstable and readily decomposes, although the decomposition kinetics are slow[68]. The slow kinetics of decomposition makes RuO_4 the main volatile ruthenium species in the containment conditions (T<413 K [73]) as partial pressures of RuO, RuO_2 and RuO_3 are expected to be negligible[62, 95, 100]. Due to the oxidizing properties and high chemical reactivity of RuO_4 it is likely that it will interact with materials available in the containment, as well as with other fission products already deposited in the containment[67, 71, 72]. This is of importance, as these interactions of RuO_4 would cause to become immobilized on the surfaces, thus

mitigating the consequences of a nuclear accident.

In Swedish BWR and PWR containments most of the concrete and steel surfaces are covered with epoxy paint[114]. In addition, many construction details in containment are made of aluminum or zinc-galvanized metals. During an accident is also likely that copper aerosols will be released from the cables during a meltdown[115]. The approximated surface areas of particular materials in a representative BWR containment are presented in Table 5.

Table 5. *Surface areas of different materials in the nuclear reactor containment.*

Material	**Containment surface area (m^2)**	**Location**
Paint	≈2000-3000 (a)[116]	Walls and floors
Aluminum	11930 (a)[117]	Sheets, fans
Zinc	6300 (a)[117]	Floor gratings, ventilation tubes
Copper	1350 (b)[117]	

(a) *Data for Forsmark 3*
(b) *Assuming 10 μm Cu-aerosol particles*

The ability of RuO_4 to interact with the mentioned materials was shown previously [67, 71]. However proper characterization of the formed deposits is still a matter of discussion due to discrepancies between the results[62, 71, 105, 118].
In general it can be concluded that the interaction of RuO_4 with the materials cited forms black-colored ruthenium rich deposits. RuO_4 decomposition is promoted by high temperatures and steam. The steam seems to be the key factor towards ruthenium stability in the gaseous phase[68]. The mechanism of RuO_4 decomposition was broadly studied in the past. Ortins de Bettencourd and Jouan proposed the simple reduction of RuO_4 according to reaction (5)[119].

$$RuO_{4(g)} \rightarrow RuO_{2(s)} + O_2 \quad (5)$$

On the other hand, Zimmerman et al. suggested that ruthenium tetroxide decomposes photochemically, through the formation of ruthenium trioxide, as presented in reaction (6)[106]. The proposed mechanism includes the formation of RuO_3 in both solid and gaseous forms.

$$2RuO_{4(g)} \rightarrow 2RuO_{3(g,s)} + O_2 \quad (6)$$

Mun et al. proposed a different decomposition mechanism of RuO_4 in both dry and humid air atmospheres[68].
Firstly, decomposition of RuO_4 to RuO_3 in the gas phase takes place.

$$RuO_{4(g)} \rightarrow RuO_{3(g)} + \frac{1}{2}O_2 \quad (7)$$

In the next step RuO_3 is reduced to the solid state Ru_2O_5.

$$2RuO_{3(g)} \rightarrow Ru_2O_{5(s)} + \frac{1}{2}O_2 \quad (8)$$

Reaction 8 can be also replaced by reaction 9, with faster kinetics, and implies a catalytic role for RuO_2 in RuO_4 decomposition.

$$RuO_{3(g)} + RuO_{2(s)} \rightarrow Ru_2O_{5(s)} \quad (9)$$

The final step then leads to the decomposition of Ru_2O_5 to RuO_2.

$$Ru_2O_{5(s)} \rightarrow 2RuO_{2(s)} + \frac{1}{2}O_2 \quad (10)$$

Regarding the kinetics, reactions 7 and 8 seem to be limiting processes. If RuO_2 is available in the system, reaction 8 will be replaced by reaction 9, with much faster kinetics[68].

In a humid environment the effect of water is explained by dissolution of RuO_4 in the water, thus forming hyperruthenic acid[68].

$$RuO_{4(g)} + H_2O \rightarrow H_2RuO_5 \quad (11)$$

Hyperruthenic acid is then reduced in two steps to the hydrated form RuO_2.

$$2H_2RuO_{5(s)} \rightarrow Ru_2O_5.2H_2O_{(s)} + \frac{3}{2}O_2 \quad (12)$$

$$Ru_2O_5.2H_2O_{(s)} + 2H_2O \rightarrow 2(RuO_2.2H_2O_{(s)}) + \frac{1}{2}O_2 \quad (13)$$

The chemical characterization of the black ruthenium-rich deposits was investigated with different results. Kim et al. proposed that deposit of ruthenium consists of condensed RuO_3 on a RuO_2 layer[105]. Sakurai et al. carried out experiments with the deposition of RuO_4 on different metal surfaces. Deposits were identified as polymeric forms of RuO_4, with ruthenium atoms bonded to each other by peroxo-bonds[118]. Mun et al. identified the deposits as a hydrated form of RuO_2 partly undergoing hydrolysis, resulting in the formation of ruthenium oxo-hydroxides on the surface[71].

Due to the different chemical and physical properties of some of the volatile elements (like iodine) will be released from the fuel in the earlier sequences of an accident then ruthenium. Thus at the time RuO_4 is transported into the containment, a part of the released I_2 has already reacted with the surface materials in the containment[120]. As shown previously, iodine is prone to form respective iodides after interaction with metal surfaces (Al, Cu, Zn)[117]. RuO_4 is known to be a strong oxidizing agent (E^0 Ru(+VIII)/Ru(+IV)=1,4V)[121]. The high standard reduction potential of Ru(+VIII) leads to a possible oxidation of metal iodides and iodides in paint to elemental iodine or higher iodine oxides. Iodine released from the surfaces can therefore contribute to a delayed volatile source term in the containment. Standard reduction potentials for the respective reactions are calculated in Table 6[122].

Table 6. *Calculated standard reduction potentials for the reactions of some metal iodides with RuO_4 at 298 K[122, 123].*

Reaction	**E_0 (V) at 298.15 K**	**log K**
$2AlI_{3(s)}+1.5RuO_{4(g)} \rightarrow 1.5RuO_{2(s)}+3I_2(g)+Al_2O_{3(s)}$	1.95	198.2
$2AlI_{3(s)}+9RuO_{4(g)} \rightarrow 9RuO_{2(s)}+ 3I_2O_5(s)+Al_2O_{3(s)}$	0.57	308.0
$2ZnI_{2(s)}+RuO_{4(g)} \rightarrow RuO_{2(s)}+2I_{2(g)}+2ZnO_{(s)}$	0.84	56.6
$2ZnI_{2(s)}+RuO_{4(g)} \rightarrow RuO_{2(s)}+ I_2O_{5(s)}+2ZnO_{(s)}$	0.39	78.9
$2CuI_{(s)}+3RuO_{4(g)} \rightarrow 3RuO_{2(s)}+I_{2(g)}+CuO_{(s)}$	0.57	38.7
$4CuI_{(s)}+7RuO_{4(g)} \rightarrow 7RuO_{2(s)}+ 2I_2O_{5(s)}+4CuO_{(s)}$	0.37	178.4

3.3. Effects of gamma radiation on the ruthenium deposits in the containment of a nuclear power plant

During an accident radiation emitted from the fission and activation products will lead to radiolysis of air and water over the fuel and in the containment building, forming both oxidizing and reducing agents. The most important are ozone, nitrogen oxides and hydroxyl radicals, as well as hydrogen peroxide in humid conditions. These species can oxidize different compounds, eventually causing a re-vaporization of the radionuclides already adsorbed on the surfaces. The formation of air radiolysis products depends on the received dose and the dose rate.

For re-volatilization, oxidation of ruthenium deposits to the form of volatile ruthenium tetroxide is necessary. The calculated standard reduction potentials of respective re-vaporization reactions and radiation yields of oxidizing agents are summed up in Table 7. Please note that the presented reactions are written as summary reactions and do not necessarily proceed in one step.

Table 7. *Standard reduction potentials for the chemical reactions possibly leading to re-vaporization of ruthenium deposits at 298 K.*

Reaction	Standard reduction potential E_0 (V)	Radiolytical yield of oxidizing agent (Mol/J)
$RuO_{2(s)}+2O_{3(g)} \leftrightarrow RuO_{4(g)}+2O_{2(g)}$	1.32E-1	2.11E-7[124]
$RuO_{2(s)}+2NO_{2(g)} \leftrightarrow RuO_{4(g)}+2NO_{(g)}$	-4.75E-1	-
$RuO_{2(s)}+2NO_{(g)} \leftrightarrow RuO_{4(g)}+N_{2(g)}$	1.57E-1	-
$RuO_{2(s)}+2H_2O_{2(g)} \leftrightarrow RuO_{4(g)}+2H_2O_{(l)}$	3.90E-1	7.26E-8[125]
$RuO_{2(s)}+4OH_{(g)} \leftrightarrow RuO_{4(g)}+2H_2O_{(l)}$	1.29	2.80E-7[125]

3.4. Possible influences of air radiolysis products and aerosols on the ruthenium transport in the RCS

The chemistry of ruthenium has been fairly well studied in simple systems such as air or oxygen atmospheres. However, in the case of nuclear accident many other chemical species can affect ruthenium chemistry. As mentioned previously the unavoidable radiolysis of air and water will take place during an accident, leading to the formation of different radicals or oxidative/reductive molecular species. The most prominent of these are nitrogen oxides, ozone, nitric acid, hydroxyl radicals and hydrogen peroxide[69, 70, 124-127]. These species can affect the stability of gaseous ruthenium oxides in the gas phase, as shown previously[69, 70, 74].

Regarding the nitrogen oxides, these can show either oxidizing or reducing properties depending on the particular reactions. For example NO_2 has the ability to oxidize lower ruthenium oxides into the form of RuO_4, thus increasing the gaseous fraction of ruthenium during the transport of ruthenium through the RCS, according to reactions (14-16)[123].

$$RuO_{2(s)} + NO_{2(g)} \leftrightarrow RuO_{3(g)} + NO_{(g)} \qquad K=0.17 \text{ at } 1500 \text{ K} \qquad (14)$$

$$RuO_{2(s)} + 2NO_{2(g)} \leftrightarrow RuO_{4(g)} + 2NO_{(g)} \qquad K=2.8 \text{ at } 1500 \text{ K} \qquad (15)$$

$$RuO_{3(g)} + NO_{2(g)} \leftrightarrow RuO_{4(g)} + NO_{(g)} \qquad K=16.8 \text{ at } 1500 \text{ K} \qquad (16)$$

On the other hand N_2O can react as both a reducing or oxidizing agent, depending on the particular reaction, as presented in equations (17-22)[123].

$$RuO_{2(s)} + 2N_2O_{(g)} \leftrightarrow RuO_{4(g)} + 2N_{2(g)} \qquad K=9.0E9 \text{ at } 1500 \text{ K} \qquad (17)$$

$$RuO_{2(s)} + N_2O_{(g)} \leftrightarrow RuO_{3(g)} + N_{2(g)} \qquad K=9.5E3 \text{ at } 1500 \text{ K} \qquad (18)$$

$$RuO_{3(g)} + 2N_2O_{(g)} \leftrightarrow RuO_{4(g)} + 2N_{2(g)} \qquad K=9.5E5 \text{ at } 1500 \text{ K} \qquad (19)$$

$RuO_{3(g)} + N_2O_{(g)} \leftrightarrow RuO_{2(s)} + 2NO_{(g)}$ K=2.2E4 at 1500 K (20)

$RuO_{4(g)} + N_2O_{(g)} \leftrightarrow RuO_{3(g)} + 2NO_{(g)}$ K=2.2E2 at 1500 K (21)

$RuO_{4(g)} + 2N_2O_{(g)} \leftrightarrow RuO_{2(s)} + 4NO_{(g)}$ K=4.8E6 at 1500 K (22)

The resulting composition of ruthenium oxides in the case of an accident will therefore be strongly dependent on the kinetics of the presented reactions due to the non-equilibrium nature of the severe accident processes. Therefore experimental evaluation of the different scenarios needs to be performed.

The transport of ruthenium can be also affected by other elements released during an accident into the atmosphere. As there will be a wide variety of aerosol or gaseous species in the RCS atmosphere during an accident different interactions will take place. For example ruthenium oxides can be reduced on the surface of metallic aerosols to form non-volatile ruthenium species[128]. On the other hand the volatility of ruthenium can be increased by compounds with oxidizing properties, as shown in reactions (23-25)[123].

$5RuO_{2(s)} + I_2O_{5(s)} \leftrightarrow 5RuO_{3(g)} + I_{2(g)}$ K=1.2E40 at 1500 K (23)

$2.5RuO_{2(s)} + I_2O_{5(s)} \leftrightarrow 2.5RuO_{4(g)} + I_{2(g)}$ K=2.4E31 at 1500 K (24)

$5RuO_{3(g)} + I_2O_{5(s)} \leftrightarrow 5RuO_{4(g)} + I_{2(g)}$ K=5.0E22 at 1500 K (25)

As ruthenium is transported through the primary circuit and the temperature drops under 1000 K, RuO_3 rapidly decomposes into solid RuO_2, according to reaction (26)[62].

$2RuO_{3(g)} \rightarrow 2RuO_{2(s)} + O_2$ (26)

Consequently, at the temperatures expected in the containment during an accident (<413 K)[75], RuO_4 will be the predominating gaseous species of ruthenium[73].

4. Experimental

4.1. Ruthenium transport in the primary circuit simulating facility

4.1.1. Facility used during ruthenium transport experiments

The basic set-up of the VTT ruthenium transport facility is schematically described in Figure 8. The set-up was slightly modified in some of the experiments when compared to the previous experiments [63, 64] using pure Ru oxides. The main component of the facility was the horizontal, tubular flow furnace (Entech, ETF20/18-II-L), which was used to heat the anhydrous RuO_2 powder (99.95%, Alfa Aesar). The furnace was 110 cm long with two heating sections, each 40 cm long. These zones were separated by a 38 mm layer of insulation. At both ends of the furnace there was 131 mm of thermal insulation.

The furnace tube was made of high purity alumina (Al_2O_3, 99.7%) and its inner diameter was 22 mm. The alumina crucible with the RuO_2 powder (mass 1 or 2 g) was placed over the second heated zone of the furnace, 25 cm from the outlet. The RuO_2 powder was heated to the temperature desired for experiment (1300 K-1700K) in an oxidizing flow and the formation of gaseous ruthenium oxides took place. In experiments with NO_2, N_2O and HNO_3 precursors, a second alumina tube (Al_2O_3, 99.7%, outer diameter 6 mm with a wall thickness of 1 mm) was inserted inside the furnace tube, the outlet of which was located directly after the crucible to avoid the effect of precursors on the ruthenium vaporization rate.

The total flow rate through the facility was 5 l/min (NTP; NTP conditions 0 °C, 101325 Pa).

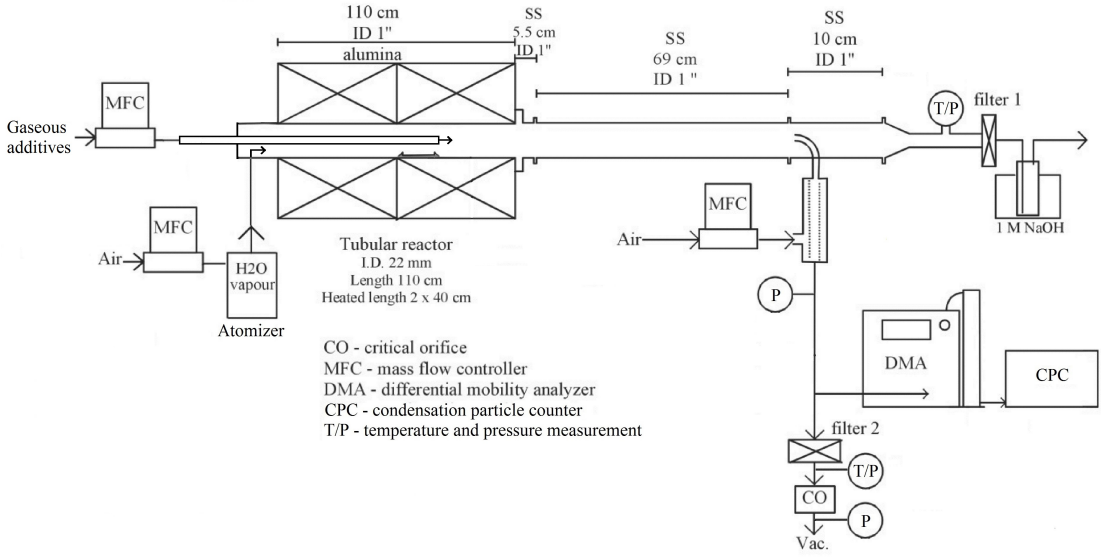

Figure 8. *The basic set-up of the experimental facility for ruthenium tests*[63].

After the gas flow passed through the outlet of the furnace, it was cooled in a stainless steel (SS; AISI 316L) tube. The aerosol products from the possible reaction of ruthenium oxides with the seed particles or the gaseous medium within the facility were filtered out at a point 106 cm downstream of the furnace. The filter used was 90 mm in diameter and it was made of Mitex® (pore size 5 µm, Millipore). The temperature of the gas flow going through the filter was *ca.* 30 °C. Downstream of the filter, the gaseous ruthenium was trapped in a 1 M NaOH solution of Milli-Q water with two sequential liquid traps (400 ml of solution per trap) at *ca.* 25 °C. A NaOH solution was previously found to be an

efficient trap for gaseous RuO_4 [129], in which RuO_4 is reduced into the form of ruthenate and perruthenate salts. The flow rate through the filter and traps was 4 l/min (NTP).
Aerosol gas-phase sampling was done at a point 74 cm downstream of the furnace using a J-shaped probe (inner diameter 4.6 mm) pointing upstream in the flow. The sample flow (1 l/min, NTP) was diluted and quenched to *ca.* 25 °C with a porous tube diluter in order to minimize losses. The dilution ratio was *approx.* 11. The formed particles were collected on a carbon/nickel grid (400 mesh, Agar Scientific) directly from the gas phase by directing a flow of 0.3 l/min [NTP] through the grid. The sampling flow rate was controlled using a critical orifice connected to a vacuum pump. Particles were also collected on an analysis filter (pore size 5 µm, diameter 47 mm, Mitex®, Millipore). The sampling flow rate (2 l/min, NTP) through the analysis filter was also controlled with a critical orifice.

All gases fed into the facility were controlled with mass flow controllers (Brooks S5851). Pressure (Druck pressure meter, model DPI 145) and temperature (K-type thermocouple with a tip diameter of 1.5 mm) measurements were conducted upstream of the aerosol filter and at locations downstream of both the diluter and the analysis filter.

4.1.2. Experimental procedures and matrix

The experiments were started by placing a crucible filled with RuO_2 powder (99.9%, Sigma-Aldrich), (1 g or 2 g depending on the experiment) into the furnace and then heating up the system (heating rate of 10 degrees per minute) under a nitrogen atmosphere. The gas flow through the facility was started when the set-point of the experiment (1300/1500/1700 K) was reached. The duration of the experiments was from 20 to 60 minutes. In the experiments, particulate and gaseous reaction products were collected on a filter and trapped in a 1M NaOH solution, respectively. At the same time, particles in the gas phase were analysed online and additional samples of the particles were collected for the analyses to be conducted later. After the experiment, the gas flow was stopped and the facility was cooled down (cooling rate of 10 degrees per minute) before the collected samples were removed.
The experimental matrix with the details of the experiments is presented in Table 8. Experiments with air atmosphere were reference experiments, in which RuO_2 powder was oxidized and transported. The release and transport results of vaporized ruthenium oxides were then compared with the other experiments.
The release rates of ruthenium from the crucible in the furnace were determined by weighing the mass of the crucible containing RuO_2 before and after the experiments. The mass of released RuO_2 was converted to the corresponding mass of metallic ruthenium for the evaluation of results.
In experiments with nitrogen oxides and HNO_3 an experimental setup with inner tube was used. A flow of N_2O, NO_2 or HNO_3 gases (2.5±0.1 l/min, NTP) was fed through the inner furnace tube. NO_2 and N_2O were diluted with N_2 to obtain a desired concentration of precursor in the gas. As HNO_3 was fed with an additional atomizer (located at that time before the inlet of inner furnace tube, not shown in Figure 8), a carrier gas of nitrogen was used to transport HNO_3 droplets (solution of HNO_3 and Milli-Q water) via the heated line (120 °C) into the inlet of the inner furnace tube. After the outlet of the inner tube the

precursors were mixed with the ruthenium volatile oxides in the gas stream, thus overall flow rate at the outlet of the furnace was again 5 l/min, NTP.
The effect of seed CsI particles on the transport of ruthenium was investigated as follows. Air (flow rate of 5 l/min, NTP) was used to transport the droplets containing a 4% w/w CsI solution in the atomizer to the furnace by the main alumina tube. Water evaporated from the droplets inside the heated furnace and solid particles were formed. A low concentration of steam was therefore generated into the airflow.
The steam concentration in all experiments was dependant on the flow rate through the atomizer.
Ruthenium in the sodium hydroxide liquid traps was quantitatively precipitated with injection of EtOH (96%, Sigma-Aldrich). Samples were then centrifuged and precipitates of ruthenium were filtered from the solution. The filters used for trapping aerosols in the gas stream at the sampling point of the facility were used as they were, without additional manipulation. Both precipitates from the sodium hydroxide traps and aerosol filters were afterwards used for neutron activation and consequent quantification of transported elements.

Table 8. *Experimental matrix for ruthenium transport experiments*

T [K]	Gas	Flow rate over the crucible [l/min]	Precursor[a]	Additive precursor conc.	Humidity[b] [ppmV]	Other
1300±12 1500±12 1700±12	Air	5/2.5	RuO_2	-	2.14E+04 ±2.1E3	Atomizer with water only
1500±12	Air	5/2.5	RuO_2	-	<60	-
1300±12 1500±12 1700±12	Air+NO_2	2.5	RuO_2+NO_2	NO_2 50 ppmV	2.14E+04 ±2.1E3	Atomizer with water only
1300±12 1500±12 1700±12	Air+N_2O	2.5	RuO_2+ N_2O	N_2O 50 ppmV	2.14E+04 ±2.1E3	Atomizer with water only
1300±12 1500±12 1700±12	Air+HNO_3	2.5	RuO_2+ HNO_3	HNO_3 5 ppmV	2.14E+04 ±2.1E3	Atomizer with HNO_3 solution
1300±12 1500±12 1700±12	Air+CsI	5	RuO_2+ CsI	CsI 0.4 mg/l air	2.14E+04 ±2.1E3	Atomizer with CsI 4% (w/w) solution

[a] *The mass of RuO_2 powder in the crucible was 1 g for temperatures 1300 K and 1500 K and 2 g for temperature 1700 K.*
[b] *The humidity in the gas flow came from the water-based precursor solution of the atomizer.*

4.2. Ruthenium containment chemistry experiments

4.2.1. Preparation of samples for RuO_4 and I_2 deposition

The metals used in this study were aluminum (99.5%, Alfa Aesar), zinc (99.5%, Alfa Aesar) and copper (99.5%, Goodfellow). The aluminum and the zinc samples were supplied in rod shapes with a diameter of 19 mm and 13 mm, respectively. The rods were cut into round plates with a thickness of 3 mm. The copper was supplied as a 3mm thick metal plate with and was cut into squares with a 10mm side length. Metal samples were cleaned with acetone and ethanol (96% Sigma-Aldrich), and then consequently washed with Milli-Q water (18 MΩ, Millipore) to wash off any organic impurities prior the depositions.

Teknopox Aqua VA™ epoxy paint was used during the experiments, which is also used in the containment of the Ringhals NPP[130]. Paint coupons were

prepared by painting an approximately 100 μm thick layer on one side of ca 3mm thick glass slide. Each paint coupon was square shaped, with a side length of 15 mm. After painting the coupons were left to cure and evaporate excessive solvents for one month at room temperature in the laboratory (294±1 K).

4.2.2. Wet method of RuO_4 preparation and deposition

As ruthenium tetroxide is a rather unstable compound, it is not commercially available. It was therefore necessary to perform in house preparation prior to use in the experiments.

RuO_4 was produced by the method developed by Krtil et al.[131] with some minor changes. Ruthenium trichloride was oxidized in a slightly basic solution with $K_2S_2O_8$[131]. In the experiments, 60 mg of $RuCl_3$ (99.9%, Sigma-Aldrich) was dissolved in 1 ml of Milli-Q water (18 MΩ). Thereafter the solution was quantitatively transferred into a triple neck round-bottomed flask. Then 2 ml of Milli-Q water and 2 ml of a 2 M K_2CO_3 (99.9%, Merck) solution was added to the flask. In the next step, 0.5 g of $K_2S_2O_8$ powder (99%, Sigma Aldrich) was dissolved in the mixture. A trace amount of ^{103}Ru radiotracer, in the form of $RuCl_3$, was spiked into the mixture for the quantification of the deposited ruthenium amount. The temperature during the reaction was kept at 353±1 K by water bath to increase the rate of the reaction. An illustration of the laboratory setup is presented in Figure 9. To increase the mass transfer of synthesized RuO_4 from the solution to the gas phase, a stream of nitrogen gas with a flow rate of 200 ml/min was bubbled through the solution. The gas flow was directed to the reaction vessel through glass connecting tubing. The 500 ml reaction vessel was sealed with a 5-neck lid. A coldfinger filled with a dry ice was placed in one of the necks in order to condense RuO_4 from the gas phase at the outer surface of the vial. Necks that were not used as an inlet or outlet for the gas or for the coldfinger were sealed with glass stoppers. Paint coupons or metal samples for the deposition were positioned in the bottom of the reaction vessel. The stream of gas, after passing through the reaction vessel, was introduced to the liquid trap containing a 1 M KOH solution.

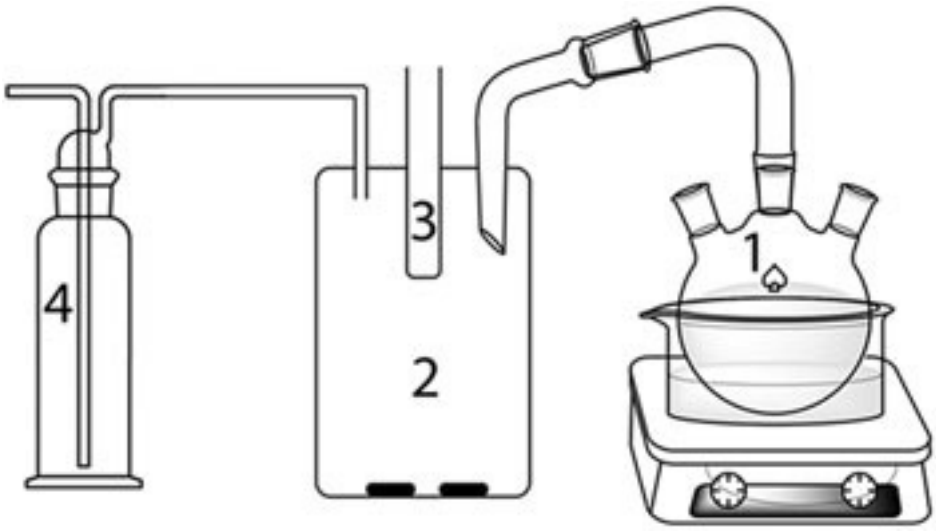

Figure 9. *Schematic illustration of the laboratory setup for RuO_4 production and deposition. 1.Triple neck flask for oxidation of $RuCl_3$, 2.Reaction vessel with samples in the bottom, 3.Cold trap for RuO_4, 4.Hydroxide trap for excessive RuO_4*[132].

Potassium hydroxide solution is known for its ability to reduce ruthenium tetroxide to the perruthenate (+VII) (RuO_4^-) and ruthenate (+VI) (RuO_4^{2-}) form, which is not volatile and stays in the hydroxide solution[84]. Thus works as an efficient trap for the gaseous RuO_4. During the RuO_4 production it took 30 minutes until the solution changed color from brownish to transparent, with no visible yellow fumes of RuO_4 present in the flask. The gas flow was then turned off and the reaction vessel was disconnected from the round-bottomed flask for RuO_4 generation and from the ruthenium trap on the other side. The reaction vessel was thereafter sealed and the crystals of RuO_4 on the coldfinger were left to sublimate and interact with the samples for 18 hours. The temperature during deposition was 295±1 K and the relative humidity was 99±1 %. The humidity and temperature in the reaction vessel during depositions were measured with a humidity meter (Testo 635, Thermo Hygrometer).

4.2.3. Dry method of RuO_4 preparation and deposition

For the deposition of RuO_4 in a dry atmosphere a different method of ruthenium tetroxide generation was used. Schematics of the ruthenium preparation column were the same as in the humid deposition experiments. The only minor difference was that the triple-neck flask was heated in a heating nest rather than in a water bath. In order to decrease humidity content in the system powders were used throughout the process instead of solutions. A mixture of 100 mg $RuCl_3$ powder (99.9%, Sigma Aldrich) was milled with 10 g of $K_2S_2O_8$ (99%, Sigma Aldrich) and 1 g of K_2CO_3 (99.9%, Merck) to obtain a fine mixture of ruthenium in $K_2S_2O_8$ powder. The powder was then transferred to a triple-neck flask placed in a heating nest pre-heated to 473±10 K. After the transfer of the ruthenium and potassium peroxodisulphate powder, nitrogen gas with a flow rate of 500 ml/min was introduced to the flask in order to increase the mass transfer of RuO_4 from the powder into the reaction vessel. The evolution of the gas was left to proceed for 10 minutes, as the kinetics of RuO_4 production were faster than in the case of the wet method of production. The gas flow was

subsequently turned off and the reaction vessel was disconnected from the triple-neck round-bottomed flask and the ruthenium trap. The reaction vessel was sealed and crystals of RuO_4 on the inner vial were left to sublimate and interact with the samples. After 18 hours the reaction vessel was opened and the samples were taken out. During this procedure the ^{103}Ru radiotracer was used in the form of $RuCl_3$ powder. The atmosphere during deposition was nitrogen with 99% purity. Humidity during the experiments did not exceed 2%. The temperature during deposition was 295 ± 1 K. The humidity and temperature in the reaction vessel during depositions were measured with a humidity meter (Testo 635, Thermo Hygrometer).

4.2.4. Deposition of I_2 on samples

. Deposition of I_2 on samples was performed as follows. Gaseous ^{131}I labeled iodine (I_2) vapor (ca. 250 kBq) was produced by the oxidation of potassium iodide with potassium permanganate and a few drops of concentrated sulfuric acid in a round-bottom flask. The generated I_2 vapor was deposited as elemental iodine crystals on an ice-cooled cold finger. The samples to be exposed with iodine as I_2 were placed in the bottom of the exposure vessel. The cold finger was thereafter transferred and inserted into the lid of the exposure vessel. When the cold finger reached room temperature (about 20 min) all elemental iodine crystals were evaporated as I_2 vapor and were available for sorption on the samples. The elemental iodine exposure was visible on all studied surfaces. Paint samples changed to a yellow or brown color with increasing amount of iodine deposited on samples[122].

4.3. Experiments on gamma radiation effects on ruthenium-deposited material

To examine the effects of gamma radiation on ruthenium deposits on different materials the following experimental procedure was used. In the experiments regarding the gamma radiation effects on ruthenium deposits the samples were prepared according to the wet method of RuO_4 deposition. All the irradiated samples discussed in this work were placed into a 25 ml glass beaker that was placed into an Erlenmeyer flask with a volume of 250 ml and an air atmosphere. Irradiation setup is demonstrated in Figure 10. The impact of humidity on the re-vaporization rate of ruthenium deposits was tested by injecting 30 ml of Milli-Q water into the Erlenmeyer bank in one set of the experiments. The experiments without water are referred to as experiments in dry air. The ruthenium deposits re-vaporization experiments were performed in a MDS Nordion Gammacell 220 irradiation device. The gamma source was loaded with 910 TBq ^{60}Co in May 2010. The dose rate in the irradiation chamber during the experiments was about 11 kGy per hour. This value was obtained by measurements using a Ferrous-Cupric chemical dosimeter[133]. The temperature inside the irradiation chamber during irradiation was 317 ± 1 K.

The dose that the samples received ranged from 11 to 264 kGy. As a blank (control) sample a paint coupon or metal samples were placed, for the same time as the irradiation, into an oven with a temperature of 317 ± 1K in the humid or dry atmospheres according to the performed experiment.

For examination of the re-vaporized ruthenium fraction a ^{103}Ru radiotracer was used in connection to HPGe measurements performed before and after irradiations.

Figure 10. *Setup used for the irradiation of ruthenium deposited materials.*

4.4. Chemical characterization of transported compounds and deposits formed in the experiments.

4.4.1. UV-VIS spectrophotometry

The spectrophotometric data were measured with the Perkin-Elmer Lambda 19 spectrophotometer. Spectra were measured within the range of 800-190 nm with the use of 10 mm path length quartz cuvettes (Fisher Scientifics). The background for each measurement consisted of the same sample but without ruthenium. The obtained data were analyzed using UV WinLab software.

4.4.2. SEM/EDX

A scanning electron microscope (SEM) (Hitachi TM 3000) with a backscatter electron system was used for analysis of the physical appearance of the deposits. Energy Dispersive X-ray spectroscopy (EDX) (Oxford Inca 300 EDS System) in conjunction with the SEM supplied quantitative data regarding the chemical composition of the deposits. EDX data were processed using Quantax 70 software.

4.4.3. X-ray electron photospectroscopy (XPS)

X-ray electron photospectroscopy (XPS) measurements were performed using a Perkin Elmer Phi 5500 Multi Technique System at the department of Materials and Manufacturing Technology at Chalmers Technical University. During the measurements X-rays emitted from the Al source (1486.6eV) in the XPS device ionize electrons on the surface of the samples. The kinetic energy spectra of the emitted photoelectrons are collected. These energies correspond to the binding energies (BE) of the elements that can be estimated during the normalization

process. Based on the binding energies, sufficient characterization of the chemical composition was possible.
During the measurements the X-ray voltage and power were 14 kV and 350 W, respectively. The acquisition conditions for the survey spectra (0–1100 eV) were 93.9 eV pass energy, 45° take-off angle and 0.4 eV/step. The acquisition conditions for the detailed scans were then 23.5 eV pass energy, 45° take-off angle and 0.1 eV/step. For determination of the binding energies three standard lines were used as references (Au 4f7/2: 84.0 eV, Ag 3d5/2: 368.3 eV, Cu 2p3/2: 932.7 eV). Calibration was carried out before each measurement under the same conditions as that of the selected region spectra. It was estimated that the experimental uncertainty of the binding energy was ±0.1 eV. The ruthenium 3d5/2 peak has a position near to the binding energy of the carbon C1s peak with binding energy of 284.5 eV. This can lead to the uncertain determination of the carbon peak position if charging of sample occurs. A compensation for the charging of the samples was therefore made with the use of gold foil conductively connected to the measured sample. After this the Au 4f7/2 peak with binding energy 84 eV was used for the charge corrections if necessary. Curve fitting of recorded photoelectron peaks was performed using the PHI Multipak software by assuming Shirley background. During the curve fitting process, asymmetrical or Gauss (20%)/Lorentz (80%) shape of the peaks was used. Reference values for RuO_2 in the forms of both hydrated and anhydrous powder were obtained by measurements of commercial powders (99.9%, Sigma-Aldrich).
An ESCA spectrum analysis was performed with a focus on the most significant ruthenium, cesium, iodine and oxygen lines (Ru3d5/2, Ru3d3/2, I3d5/2, I3d3/2, Cs1s, O 1s). To obtain further insight into the chemical composition of the samples, analysis of the O 1s peak binding energies was performed.

4.4.4. The Extended X-ray Absorption Fine Structure (EXAFS)

4.4.4.1. EXAFS - Data collection

The Extended X-ray Absorption Fine Structure (EXAFS) measurements of the ruthenium species adsorbed to the different matrices described in sections 2.1 and 2.2 were performed at the Ru K X-ray absorption edge (22118.0 eV)[134]. The data were collected at the wiggler beamline I811 at MAX-lab, Lund University, which operated at 1.5 GeV and a maximum current of 220 mA. The EXAFS station was equipped with a Si[111] double crystal monochromator. Higher order harmonics were reduced by detuning the second monochromator crystal to reflect 80% of maximum intensity at the end of the scans. All measurements were performed in fluorescence mode using a Passivated Implanted Planar Silicon (PIPS®) detector[135]. For each sample six 10 minute continuous scans were averaged by means of the EXAFSPAK program package[136].

4.4.4.2. EXAFS - Data Analysis

The EXAFS functions were extracted using standard procedures for pre-edge subtraction, spline removal and data normalization[137]. In order to obtain quantitative information the k^3-weighted EXAFS oscillations were analyzed by non-linear least squares fitting of the model parameters. All data treatment was made by the use of the EXAFSPAK program package[136]. Model fitting was

performed with theoretical phase and amplitude functions, including both single and multiple scattering paths using the *ab initio* code FEFF (version 6.01)[138].

The standard deviations reported for the refined parameters in Table 30. were obtained from k^3 weighted least squares refinements of the EXAFS function χ (k), and do not include systematic errors of the measurements. These statistical error values allow reasonable comparisons e.g. of the significance when comparing relative shifts in the distances. However, the variations in the refined parameters, including the shift in the E_o value (for which k = 0), using different models and data ranges, indicate that the absolute accuracy of the distances given for the separate complexes is within ±0.005 to 0.02 Å for well-defined interactions. The "standard deviations" presented in the text have been increased accordingly to include estimated additional effects of systematic errors.

4.4.5. X-ray diffraction analysis (XRD)

Crystallographic structure of the collected aerosols was examined by means of X-ray diffraction analysis (XRD). Combination of XPS and XRD analysis allowed characterization of both crystalline and potentially amorphous compounds in the collected aerosols. XRD measurements were performed using Bruker D2 Phaser diffractometer with Cu K**α** characteristic radiation, equipped with scintillation detector. Rotation speed of the sample holder was 360°/min and the measurement angle interval was 20-80° 2-theta. Comparing the obtained data with standards in the Joint Committee of Powder Diffraction Standards database[139] led to the identification of compounds.

4.5. Quantification of transported compounds and deposits formed in the experiments.

4.5.1. Neutron Activation Analysis (NAA)

The quantification of ruthenium aerosols collected on filters and gaseous ruthenium trapped in the sodium hydroxide liquid traps from the experiments regarding the ruthenium transport was done using of Neutron Activation Analysis. Ruthenium in the liquid traps was precipitated by the addition of EtOH (96% Sigma-Aldrich), centrifuged and then filtered from the solution. Aerosols collected on the PTFE filters were used as they were after the experiment. Samples were then irradiated in the research reactor at VTT (Triga mark II reactor in Otaniemi, Espoo). Irradiations were carried out with a thermal neutron flux of $8.7 \cdot 10^{12}$ n·cm^{-2}·s^{-1} and epithermal flux of $4.6 \cdot 10^{12}$ n·cm^{-2}·s^{-1}. Samples were irradiated for 10 minutes up to 4 hours depending on the ruthenium content in the sample. After a week of cooling time the samples were measured by means of gamma spectrometry. Cross sections used for the data evaluation were taken from [140].

4.5.2. Gamma spectrometry

For the measurements of radioisotope activity a p-type High Purity Germanium (HPGe) detector (Ortec model GEM-15180-S) with a relative efficiency 17.7% and resolution of 1.7keV at 662 keV was used. The evaluation of data was performed with GammaVision software version 7.01.03. (Ortec). The detector was empirically calibrated for both energy and efficiency with QCYA18189 (Eckert & Ziegler) standard radionuclide source solution with the same geometry as the irradiated samples. The activity of ^{103}Ru was determined from

counts at the 497keV peak, where absolute efficiency at the given geometry was determined to be 1.7%. The detection limit for ruthenium in the samples was determined to be 1.0E-2 μg, based on the times of irradiations and measurements. Uncertainties of the measurements according to GUM (the Guide to the Expression of Uncertainties in Measurements)[141] were calculated to be from 0.67% to 10%, depending on the experiment.

4.5.3. Inductively coupled plasma–mass spectrometry (ICP-MS)

For the analyses of sodium hydroxide traps for cesium and iodine content ICP-MS was used, after the precipitation and filtration of ruthenium. A Thermo Scientific™ HR ICP-MS Element2™ Inductively Coupled Plasma Mass Spectrometer was used to measure the concentrations of minor and trace iodine and cesium in aqueous solution of sodium hydroxide 0.1 M. The mass resolution (m/Δm) of the ICP-MS was 300.

The optimization of the experimental parameters (see Appendix A table A1) was performed using the maximum ion intensity of ^{127}I, ^{133}Cs and ^{103}Rh. All solutions were prepared using sodium hydroxide solution (0.1 M). In addition, the elution buffer contained an internal standard of 10 μg/l Rh (Rhodium, element standard for atomic spectroscopy 1000±5 μg mL^{-1}, 20°C, Spectrascan). Iodine-standard solutions were prepared by dissolving the appropriate amount of potassium iodide (PA grade) in MilliQ water after dilutions with sodium hydroxide. The Cs-standard solutions were prepared by diluting standard solutions obtained from SPEX CertiPrep (CLMS-2 Claritas PPT ICP-MS solution, see Appendix A table A2 for the contents of CLMS-2). The ICP-MS was rinsed with 1% nitric acid solution and 0.1 M sodium hydroxide solution for a total of 7 minutes between aliquot measurements to reduce the memory effect of iodine. After samples with an assumable high concentration of iodine, 5% nitric acid solution was used for rinsing instead of 1% nitric acid solution.

No specific sample preparation was required and dilutions were performed in the same matrix. Data evaluation was performed with The Element ICP-MS Software (version 3.12.242).

4.5.3.1. Choice of standard calibration

Calibration was done at the beginning of analysis and again as needed based on the outcomes from quality control. The calibration curves were prepared from standard solutions with concentrations framing the concentration of test samples. The solutions were prepared by serial dilutions of stock solutions in an identical matrix to the samples. Concentration in the sample was determined using the following equation (27):

$$C_{sample} = \frac{\left(\frac{S_{analyte}}{S_{internal\_standard}} \right)}{m} \qquad (27)$$

where

C_{sample} is the concentration of the analyte in solution (ng/ml)

$S_{analyte}$ is the signal of the analyte

$S_{internal\_standard}$ is the signal of the internal standard

m is the slope of the calibration curve.

5. Results and discussion

5.1. Ruthenium transport in the primary circuit simulating facility

5.1.1. Ruthenium release

It was assumed that the release rate of ruthenium from the crucible was constant during the course of each experiment, as has been shown previously[63]. In addition, ruthenium was assumed to release only when air was introduced into the gas flow, i.e. when the furnace was heated to the set-point temperature (1300 K-1700 K). The ruthenium release rate results are presented in Figure 11.

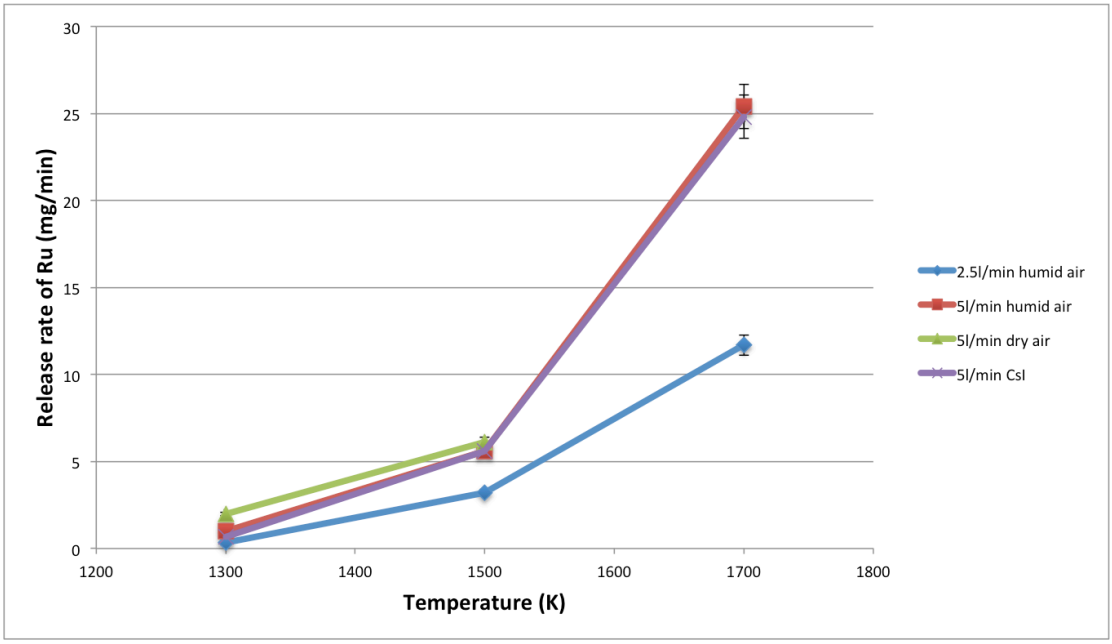

Figure 11. *Dependence of ruthenium release rates from the crucible on temperature. The results are given as 2 standard deviations. Points for flow of 5 l/min in the humid air at 1300 K and 1700 K are taken from* Kärkelä *et al.[63].*

As can be seen from Figure 11. the release rates were fairly similar when the sample temperature and airflow over the crucible were kept constant. Increase of temperature lead to significant increase of ruthenium release rate from RuO_2 powder. When the airflow over the sample was decreased to 2.5 l/min the release rate of ruthenium from the crucible was decreased to approximately half when compared to 5 l/min. Humidity in the atmosphere or CsI aerosols did not seem to have a significant effect on the release rate of ruthenium from the crucible.

5.1.2. Ruthenium transport

The amount of ruthenium transported as aerosol particles on the filter and as gaseous RuO_4 to the liquid traps of 1 M NaOH solution was quantified with the use of instrumental neutron activation analysis. In the experiments with CsI aerosols in the airflow, liquid traps were also analysed using ICP-MS in order to evaluate the content of cesium and iodine in the traps. Based on these measurements the quantities of ruthenium in the form of aerosols and gas could

be determined. Effects of different precursors, temperatures and flow rates are discussed in the following sections.

5.1.2.1. The effect of temperature on ruthenium transport in air

The masses of ruthenium transported in gaseous and aerosol form in an air atmosphere under different temperatures and humidity are summarized in Table 9. The corresponding percentage of the total ruthenium released is summarized in Table 10.

Table 9. *Mass of ruthenium transported as aerosol particles and gas through the model primary circuit. The uncertainties are given as 2 standard deviations.*

Exp. [#]	**Total Ru transported (mg)**	**Ru in the form of RuO_2 aerosol (mg)**	**Ru in the form of RuO_4 gas (mg)**	**Ru deposited inside the facility (mg)**
1 1500 K dry 5 l/min	26.1±2.6	25.1±2.5	1.0±0.1	288.0±3.0
2 1300 K humid 5 l/min[a]	7.0±0.7	3.9±0.4	3.1±0.3	53.0±1.0
3 1500 K humid 5 l/min	23.6±2.4	23.4±2.3	0.30±0.02	280.0±3.0
4 1700 K humid 5 l/min[a]	380.7±38.1	378.0±38.0	2.7±0.3	1142±90
5 1300 K humid 2.5 l/min	0.64±0.01	0.62±0.001	0.02±0.001	8.4±0.1
6 1500K humid 2.5 l/min	8.3±0.4	8.3±0.4	0.010±0.001	76.7±0.8
7 1700 K humid 2.5 l/min	57.9±2.9	57.9±2.9	0.001±0.001	475.8±4.8

a) data taken from Kärkelä *et al.*[63].

Table 10. *The fractions of ruthenium transported as RuO_2 aerosol particles and RuO_4 gas through the model primary circuit, as well as the fraction of ruthenium deposited inside the circuit. All values are given as % of the released Ru. The uncertainties are given as 1 standard deviation.*

Exp. [#]	**Total Ru transported (%)**	**RuO_2 transported (%)**	**RuO_4 transported (%)**	**Ru deposited (%)**
1 1500 K dry 5 l/min	3.40±0.30	3.30±0.30	0.13±0.01	96.6±1.0
2 1300 K humid 5 l/min[a]	11.6±1.2	6.5±0.7	5.2±0.5	88.4±1.3
3 1500 K humid 5 l/min	21.3±2.1	21.2±2.1	0.20±0.02	78.7±2.8
4 1700 K humid 5 l/min[a]	25.0±2.5	24.8±2.5	0.18±0.02	75.0±3.1
5 1300 K humid 2.5 l/min	9.3±0.9	9.1±0.5	0.024±0.012	90.7±1.4
6 1500 K humid 2.5 l/min	12.8±1.3	12.8±0.6	0.010±0.005	87.2±1.9
7 1700 K humid 2.5 l/min	14.3±1.4	14.3±0.7	0.001±0.005	85.7±2.0

a) data taken from Kärkelä *et al.*[63].

From the results it can be concluded that both increased humidity and increased temperature significantly increased the transport of ruthenium through the facility. The increased transport due to humidity in the atmosphere mainly took place in the form of RuO_2 aerosol, with a decreased RuO_4 fraction when compared to dry air conditions. The proposed explanation is that steam passivizes the surfaces of the outlet tube, which is made of stainless steel, and thus decreases the catalytic decomposition of RuO_3 to RuO_2 and the deposition of RuO_2 taking place on the surface when the temperature decreases to below 1000 K. Therefore, the gas phase formation of RuO_2 particles is increased and the transport of particles is enhanced. Temperature had similar effects on the increase of RuO_2 and the decrease of the RuO_4 transported fraction. An explanation of this behaviour is that according to the thermodynamic calculations a higher fraction of RuO_3 is released from the RuO_2 in the crucible with increased temperature. Additionally, at 1700 K the non-negligible volatilization of RuO_2 itself and consequent condensation when the temperature decreases contribute to the transport of ruthenium in the form of aerosols.
The airflow seems to affect both the absolute amount of transported ruthenium and the RuO_4 transported fraction. This behaviour can be explained due to the longer residence time of the RuO_4 in the facility, therefore resulting in more time for the decomposition on the surfaces within the facility.

In all experiments the major part of the released ruthenium was deposited inside the facility, as can be seen in Tables 9 and 10. The highest retention of ruthenium in the facility was observed at the outlet of the furnace, where the temperature decreased rapidly. This behaviour was attributed to the decomposition of RuO_3 into solid ruthenium deposits. Similar effect was observed in the previous experiments with the same facility[63, 66].

5.1.2.2. The effect of temperature on ruthenium transport in air with 50ppmV NO_2

The results of transported ruthenium under the humid air atmosphere with addition of 50 ppmV of NO_2 are presented in Table 11. The corresponding percentage of the total ruthenium released is summarized in Table 12. Introduction of NO_2 into the airflow strongly affected the resulting composition of transported ruthenium. As a result a higher transport of gaseous RuO_4 through the facility was observed when compared to the pure humid air atmosphere at temperatures of 1300 K and 1500 K.

Table 11. *Mass of ruthenium transported as aerosol particles and RuO_4 through the model primary circuit under a humid air atmosphere with 50 ppmV of NO_2. The uncertainties are given as 2 standard deviations.*

Exp.	Total Ru transported (mg)	Ru in the form of RuO_2 aerosol (mg)	Ru in the form of RuO_4 gas (mg)	Ru deposited inside the facility (mg)
1300 K	1.2±0.1	0.001±0.001	1.2±0.1	10.4±0.1
1500 K	9.0±0.5	2.6±0.1	6.4±0.3	76.0±2.2
1700 K	82.0±4.1	82.0±4.1	0.010±0.005	451.7±8.3

Table 12. *The fractions of ruthenium transported as RuO_2 aerosol particles and RuO_4 gas through the model primary circuit and the fraction of ruthenium deposited inside the circuit. The values are given as % of the released ruthenium. The uncertainties are given as 2 standard deviations.*

Exp.	Total Ru transported (%)	RuO_2 transported (%)	RuO_4 transported (%)	Ru deposited (%)
1300 K	13.9±1.4	0.010±0.005	13.9±0.7	86.1±2.0
1500 K	13.9±1.4	4.0±0.2	9.9±0.5	86.1±2.0
1700 K	20.2±2.0	20.2±1.0	0.001±0.005	79.8±3.1

The increased gaseous fraction of transported ruthenium was attributed to reaction (28).

$$RuO_{3(g)}+NO_{2(g)} \leftrightarrow RuO_{4(g)}+NO_{(g)} \qquad (28)$$

The temperature used during the experiments showed a strong effect on the form of transported ruthenium. A decreasing trend of transported gaseous

fraction was observed from 1300 K to 1700 K. This behavior was attributed to the thermal decomposition of NO_2 according to reactions (29) and (30)[142, 143]. A second reason is the decreasing equilibrium constant for the oxidation of RuO_3 over the temperature interval, as presented in Table 13[123].

$$3NO_{2(g)} \leftrightarrow NO_{2(g)} + O_{2(g)} + 2NO_{(g)} \quad (29)$$
$$2NO_{2(g)} \leftrightarrow O_{2(g)} + 2NO_{(g)} \quad (30)$$

Table 13. *Equilibrium constants for the oxidation of RuO_3 by NO_2 to RuO_4 at different temperatures[123].*

Temperature	**K_{eq}**
1300 K	28.55
1500 K	16.85
1700 K	11.3

As a result of these two factors the ratios between the aerosol and gaseous fractions of transported ruthenium are lower than the thermodynamic equilibrium calculations predict.
As can be seen from Tables 11 and 12, the absolute amount of transported ruthenium was increased at temperatures of 1300 K and 1700 K when compared to the humid air atmosphere with nearly 92% and 49% increase, respectively.

5.1.2.3. The effect of temperature on ruthenium transport in air with 50ppmV N_2O

The effect of N_2O on the transport of ruthenium is summarized in Tables 14 and 15.

Table 14. *Mass of ruthenium transported as aerosol particles and as gas through the model primary circuit under a humid air atmosphere with 50 ppmV of N_2O. The uncertainties are given as 2 standard deviations.*

Exp.	**Total Ru transported (mg)**	**Ru in the form of RuO_2 aerosol (mg)**	**Ru in the form of RuO_4 gas (mg)**	**Ru deposited inside the facility (mg)**
1300 K	0.50±0.03	0.50±0.03	0.010±0.005	11.1±0.1
1500 K	16.5±0.8	16.4±0.8	0.090±0.005	68.5±0.9
1700 K	62.9±3.1	62.9±3.1	0.010±0.005	470.8±3.1

Table 15. *The fractions of ruthenium transported as RuO_2 aerosol particles and RuO_4 gas through the model primary circuit and the fraction of ruthenium deposited inside the circuit. The values are given as % of the released ruthenium. The uncertainties are given as 2 standard deviations.*

Exp.	Total Ru transported (%)	RuO_2 transported (%)	RuO_4 transported (%)	Ru deposited (%)
1300 K	6.1±0.6	6.0±0.3	0.13±0.01	93.9±1.0
1500 K	25.5±2.6	25.4±1.3	0.14±0.01	74.5±3.8
1700 K	15.5±1.6	15.5±0.8	0.001±0.005	84.5±2.3

The injection of N_2O significantly increased the aerosol fraction of ruthenium transported through the facility when compared with the humid air experiment at 1500 K. This behavior was attributed to reactions (31) and (32) and the subsequent decomposition of RuO_3 into a solid RuO_2 at the outlet of the furnace, where the temperature decreased below 1000 K. The equilibrium constants for reactions (31) and (32) over the temperature interval used in the experiments are presented in Tables 16 and 17[123].

$$RuO_{4(g)}+N_2O_{(g)} \leftrightarrow RuO_{3(g)}+2NO_{(g)} \quad (31)$$
$$RuO_{4(g)}+2N_2O_{(g)} \leftrightarrow RuO_{2(s)}+4NO_{(g)} \quad (32)$$

Table 16. *Equilibrium constants for the reduction of RuO_4 by N_2O to RuO_3 at different temperatures[123].*

Temperature	K_{eq}
1300 K	19.03
1500 K	217.9
1700 K	137.6

Table 17. *Equilibrium constants for the reduction of RuO_4 by N_2O to $Ru0_2$ at different temperatures[123].*

Temperature	K_{eq}
1300 K	1.48 E6
1500 K	4.79 E6
1700 K	1.21 E7

The overall transport of ruthenium through the facility was increased by a factor of 2 1500 K when compared to the humid air atmosphere. The opposite effect was detected at 1300 K when the overall transport was decreased by ca. 16%. A modest increase in ruthenium transport was observed at 1700 K.

5.1.2.4. The effect of temperature on ruthenium transport in air with 5ppmV HNO_3

The results for ruthenium transport under the humid air atmosphere with 5 ppmV of HNO_3 are presented in Tables 18 and 19.

Table 18. *Mass of ruthenium transported as aerosol particles and as gas through the model primary circuit under a humid air atmosphere with 5 ppmV of HNO_3. The uncertainties are given as 2 standard deviations.*

Exp. [#]	Total Ru transported (mg)	Ru in the form of RuO_2 aerosol (mg)	Ru in the form of RuO_4 gas (mg)	Ru deposited inside the facility (mg)
1300 K	0.9±0.5	0.80±0.04	0.11±0.01	10.7±0.5
1500 K	8.5±0.4	7.6±0.4	0.86±0.04	76.5±1.0
1700 K	58.2±3.0	55.0±2.8	3.2±0.2	475.5±3.0

Table 19. *The fractions of ruthenium transported as RuO_2 aerosol particles and RuO_4 gas through the model primary circuit and the fraction of ruthenium deposited inside the circuit. The values are given as % of the released ruthenium. The uncertainties are given as 2 standard deviations.*

Exp.	Total Ru transported (%)	RuO_2 transported (%)	RuO_4 transported (%)	Ru deposited (%)
1300 K	10.4±1.0	9.1±0.5	1.2±0.1	89.7±1.6
1500 K	13.1±1.3	11.8±0.6	1.3±0.1	86.9±2.0
1700 K	14.4±1.4	13.6±0.7	0.78±0.04	85.7±2.2

The introduction of HNO_3 feed into the airflow affected the composition of transported ruthenium, resulting in a higher transport of gaseous RuO_4 through the facility when compared to the pure humid air atmosphere at all experimental temperatures. The effect of nitric acid injection was not as prominent as could be expected from the thermodynamic calculations as presented in Table 20[123].

$$3RuO_{3(g)}+2HNO_{3(g)} \rightarrow 3RuO_{4(g)}+H_2O_{(g)}+2NO_{(g)} \qquad (33)$$

Table 20. *Equilibrium constants for the oxidation of RuO_3 by HNO_3 to RuO_4 at different temperatures*[123].

Temperature	K_{eq}
1300 K	1.65 E11
1500 K	4.57 E10
1700 K	1.66 E10

An explanation for this is the thermal decomposition of HNO_3 to the lower nitrogen oxides, leading to the lower amount of precursor in the gas phase[144, 145].
As can be seen from Tables 9 and 18, the absolute amount of transported ruthenium was fairly similar when compared to the humid air atmosphere for all temperatures used in the experiments.

5.1.2.5. The effect of temperature on ruthenium transport in air with a feed of CsI aerosols

The results of transported ruthenium under the humid air atmosphere with the addition of CsI aerosols (ca. 0.8 mg/l air) into the airflow are presented in Table 21. The corresponding percentage of the total ruthenium released is summarized in Table 22.

Table 21. *Mass of ruthenium transported as aerosol particles and gas through the model primary circuit fed with CsI aerosols. The uncertainties are given as 2 standard deviations.*

Exp.	Total Ru transported in total (mg)	Ru in the form of RuO_2 aerosol (mg)	Ru in the form of RuO_4 gas (mg)	Ru deposited inside the facility (mg)
1300 K CsI	1.5±0.1	0.70±0.03	0.80±0.04	24.6±0.5
1500 K CsI	34.9±1.8	7.2±0.4	27.7±1.4	186.1±2.5
1700 K CsI	125.7±6.3	79.9±4.0	45.8±2.3	854.3±7

Table 22. *The fractions of ruthenium transported as RuO_2 aerosol particles and RuO_4 gas through the model primary circuit, as well as the fraction of ruthenium deposited inside the circuit. All values are given as % of the released Ru. The uncertainties are given as 2 standard deviations.*

Exp.	Total Ru transported in total (%)	RuO_2 transported (%)	RuO_4 transported (%)	Ru deposited (%)
1300 K CsI	7.3±0.4	3.4±0.2	4.0±0.2	92.7±0.5
1500 K CsI	20.8±1.0	4.3±0.2	16.5±0.8	79.2±1.2
1700 K CsI	16.9±0.9	10.7±0.5	6.2±0.3	83.1±1.0

Introduction of CsI aerosols fed into the airflow led to the decrease of overall ruthenium transport through the facility at temperatures of 1300 K and 1700 K. During the experiment conducted at 1500 K the overall ruthenium transport was the same as in the pure humid air atmosphere. The fraction of transported gaseous ruthenium was increased significantly at temperatures of 1500 K and 1700 K. This effect was most prominent at 1500 K where about 16.5% of the transported ruthenium was in the form of a gas when compared to the 0.2% in humid air atmosphere at the same temperature.

5.1.2.6. The transport of cesium and iodine in the experiments on ruthenium transport with CsI feed

The amounts of cesium and iodine transported through the primary circuit simulating facility during the experiments conducted at temperatures of 1300 K-1700 K were quantified using NAA and ICP-MS. The results are summarized in Tables 23-25. The quantification of iodine collected on the main filter was not possible due to iodine evaporation during the neutron activation. Data is therefore available only for iodine collected in the liquid 1 M NaOH trap.

Table 23. *Masses of cesium and iodine transported as aerosol particles and gas through the model primary circuit. The uncertainties are given 2 standard deviations.*

Exp	CsI in feed (mg)	CsI concentration (mg/l air)	Iodine as gas (mg)	Cs aerosol (mg)	Cs gas (mg)
1300 K CsI	126.9±3.1	0.81±0.02	1.1±0.005	0.25±0.01	1.2E-3±1.2E-5
1500 K CsI	123.4±3.1	0.79±0.02	1.7±0.008	0.42±0.02	9.2E-3±9.2E-5
1700 K CsI	120.1±3.1	0.77±0.02	2.8±0.01	0.45±0.02	1.0E-2±1.0E-4

Table 24. *The fractions of cesium transported as aerosol particles and gas through the model primary circuit, as well as the fraction of cesium deposited inside the circuit. All values are given as % of the injected cesium in the form of CsI. The uncertainties are given as 2 standard deviations.*

Exp.	Total Cs transported (%)	Cs aerosol transported (%)	Cs gas transported (%)	Cs deposited (%)
1300 K CsI	0.39±0.02	0.39±0.02	1.9E-3±1.9E-5	99.6±0.02
1500 K CsI	0.68±0.03	0.67±0.03	1.2E-2±1.2E-4	99.3±0.03
1700 K CsI	0.74±0.04	0.74±0.04	2.6E-3±2.6E-5	99.3±0.04

Table 25. *The fractions of iodine transported as aerosol particles and gas through the model primary circuit, as well as the fraction of iodine deposited inside the circuit. All values are given as % of the injected iodine in the form of CsI. The uncertainties are given as 2 standard deviations.*

Exp.	Total I transported (%)	I aerosol transported (%)	I gas transported (%)	I deposited (%)
1300 K CsI	1.72±0.01	-	1.72±0.01	98.28±0.01
1500 K CsI	2.76±0.01	-	2.76±0.01	97.24±0.01
1700 K CsI	4.75±0.02	-	4.75±0.02	95.26±0.02

As can be seen from Tables 23-25 iodine was partly volatilized from the feed of CsI and transferred in the form of gas to the liquid traps. The detected volatile

fraction of cesium was very minor. As discussed further, some iodine was detected on the aerosol filter measured by XPS. The overall quantification of transported of iodine is therefore underestimated.
From the measured data it is obvious that the overall transport of both cesium and iodine through the facility was very small in all the performed experiments. The fraction of transported iodine increased when the temperature increased whereas the increase of the transported cesium fraction was only minor.

5.1.3. Chemical characterization of transported ruthenium

5.1.3.1. Characterization of the gaseous ruthenium fraction from all ruthenium transport experiments

Characterization of the gaseous ruthenium speciation was not possible due to the high temperatures inside the hot zone of the facility online. However, as the thermodynamic calculations and previously published results indicate, RuO_4 is the only gaseous ruthenium specie that is relatively stable at temperatures lower than 1000 K[62, 68, 73].
As it is known that RuO_4 forms ruthenate and perruthenate salts of sodium in solutions of NaOH[84, 146, 147], the liquid traps were examined by spectrophotometry in order to determine the formation of these compounds in the solutions. A representative UV-VIS spectrum of the liquid traps is presented in Figure 12.

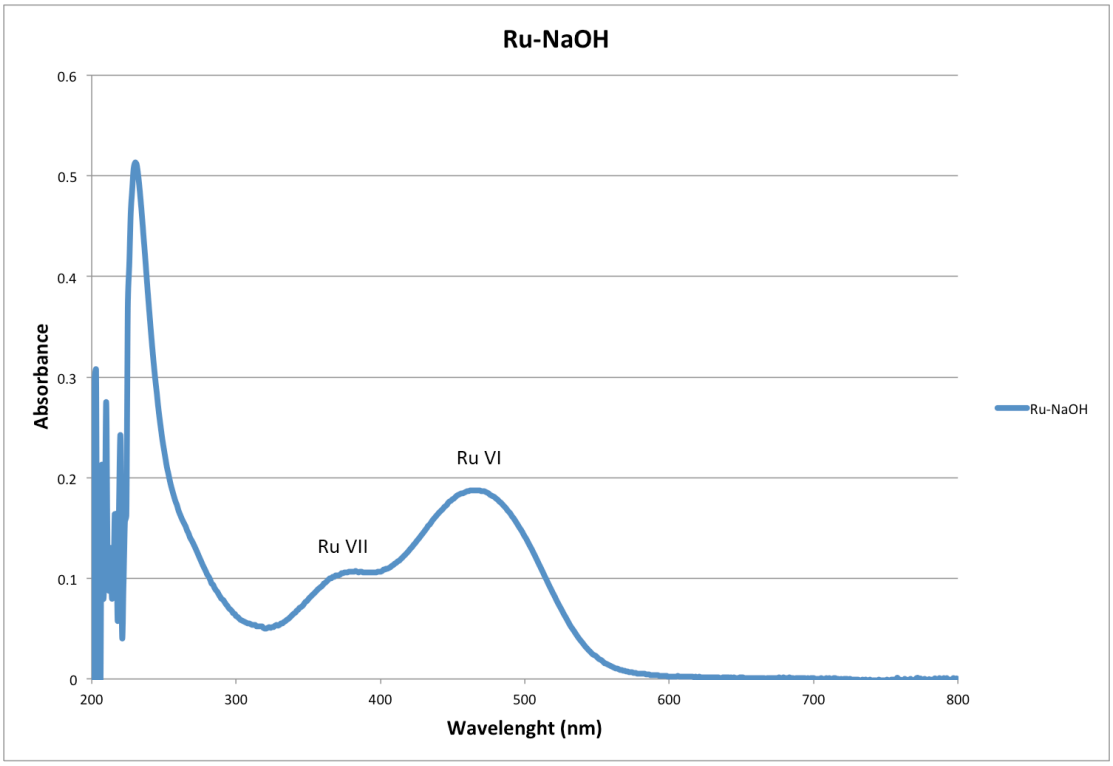

Figure 12. *UV-VIS spectrum obtained from the measured 1 M NaOH liquid trap.*

The two distinctive peaks originating from Ru^{VI+} and Ru^{VII+} could be identified in the obtained spectra from the experiments[112]. The spectra obtained from all the ruthenium transport experiments showed the same behavior. This, along with the data from the previous studies, was interpreted as a strong indication that the gaseous fraction of ruthenium collected in the 1 M NaOH traps was in

the form of RuO_4. However it should be stated that if ruthenium in oxidation states (VI-VIII) formed volatile oxyhalides with iodine and those would be retained in the liquid traps, ruthenium absorption spectra would look very similar to spectra obtained during the experiments. Thus possibility of gaseous ruthenium transport in form of oxyhalides could not be neglected in the experiments with CsI feed.

5.1.3.2. SEM/EDX characterization of aerosols collected on the filters from ruthenium transport experiments

The ruthenium particle samples collected during the experiments were analysed with a scanning electron microscope. The SEM micrographs of the particles collected from some of the experiments are presented in Figure 13. Depending on the reaction conditions, the morphology (particle size and shape) of ruthenium aerosol particles varied greatly between the samples. In experiments with humid air atmosphere the typical crystalline needle-shaped form of RuO_2 was clearly evident and was the predominant form of ruthenium in the samples. Thus this observation also supported the previous findings[63, 148].

The feed of NO_2 gas into the flow of Ru oxides seemed to have an effect on the shape and quantity of the ruthenium particles. A variety of different sized cuboid crystals were formed instead of needle shaped crystals. However, the concentration of the formed particles was very low due to the high formation of gaseous ruthenium and thus only a few particles were observed on the grid for the analysis (see Figure 13b). In the other experiments the particle concentration was high inside the Ru transport facility and this led to an agglomeration of particles in the gas phase before they were collected on the grid, as can be seen in Figures 13a and 13c.

a)

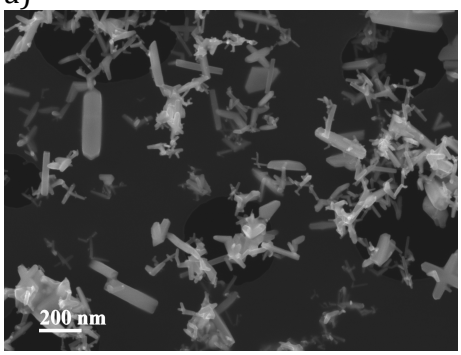

b)

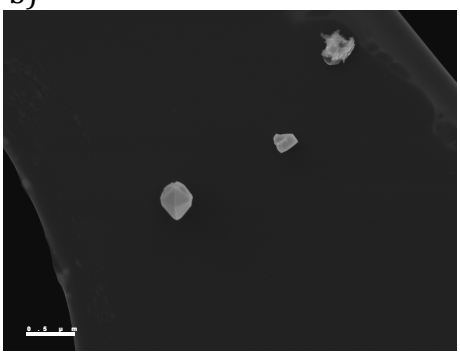

c)

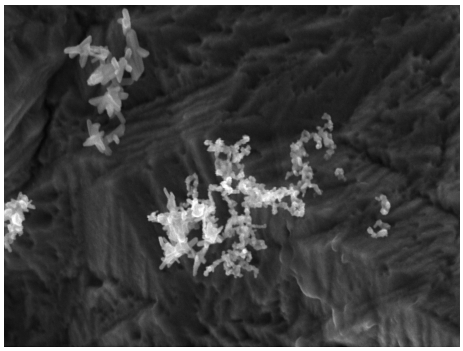

Figure 13. *SEM micrographs of ruthenium particles on a nickel/carbon grid in experiments (a) with humid air, (b) with NO_2 gas injection and (c) with feed of CsI*

The EDX analysis of two spots on the sample from the experiment conducted in air verified that the particles that were formed contained ruthenium (Figure 14). The identified characteristic X-ray line energies for Ru were for example 2.558 keV ($L_{\alpha 1}$) and 2.683 keV ($L_{\beta 1}$). In addition to Ru, signals of other elements were also observed at both analysis locations. Nickel originated from the grid and carbon from the foil, whereas the signal of aluminium was from the sample holder. Oxygen originated mainly from the oxidized Ru and the grid.

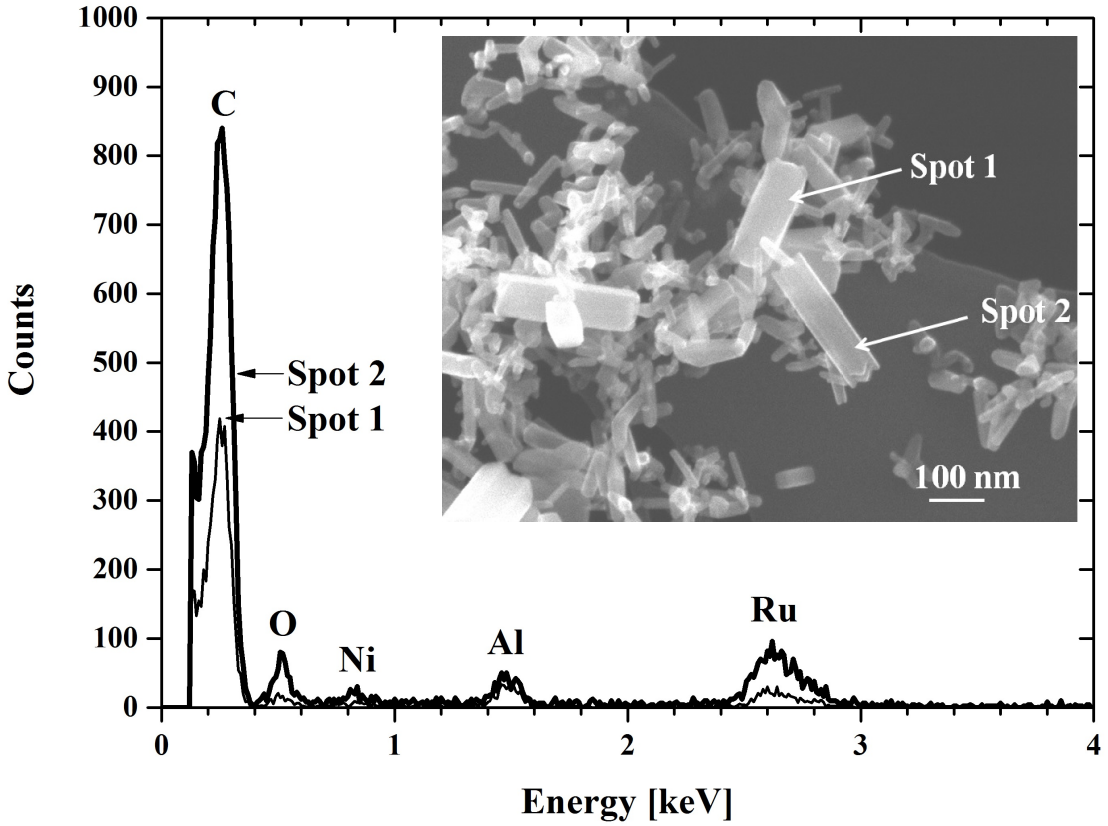

Figure 14. *EDX spectra of spots #1 and #2 of Ru particles. The recorded true counts of spot #2 are multiplied by two.*

5.1.3.3. XPS

The chemical speciation of the particles transported through the facility, which were collected directly from the gas phase on a quartz glass surface, was analyzed by XPS technique. As a result of the analysis the binding energies of ruthenium (3d5/2 peak), cesium (3d5/2 peak) and iodine (3d5/2 peak) (if used in the experiments) were obtained. The identification was based on the comparison between the identified binding energies of elements on the samples with the reference binding energy values found in the literature. The reference samples of commercial ruthenium dioxide powders, both anhydrous and hydrated (purity of 99.5%, Alfa Aesar), were analyzed and the obtained spectra were then compared with the spectra of ruthenium-containing samples. The reference values of the binding energies used in the evaluation of the data are presented in Table 26. As can be seen from Table 26, the binding energies are not only dependent on the oxidation state of ruthenium but also on its chemical

environment, e.g. the hydration of RuO_2. Thus, the comparison of all obtained spectra in the region of the Ru 3d5/2 peak gives better insight into the chemical characterization of the measured ruthenium compound.

Table 26. *The reference binding energies (eV) for Ru 3d5/2, I 3d/52, O 1s and Cs 3d5/2 peaks in various compounds.*

Compound	Ru 3d5/2	I 3d5/2	Cs 3d5/2	O 1s
Ru metal	280.0[105]	-	-	-
RuO_2	280.5[149]	-	-	-
$RuO_2 \cdot 2.3H_2O$	282.1[149]	-	-	-
$BaRuO_4$	284.2[150]	-	-	-
RuO_4	283.3[105]	-	-	-
RuI_3	281.5[a]	619.0[a]	-	-
CH_3I	-	620.5[151]	-	-
CH_2I_2	-	620.6 [152]	-	-
C_2H_5I		620.7[153]	-	-
I_2	-	620.2[154] 619.9[155, 156]	-	-
I_2O_5	-	623.3[155]	-	529.9[157]
HIO_3	-	623.1[155]	-	-
$NaIO_4$	-	624[155]	-	-
AlI_3	-	618.0-619.7 [b]	-	-
ZnI_2	-	619.5 [154]	-	-
CuI	-	619.6 [158]	-	-
CsI	-	618.4[159]	724.1[159]	-
CsOH	-	-	724.15[154]	530.6[160]
Cs_2O	-	-	725.2[161]	527.0[161]
$CsClO_4$	-	-	724.4[159]	
OH^-	-	-	-	≈530.5-531.7[71, 154, 162]
H_2O	-	-	-	≈532.1-533.3[71, 163]

(a) *Value obtained from measurements with commercial RuI_3 (98% Sigma Aldrich).*
(b) Estimated value.

5.1.3.3.1. XPS measurements of samples from experiments with air, N_2O, NO_2, and HNO_3 atmospheres

The binding energies for the Ru 3d5/2 peak in all samples were within the region of 280.4 eV-280.5 eV, regardless of the atmosphere used, as can be seen in Figure 15. This provides a strong indication that the transported ruthenium aerosols were in the form of anhydrous RuO_2 in all experimental conditions. The

overall characteristics of the spectra are very similar to each other, which strengthens the assumption that all spectra originate from the same compound. During the XPS measurements no nitrogen was detected in the collected samples, thus the possible formation of ruthenium nitrosyl compounds was ruled out during the data evaluation process[164, 165].

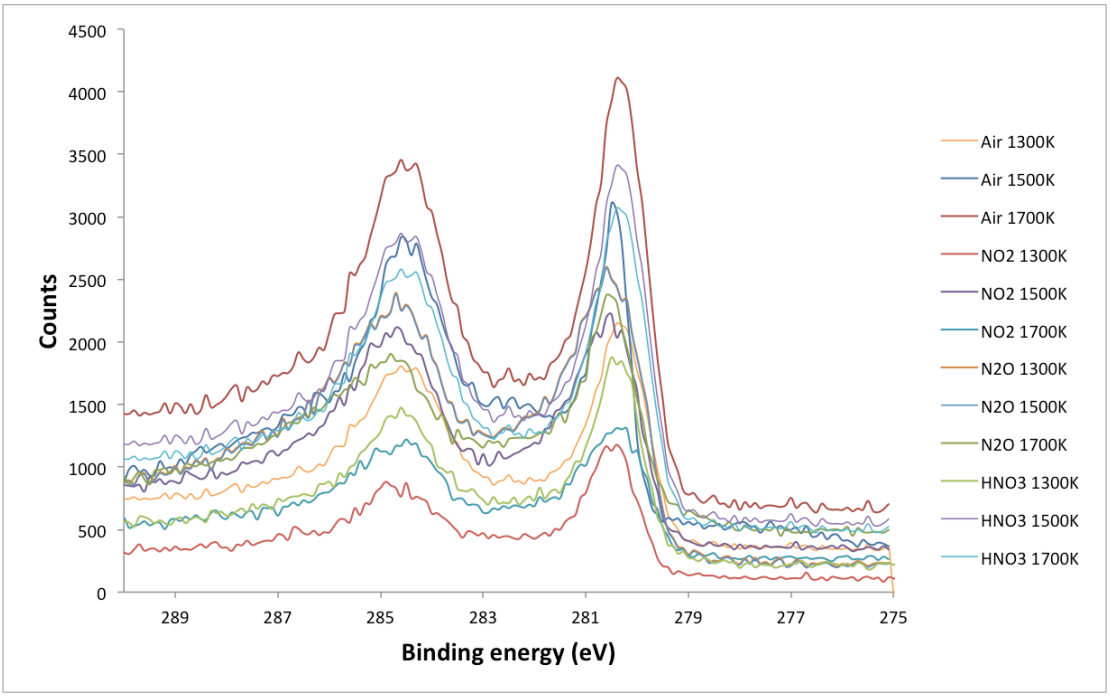

Figure 15. *The XPS spectra obtained from the analysis of collected aerosols on filters. Spectra were scaled to fit the figure.*

5.1.3.3.2. XPS measurements of samples from experiments with CsI aerosols

The results obtained from XPS analysis of aerosols collected during the experiment conducted under temperatures of 1300 K, 1500 K and 1700 K with CsI aerosol injection are presented in Table 27. As can be seen from Table 27 ruthenium in the aerosols was in the form of RuO_2. The binding energy of the Ru 3d5/2 peak was slightly higher than the reference binding energy for anhydrous RuO_2 in all experiments. Additionally the hydration of RuO_2 decreased with the increased temperature used in the experiments. Therefore it can be assumed that RuO_2 was in a partially hydrated form, where the amount of adsorbed moisture was lower than the stoichiometry of the $RuO_2 \cdot 2.3\ H_2O$ used as a reference sample. The determined binding energies were also significantly lower than for the ruthenium in its perruthenate form. This eliminates the possibility of ruthenium transportation to the containment in a form of $CsRuO_4$ or Cs_2RuO_4 when cesium iodide and ruthenium are transported at the same time through RCS, as was previously proposed in some works[63, 94, 166].

Table 27. *Obtained binding energies and identified compounds from the collected aerosols from experiments with CsI aerosol injection.*

Temperature	Peak	Ru 3d5/2	I 3d5/2	Cs 3d5/2
1300 K	**Binding energies**	281.3±0.1	618.9±0.1 624.0±0.1	724.2±0.1
1300 K	**Chemical state of element**	RuO_2	I^- IO_4^-	Cs^+
1500 K	**Binding energies**	281.0±0.1	618.5±0.1 623.0±0.1	724.0±0.1
1500 K	**Chemical state of element**	RuO_2	I^- IO_3^-	Cs^+
1700 K	**Binding energies**	280.8±0.1	618.4±0.1 620.4±0.1 622.9±0.1	724.0±0.1
1700 K	**Chemical state of element**	RuO_2	I^- I_2 IO_3^-	Cs^+

The binding energies for the iodine species were dependent on the temperature. At the temperature of 1300 K both iodide (62%) (BE 618.9±0.1 eV) and periodate (IO_4^-) (38%) (BE 624±0.1 eV) forms were detected (where the iodide form originated most probably from the CsI compound). At the temperature of 1500 K the iodine in the collected aerosols was found to be in 2 different oxidation states. The most dominant form was iodide (I^-) (42%) with a determined binding energy for I3d 5/2 peak of 618.5±0.1eV (60%). The second identified form of iodine was iodate (IO_3^-) with a binding energy of 623.0±0.1eV (40%). At the temperature of 1700 K iodine was identified to be in 3 different chemical forms. The most prominent was the iodide form (I^-) (60%) (BE 618.4±0.1 eV) followed by adsorbed elemental iodine (I_2) (30%) (BE 620.4±0.1 eV), and iodate (IO_3^-) (10%) (BE 622.9±0.1 eV). The content of iodine on the filter was very low in this sample (<0.5 mass %), thus analysis of iodine species partitioning was less reliable even after long acquisition times.
Cesium was detected only in one oxidation state with a binding energy for the Cs 3d5/2 peak of 724.2-724.0 eV under all experimental conditions. This binding energy corresponds to the form of cesium as Cs^+ ion. The obtained spectra can be found in Appendix B, Figures B1-B9.

5.1.3.4. XRD measurements of samples from experiments with air, N_2O, NO_2, and HNO_3 atmospheres

The results from the qualitative crystallographic X-ray diffraction analysis of the samples are shown in Figure 16. The recorded XRD spectra in experiments with air, N_2O, NO_2 and HNO_3 show the same diffraction pattern, which corresponds to the rutile structure of RuO_2[139, 167, 168]. This is in good agreement with the XPS analysis, leading to the conclusion that aerosols collected from the gas flow were in the form of anhydrous ruthenium dioxide.

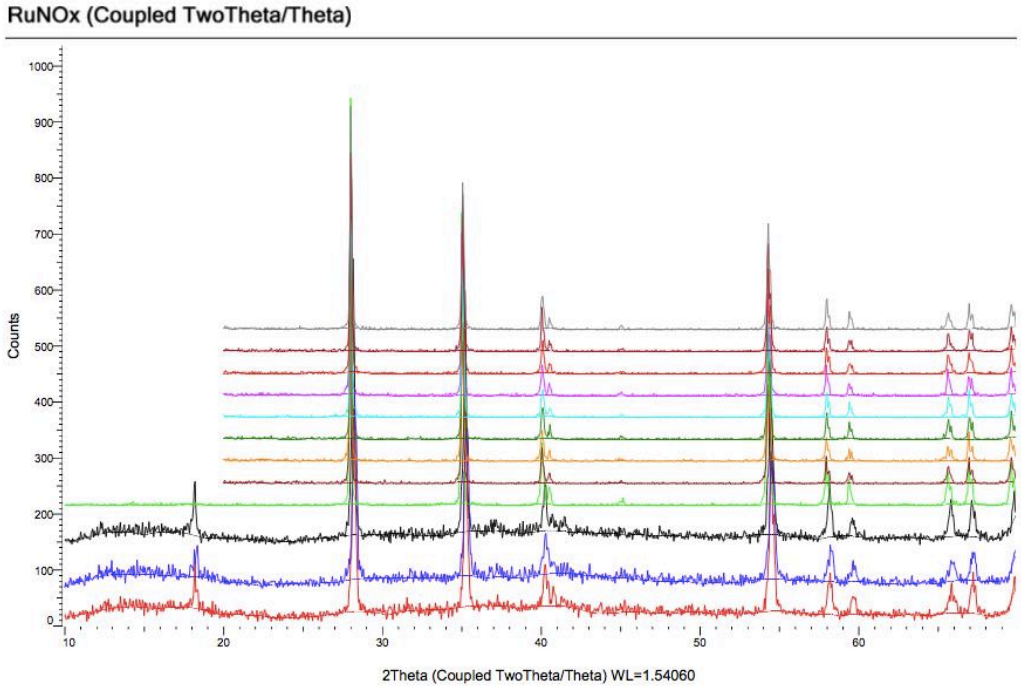

Figure 16. *The obtained XRD spectra from the samples from experiments with air, N_2O, NO_2 and HNO_3. The height of the peaks was scaled in order to fit in the figure.*

5.2. Ruthenium containment chemistry

5.2.1. Distribution of ruthenium between the metals in the containment of NPP

The surface areas of the samples used were determined by the Brunauer–Emmett–Teller theory (BET) method. Quantification of the deposited ruthenium was determined by gamma spectroscopic determination of ^{103}Ru on the samples. The weights of deposited ruthenium per square centimeter of the sample surface for the humid and dry atmospheres could therefore be determined and are presented in Table 28. The absolute amount of deposited ruthenium on the metal samples varied in each experiment, even if the same amount of ruthenium trichloride was used for the RuO_4 synthesis. This variation occurs because ruthenium tetroxide also shows an ability to decompose on glass surfaces[67]. The amount of ruthenium transported through the experimental setup to the reaction vessel was therefore slightly different between the experiments. However it seems that this variation in the absolute amount of deposited ruthenium had no impact on the distribution ratio of ruthenium.

Table 28. *Distribution of ruthenium in μg/cm² on metallic zinc, copper and aluminum in dry and humid atmospheres.*

Zinc	Copper	Aluminum	Zinc	Copper	Aluminum
Dry atmosphere			**Humid atmosphere**		
2.7±0.5	9.4±0.2	103.3±0.7	15.3±0.3	18.0±0.3	31.6±0.6
0.76±0.02	0.4±0.1	86.8±0.6	13.2±0.2	12.1±0.2	24.8±0.5
2.2±0.4	2.5±0.5	98.4±0.7	18.5±0.3	19.2±0.4	38.9±0.7

From the presented data it is obvious that a different distribution of ruthenium among the metal samples occurred at humid and dry conditions. The general reason for this is formation of a thin water layer on the samples in the humid conditions. The water layer formation is caused by the high humidity (99%) and relatively low temperature of the samples (295 K) during the deposition. As the dew point at 99% relative humidity is 313 K, the lower temperature of the samples leads to the formation of a condensed water layer on their surfaces. During the experiments under dry conditions, the low humidity (<2%) prohibited the formation of the water layer on the samples [132].

As can be seen from Table 28, the interaction of RuO_4 with the metals in both humid and dry atmospheres leads to a stronger attraction of the ruthenium to aluminum, when compared to the other metals,. As the protective oxide layer formed on the aluminum surface in the air prohibits the direct oxidation of the metal[169]. The explanation of the ruthenium reduction on the aluminum as a product of metal oxidation therefore does not seem satisfactory. The possible explanation for decomposition of RuO_4 on the aluminum surface is based on the observation of the oxygen-rich layer on the aluminum surface. The oxygen surface site density of oxides on the different metal surfaces was studied previously[170]. A high oxygen surface site density when compared to other metallic oxides e.g. ZnO was shown. The high oxygen site density may lead to an increased reactivity of the aluminum surface towards ruthenium tetroxide. This is due to the catalytic effect of this layer in the process of RuO_4 decomposition.

The difference between wet and humid depositions is caused by the fact that hydration of the surface oxygen atoms leads to a decreased negative surface charge, thus lowering the surface reactivity. This results in the lower attraction of ruthenium to the aluminum surface in the humid atmosphere.

In contrast to the aluminum samples, the relative amounts of the deposited ruthenium on the copper and the zinc were higher in the humid atmosphere experiments than in the dry conditions.

Both zinc and copper exposed to air normally have a layer of metal oxides on their surfaces. In contrast to the aluminum, the oxide layers of zinc and copper have semi-conductive properties and allow transfer of electrons from the metals to the RuO_4 [171, 172]. Electrochemical reduction of RuO_4 can therefore proceed on the zinc and copper surfaces in the humid atmosphere. The standard redox potential for the couple RuO_4/RuO_2 is 1.4 V in a neutral solution[173]. The standard redox potential for the couple Zn/Zn^{2+} is -0.762 V and for the couple Cu/Cu^{2+} is -0.337 V[174]. The electrochemical oxidation of zinc and copper metal

through the water layer is therefore possible due to the potential difference. In contrast to this behavior, in the dry atmosphere no water layer is formed on the samples. The loss of the water layer as an electrolyte prohibits the electrochemical reduction of RuO_4 on the zinc and copper samples, consequently lowering the adsorption of ruthenium on these materials.

5.2.2. Characterization of the ruthenium deposits on metals and epoxy paint samples

5.2.2.1. SEM/EDX

Micrographs obtained from SEM analysis revealed a different smoothness and deposit coverage on the samples. The EDX analysis showed a different elemental composition in different spots on the samples. A significant formation of ruthenium-rich grains was observed by EDX analysis. The EDX measurements of aluminum and zinc samples showed ruthenium-rich grains surrounded by areas containing less ruthenium. The copper and epoxy paint samples were covered with ruthenium more evenly. The highest concentration of ruthenium among the samples according to the EDX analyses was in the epoxy paint samples. The cracks on the paint samples were probably caused by the manipulation of the sample between deposition and photographing.

a)

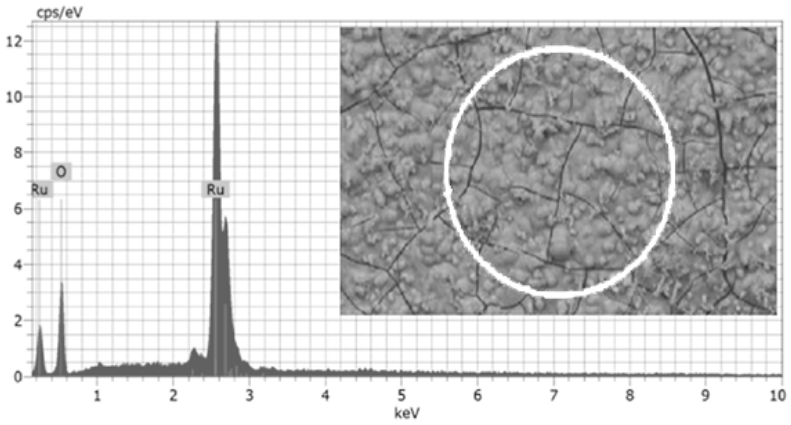

b)

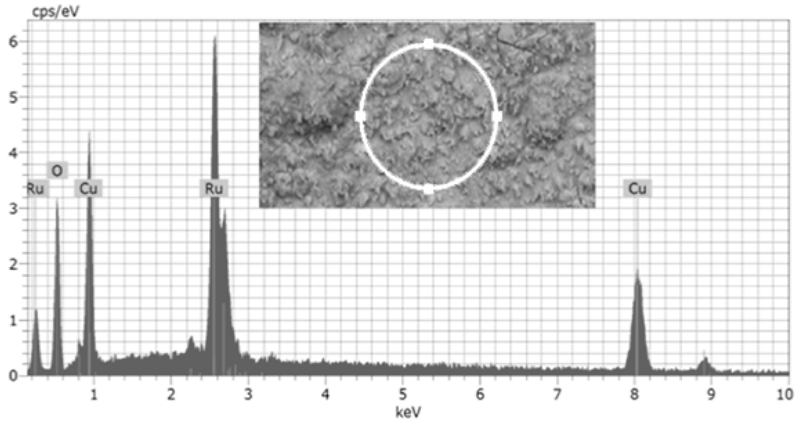

c)

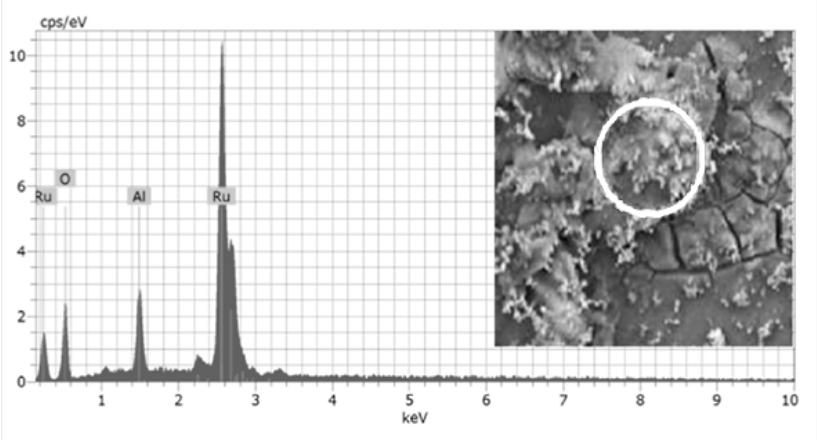

d)

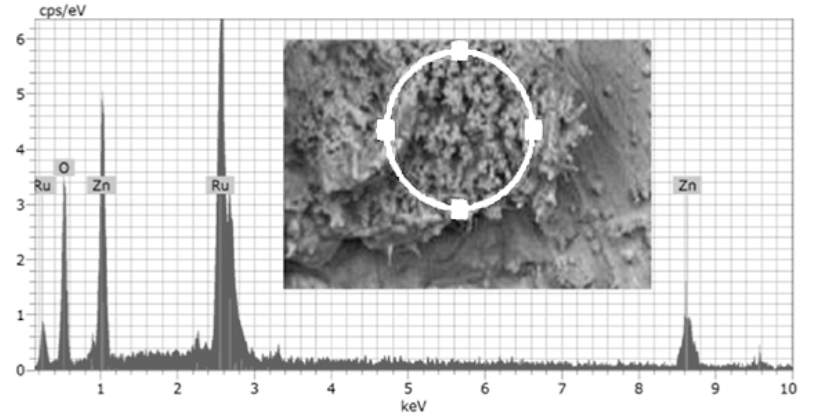

Figure 17. *SEM/EDX micrographs of ruthenium deposits on (a) paint, (b) copper, (c) aluminum, and (d) zinc.*

5.2.2.2. XPS

The chemical speciation of the ruthenium deposits formed on the samples was analyzed using XPS. As a result of the analysis the binding energies of ruthenium (3d5/2 peak) and oxygen (1s) were obtained and are presented in Table 29. The binding energies obtained were then compared with the reference binding energy values, as presented in Table 26.

Table 29. *Binding energies (eV) obtained from the XPS measurements of aluminum, zinc, copper and epoxy paint samples deposited with RuO_4.*

Sample	Ru 3d5/2	O1s	Identified Ru compound
Aluminum	281.8±0.1	529.6±0.1 530.9±0.1 532.4±0.1	$RuO_2.xH_2O/Ru^{(IV)}O_{(2-y)}OH_y$
Zinc	281.7±0.1	529.3±0.1 531.2±0.1	$RuO_2.xH_2O/Ru^{(IV)}O_{(2-y)}OH_y$
Copper	281.7±0.1	529.8±0.1 531.2±0.1 532.2±0.1	$RuO_2.xH_2O/Ru^{(IV)}O_{(2-y)}OH_y$
Epoxy paint	281.8±0.1	529.9±0.1 532.3±0.1	$RuO_2.xH_2O/Ru^{(IV)}O_{(2-y)}OH_y$

From the XPS measurements it was found that the binding energy of the Ru 3d5/2 peak had a similar value in all deposited samples that was in good agreement with the value estimated for the reference hydrated RuO_2 powder. This implies that the substrate material had no effect on the chemical speciation of the ruthenium deposits.

Identification of the oxygen species showed strong hydroxylation of the oxygen in the samples. Ruthenium dioxide as a hygroscopic oxide readily absorbs water during deposition in high humidity conditions. The occurrence of water in the sample can therefore lead to hydrolysis of the deposit upper layers. This is the most probable explanation of the hydroxyl group occurrence in the deposits. The process of hydration of the RuO_2 deposits on the samples, followed by further hydrolysis, leads to the formation of ruthenium oxo-hydroxide species with the ruthenium in a formal oxidation state +IV on the surface of deposits.

5.2.2.3. EXAFS

The EXAFS results for the ruthenium deposits on metallic aluminum, copper and zinc, and on epoxy paint show a mean Ru-O bond distance of 1.92-1.96 Å, and Ru···Ru distances of ca. 3.10 and 3.55 Å. These results strongly indicate that ruthenium is present mainly as RuO_2 in either tetragonal or orthorhomic forms, while the cubic forms can be ruled out. The distances around ruthenium in solid RuO_2 in its different forms, as reported in crystallgraphic studies, are summarized in Appendix B - Table 1. The different distribution ratios of ruthenium on the samples caused significant differences in the observed EXAFS signal. The lower the amount of the ruthenium deposit the lower the signal-to-noise ratio obtained, and thereby also a lower accuracy in the structure parameters in the deposits. From a comparison of the EXAFS spectra obtained in this study with EXAFS spectra of anhydrous RuO_2, $RuO_2 \cdot 0.29\ H_2O$ and $RuO_2 \cdot 2.32\ H_2O$ reported by McKeown, et al.[175], and of the EXAFS spectrum for a RuO_2 sample (denoted as +1.20 V) reported by Mo et al.[176], it was found that the ruthenium deposits on all surfaces studied have the most close similties with $RuO_2 \cdot 0.29\ H_2O$. As the data quality of ruthenium deposits is limited, mainly due to the small amounts of material, the resolution in the obtained distances is small. This causes that it is only possible to obtain a mean Ru-O bond distance with a Debye-Waller coefficient larger than expected for a regular octahedral configuration around a metal ion.

The refined structure parameters for the ruthenium deposists are presented in Table 30, and the fit of the EXAFS data and corresponding Fourier transforms are shown in Figures 18 and 19[132].

Table 30. *Mean bond distances (R/Å), Debye-Waller factors (σ^2) and degeneracy number of distances (N) of ruthenium(IV) oxide formed by reduction of ruthenium(VIII) oxide on different surfaces*[132].

Interaction	*N*	*R*	σ^2	*k*-range
Ru_Al				
Ru-O	6	1.959(1)	0.0095(1)	2-10
Ru···Ru	2	3.143(2)	0.0115(2)	
Ru···Ru	8	3.583(4)	0.0239(4)	
MS RuO_6	6x3	3.914(6)	0.012(1)	
Ru_Zn				
Ru-O	6	1.929(1)	0.0095(2)	2-10
Ru···Ru	2	3.101(1)	0.0073(1)	
MS RuO_6	6x3	3.86(1)	0.021(2)	
Ru_Cu				
Ru-O	6	1.919(1)	0.0055(1)	2-10
Ru···Ru	2	2.992(2)	0.0145(2)	
Ru···Ru	8	3.53(4)	0.012(4)	
MS RuO_6	6x3	3.84(6)	0.004(1)	
Ru_paint				
Ru-O	6	1.946(3)	0.008(1)	2-8
Ru···Ru	2	3.12(1)	0.014(2)	
MS RuO_6	6x3	3.90(3)	0.012(3)	

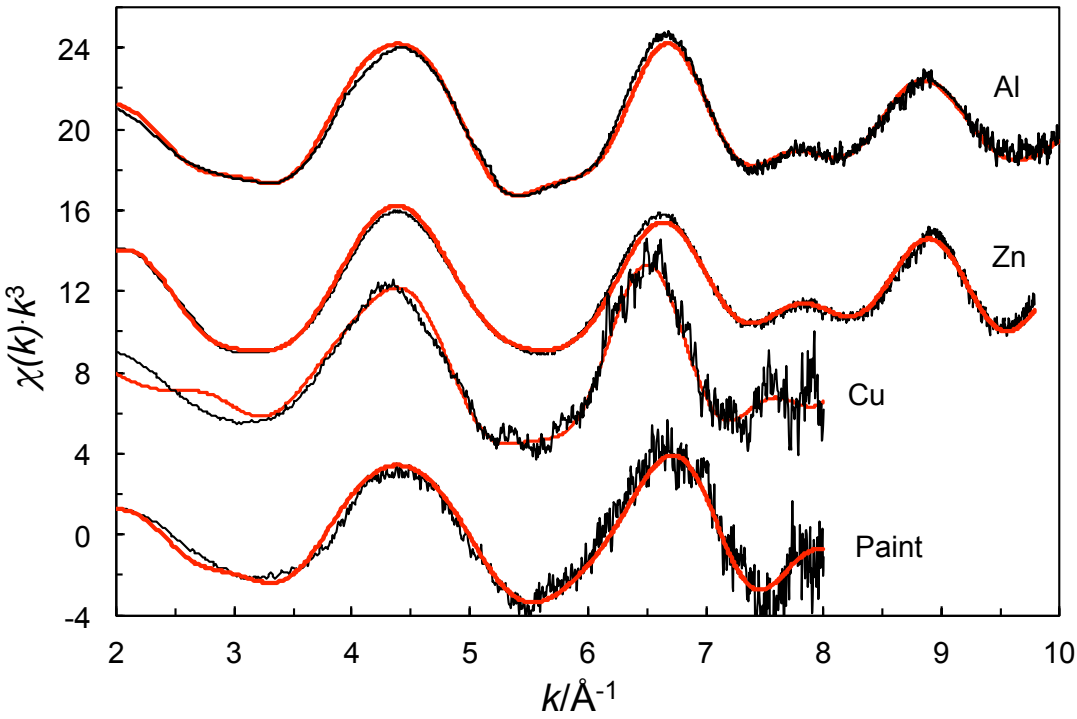

Figure 18. *Fitted raw EXAFS data of ruthenium deposists on metallic aluminum, zinc, copper, and epoxy paint*[132].

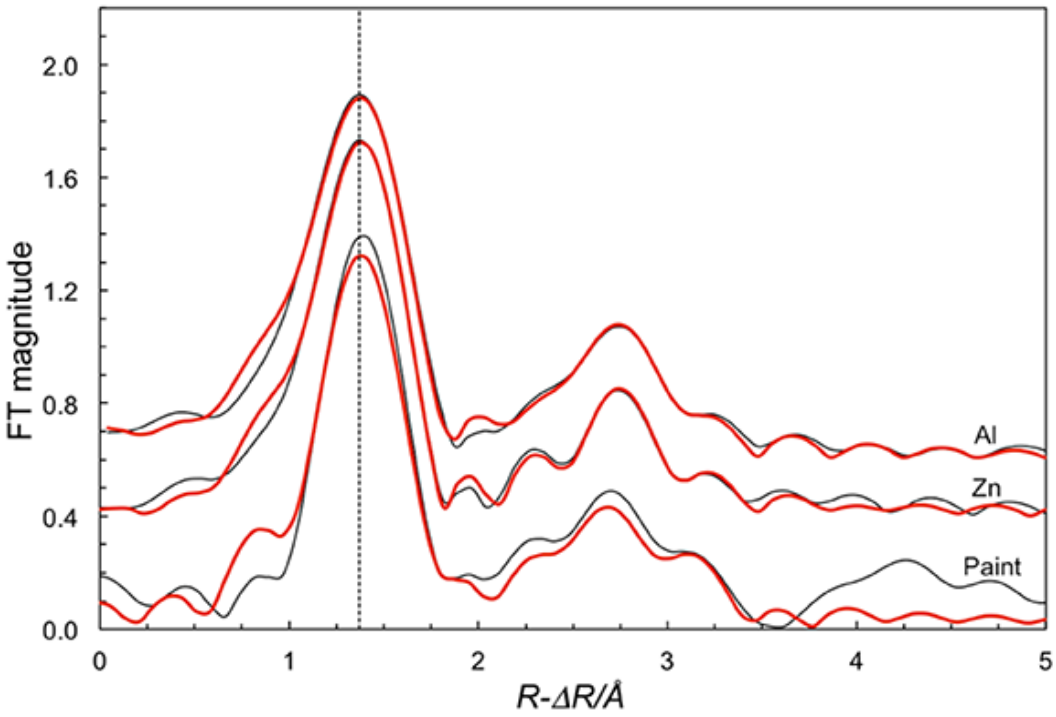

Figure 19. *EXAFS data collected on different samples with fitted RuO_2 model. Black lines represent the EXAFS data obtained after Fourier transform and the red lines represent the fitted Ab initio model*[132].

5.2.3. Interaction of RuO_4 with iodine covered zinc, aluminum, copper and epoxy paint surfaces

5.2.3.1. Revaporization of iodine from the samples after interaction with RuO_4

After the deposition of RuO_4 onto materials covered with iodine a significant release of iodine from the zinc and aluminum samples was detected. The revaporized fractions of iodine are presented in Table 31.

Table 31. *Fractions of revaporized iodine from the samples after interaction with RuO_4. The uncertainties are given as 2 standard deviations.*

Sample type	Aluminum	Zinc	Copper	Paint
Revaporized iodine fraction (%)	21.7±2.1	29.3±2.2	1.5±1.7	0.43±1.7

There was a noticeable difference between revaporized fractions of iodine from the zinc and aluminum samples compared to the fractions from copper and epoxy paint. The proposed chemical reactions for the revaporization of iodine from aluminum and zinc samples are presented as equations (34) and (35).

$$4AlI_{3(s)}+3RuO_{4(g)} \rightarrow 6I_{2(g)}+2Al_2O_{3(s)}+3RuO_{2(s)} \quad (34)$$

$$2ZnI_{2(s)}+RuO_{4(g)} \rightarrow 2I_{2(g)}+RuO2_{(s)}+2ZnO_{(s)} \quad (35)$$

The difference in the revaporized iodine fractions from different materials can be explained by the different solubility of the iodine compounds formed on the metals. The solubility of ZnI_2 (438g/100g H_2O)[177] and AlI_3 (which dissolves and reacts with water)[177] are orders of magnitude higher than the solubility of CuI (2E-5g/100g H_2O)[177]. Additionally, both ZnI_2[178] and AlI_3[177] are strongly hygroscopic. Therefore zinc and aluminum iodides were at least partly dissolved to the form of solutions on the samples. The oxidation of these iodides therefore takes place in the thin water layer formed on the surfaces of the samples. This can have an effect on the kinetics and on the mechanism of iodine oxidation. Due to the low solubility of I_2 in water (0.03g/100g H_2O)[177], I_2 formed by oxidation of iodides will be easily transferred to the gaseous phase[179]. As the solubility of copper iodide is much lower only negligible dissolution of CuI occurred during the experiments. This suggests a different mechanism of iodide oxidation compared to the zinc and aluminum samples.

The work of Brown et al. on the potassium iodide oxidation by O_3 in dry and humid conditions showed a preferred formation of molecular iodine (I_2) in humid conditions, whereas IO_3^- was formed in a dry atmosphere[180]. This indicates that the different results between AlI_3, ZnI_2 and CuI in the performed experiments were caused by different solubility and hygroscopicity of iodides.

During the experiments the dependence between the mass of ruthenium needed to volatilize 1 mg of iodine from deposits and the mass of originally deposited iodine on aluminum and zinc samples was determined. The results obtained are presented in Figure 20. It was observed that the lower was the

mass of the deposited iodine; the higher was the mass of the ruthenium tetroxide required for elemental iodine to be released.

a)

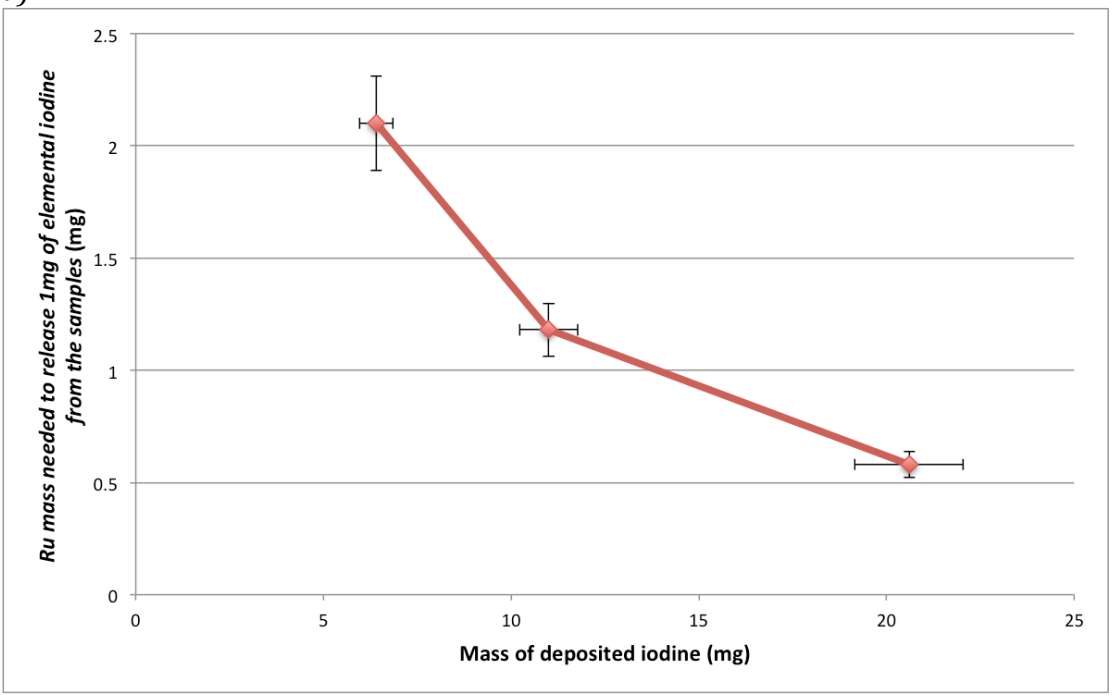

b)

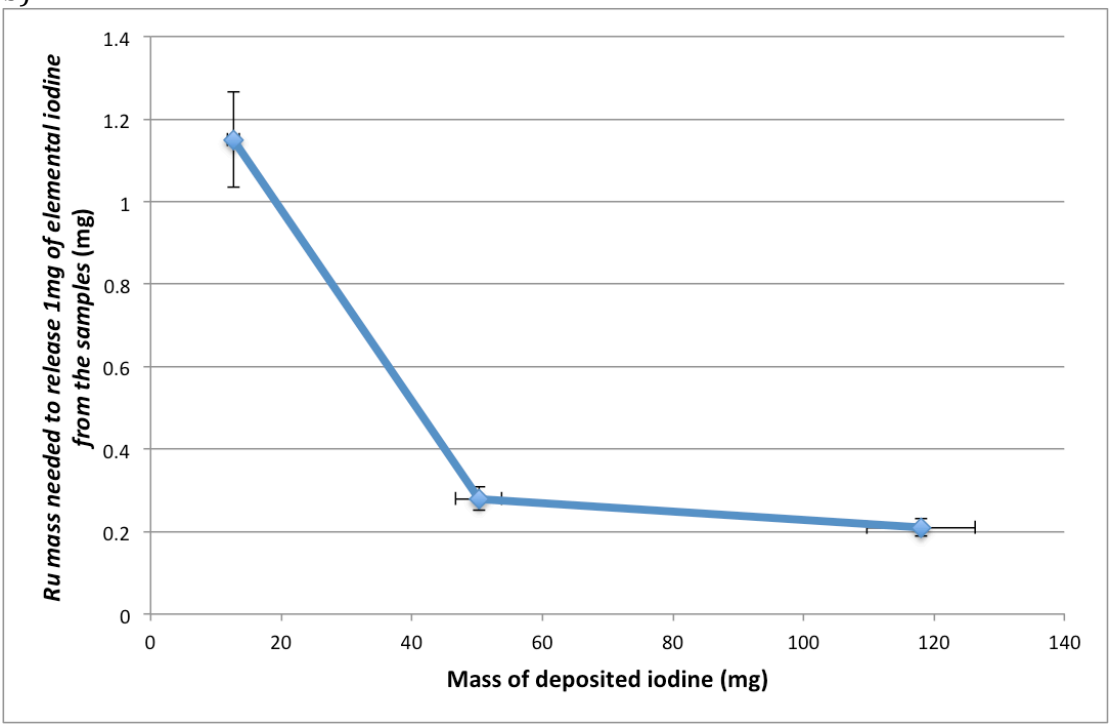

Figure 20. *Dependence of Ru mass needed to release 1 mg of elemental iodine from a) aluminum, and b) zinc deposited with I_2. Uncertainties originate from triplicates.*

5.2.3.2. Retention of ruthenium on the iodine-covered surfaces

After the interaction of iodine deposited samples with RuO_4 the ruthenium deposits formed on the samples were quantified. As a reference non-iodine exposed samples were deposited at the same time as the iodine-covered samples. The evaluations of the ratios of ruthenium adsorbed on non-exposed and iodine exposed surfaces are presented in Table 32.

Table 32. *Increase of ruthenium sorption on samples with pre-deposited iodine compared to ruthenium sorption on non-iodine exposed samples[122].*

Sample type	**Aluminum**	**Zinc**	**Copper**	**Paint**
Fold increase in Ru adsorption	30x	38x	3.2x	1.5x

As can be seen from the obtained results, iodine-covered surfaces strongly attract RuO_4 in comparison to the non-iodine exposed samples. The increase of ruthenium adsorption on the copper and paint samples pre-deposited with iodine was not as prominent as on zinc and aluminum. A correlation between increased adsorption of ruthenium and the revaporized fraction of iodine can be seen from the data on aluminum and zinc samples in Tables 31 and 32.

5.2.4. Characterization of the iodine and ruthenium deposits formed on surfaces

5.2.4.1. SEM/EDX

Micrographs obtained from SEM measurements revealed morphology changes on the samples after the deposition of RuO_4 on iodine-covered surfaces. Micrographs of the samples after elemental iodine and after RuO_4 deposition are presented in Figure 21. As can be observed, smooth iodine deposits were formed on the zinc, copper and epoxy paint samples. On the aluminum sample iodine-rich spots were formed due to the hygroscopic nature of AlI_3. Interaction of RuO_4 with iodine deposits led to significant physical changes on the microscopic scale, as can be seen in Figure 21. EDX analysis showed that the iodine quantity was much higher inside the cracks than that of ruthenium. In the areas where the layer was in one piece ruthenium was predominant over iodine on the surface.

a)

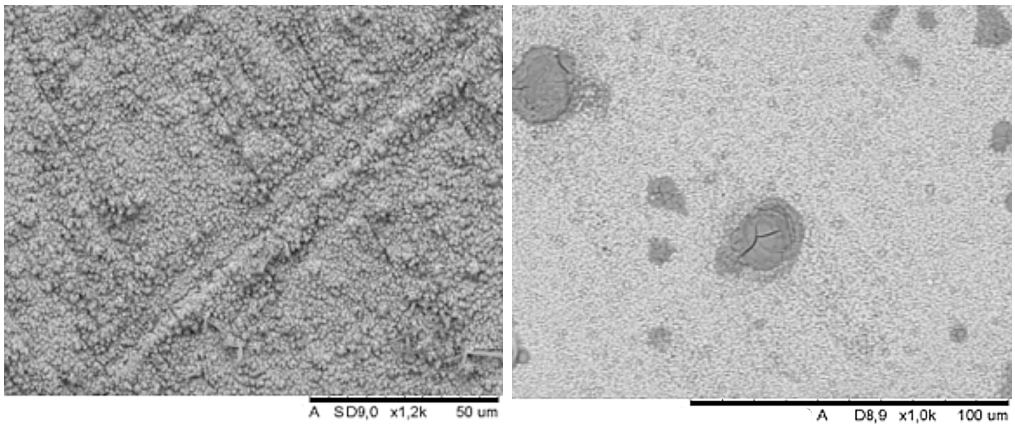
A SD9,0 x1,2k 50 um
A D8,9 x1,0k 100 um

b)

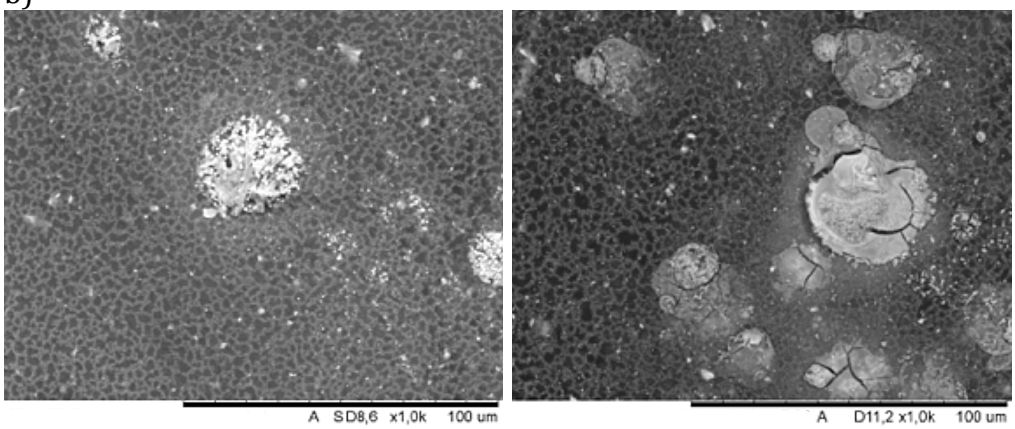
A SD8,6 x1,0k 100 um
A D11,2 x1,0k 100 um

c)

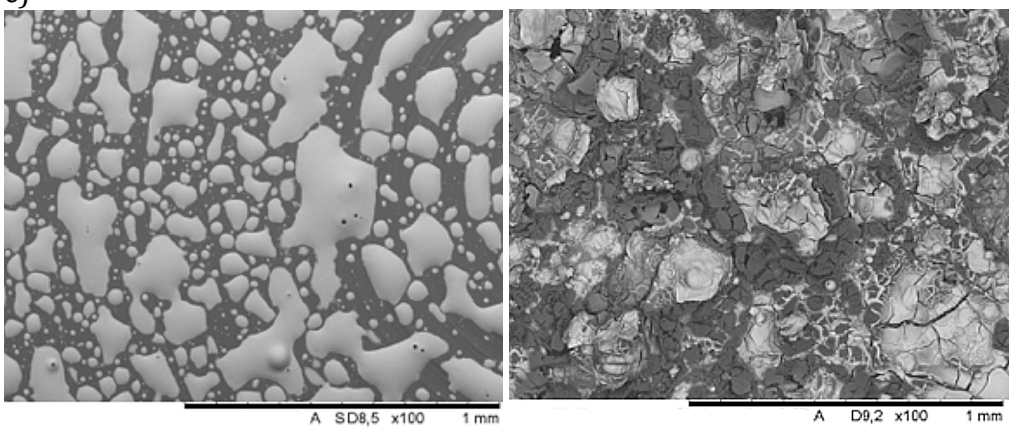
A SD8,5 x100 1 mm
A D9,2 x100 1 mm

d)

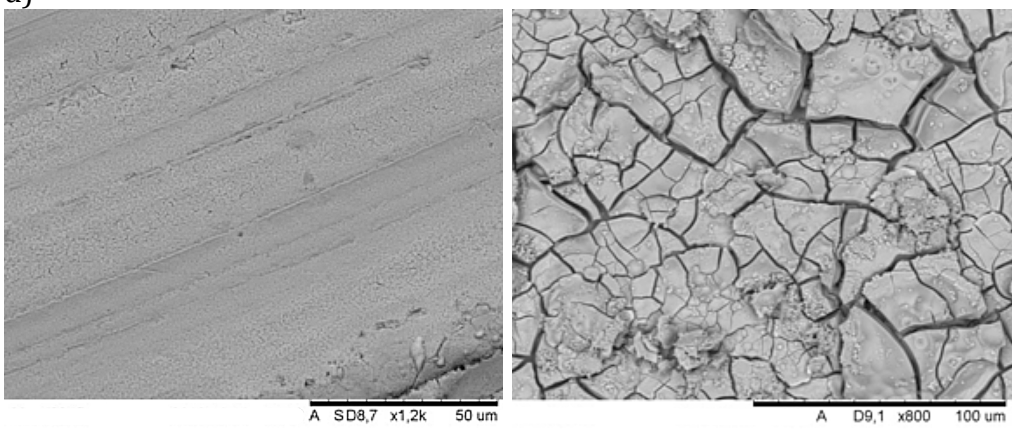

Figure 21. *SEM micrographs of copper(a), paint(b), aluminum(c), and zinc(d) surfaces deposited with I_2 (left side) and afterwards with RuO_4 (right side)[122].*

5.2.4.2. XPS

The chemical speciation of the ruthenium deposits formed on the samples was analyzed by XPS. As a result of the analysis, the binding energies of ruthenium (3d5/2 peak) and iodine (3d5/2 peak) were obtained and are presented in Table 33 (iodine only deposited) and Table 34 (after deposition of RuO_4). The obtained binding energies were then compared with the reference binding energy values, as presented in Table 26.

Table 33. *Binding energies (eV) for I 3d5/2 line on samples analyzed with XPS after the deposition of iodine.*

Sample	**Aluminum**	**Zinc**	**Copper**	**Paint**
Binding energy I 3d5/2 (eV)	619.5±0.1	619.3±0.1	619.7±0.1	618.7±0.1 620.4±0.1
Identified compound	AlI_3	ZnI_2	CuI	I- (organic) I_2

Table 34. *Binding energies (eV) for Ru 3d5/2 and I 3d5/2 lines on samples analyzed with XPS after the deposition of iodine and ruthenium tetroxide.*

Sample	**Aluminum**	**Zinc**	**Copper**	**Paint**
Binding energy I 3d5/2 (eV)	619.0±0.1	619.4±0.1 620.3±0.1	619.5±0.1 623.4±0.1	619.4±0.1 623.4±0.1
Binding energy Ru 3d5/2 (eV)	281.8±0.1	281.9±0.1	281.9±0.1	281.8±0.1
Identified compound	AlI_3 $RuO_2.xH_2O$	ZnI_2, I_2 $RuO_2.xH_2O$	CuI I_2O_5/HIO_3 $RuO_2.xH_2O$	I^-(organic) I_2O_5/HIO_3 $RuO_2.xH_2O$

The binding energies of the I 3d5/3 peak obtained from the measurements after iodine deposition showed a good agreement with iodine in the form of the respective iodides of the metal samples. The iodine speciation on the paint sample revealed two different species of iodine. The peak with an I 3d5/2 binding energy of 618.7 eV was attributed to the iodide form of iodine. The I 3d5/2 peak with a binding energy of 620.4 eV most probably originates from the organic or elemental form of iodine.
After the deposition of RuO_4 on the samples a new speciation of iodine was detected on the zinc, copper and paint samples. The zinc sample showed a new binding energy for a I 3d5/2 peak (620.3 eV) corresponding to the binding energy in elemental iodine that was probably physically adsorbed on the surface. On the copper and paint samples a new I 3d5/2 peak with a binding energy of 624.3 eV was observed, indicating that iodine was in the oxidation state +V, thus corresponding to the I_2O_5. As this oxide is strongly hygroscopic under humid conditions it was probably converted into the form of HIO_3. As binding energies for these two species are very close to each other (623.3 for I_2O_5 and 623.1 for HIO_3) it was impossible to distinguish between these two forms of iodine[157].
The ratio of the areas under the decomposed peaks for iodine species on the epoxy paint for iodine ($+V/I^-$) forms indicated that about 68% of iodide on the paint sample was oxidized into the I_2O_5/HIO_3 form. The copper sample showed the ratio between areas of iodine ($+V/I^-$), corresponding to ca. 40% of iodide oxidation into the form of I_2O_5/HIO_3.
It was shown that the binding energy of the Ru 3d5/2 peak had a similar value in all deposited samples and that this was in good agreement with the value estimated for the reference hydrated RuO_2 powder. Also, there was no difference in the Ru 3d5/2 peak binding energy on the ruthenium deposits from the non-iodine deposited samples and samples previously deposited with iodine. This implies that the iodine deposits had no effect on the chemical speciation of the deposited ruthenium.

5.2.5. Impact of gamma radiation on the ruthenium-deposited samples

5.2.5.1. Gamma radiation induced revaporization of ruthenium on epoxy paint samples in a dry atmosphere

The quantity of revaporized ruthenium from epoxy paint samples irradiated in the dry experimental conditions was actually lower than the uncertainty of measurements under the whole interval of received dose. This can be seen in Figure 22. From these results it was concluded that no revaporization of ruthenium from the deposits was detected. The blank, non-irradiated samples stored in the oven at the same temperature as in the gamma source did not show any decrease of ruthenium content during the experiments.

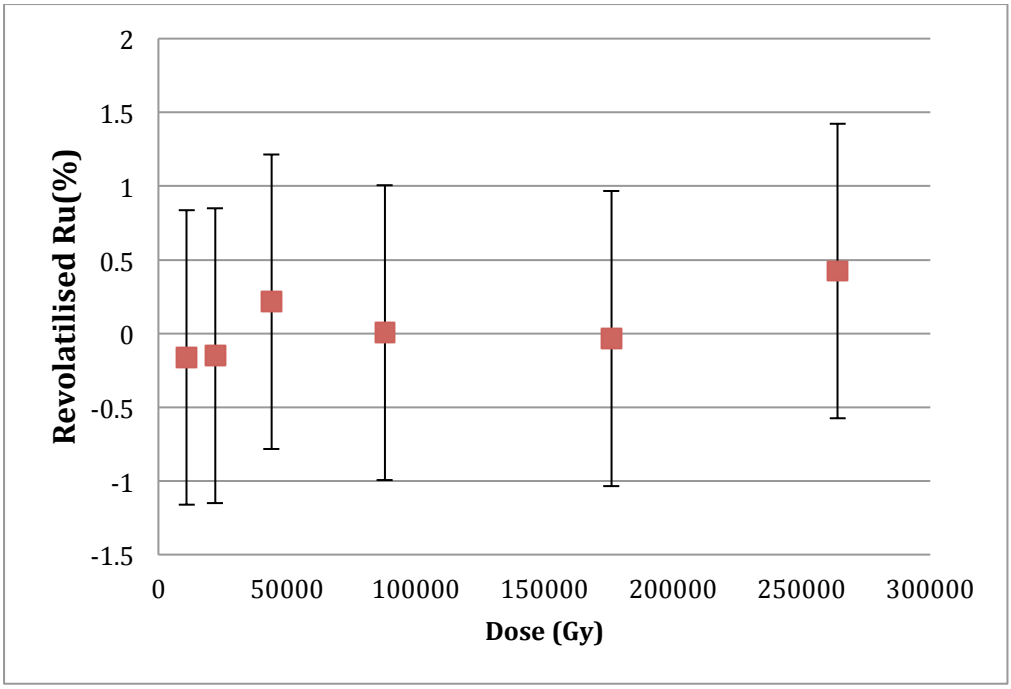

Figure 22. *Revaporized fractions of ruthenium from epoxy paint samples irradiated in a dry atmosphere. The uncertainties originate from triplicates.*

5.2.5.2. Gamma radiation induced revaporization of ruthenium on epoxy paint samples in a humid atmosphere

In the humid atmosphere the revaporized fraction of ruthenium was significantly higher in comparison to the dry atmosphere experiments. The detected revaporized fractions are shown in Figure 23. The points in the lower dose region are not statistically significant, however these were kept in the figure to show the trend in the lower dose interval.

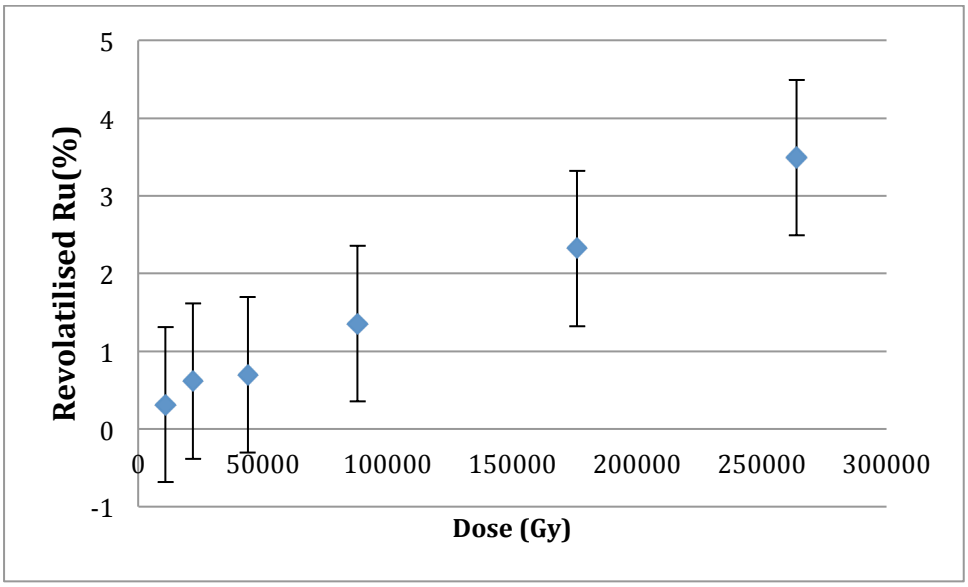

Figure 23. *Revaporized fractions of ruthenium in the humid atmosphere. The uncertainties originate from triplicate experiments.*

A linear increase of the re-vaporized ruthenium fraction was observed over the entire received dose interval used in the experiments.

The difference between the re-vaporized ruthenium fractions in the dry and humid atmospheres can be explained by the formation of different species by the radiolysis of dry and humid air. When compared to the dry air, in the case of humid air the hydrogen peroxide and hydroxyl radical are additionally formed as products of air radiolysis. The proposed reactions of H_2O_2 and $O\cdot$ with RuO_2 that lead to the formation of RuO_4 are presented in equations (36) and (37).

$$RuO_{2(s)}+4OH\cdot \rightarrow RuO_{4(g)}+2H_2O \qquad E_0= 1.29\ V\ (298K) \qquad (36)$$

$$RuO_{2(s)}+2H_2O_2 \rightarrow RuO_{4(g)}+2H_2O \qquad E_0= 3.90E\text{-}1\ V\ (298K) \qquad (37)$$

5.2.5.3. Gamma radiation impact on metals with ruthenium deposits

The irradiation of metal samples with ruthenium deposits had different effects on the samples, as in the case of epoxy paint. A notable corrosion of samples was observed after irradiation. As a result a physical shedding of ruthenium-containing flake particles was observed. This behavior was most prominent in the cases of the zinc and aluminum samples. Photographs of the samples before and after irradiation are presented in Figure 24.

(a)

(b)

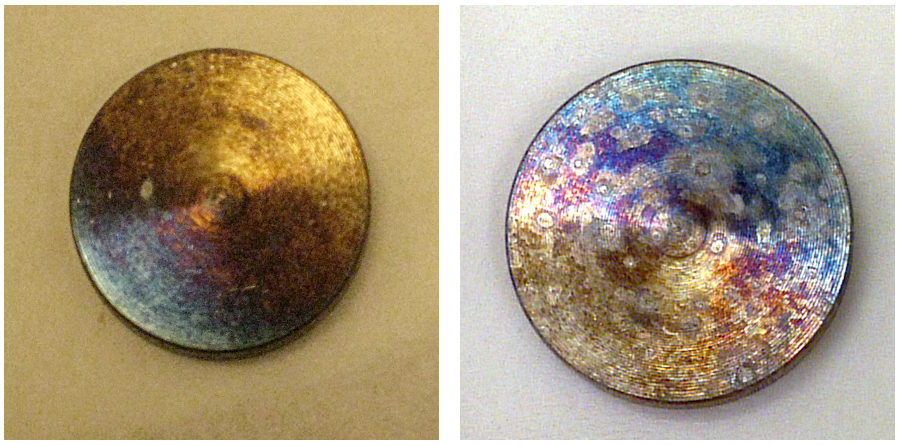

Figure 24. *Zinc (a) and aluminum (b) samples before (left side) and after irradiation (right side).*

The aluminum samples showed a color change of the deposited ruthenium layer after irradiation. However, the chemical speciation (hydrated RuO_2) of ruthenium deposits remained the same as before irradiation. This was proved by examination by XPS.
The amount of ruthenium released from the samples varied between different metals, as can be seen in Table 35.

Table 35. *Loss fractions of ruthenium from metal samples after irradiations with a received dose of 264 kGy*

Sample	**Aluminum**	**Copper**	**Zinc**
Loss fraction (%)	4.7±1.3	3.7 ±1.4	19.0±4.2

The most prominent loss of ruthenium occurred in the case of the zinc sample. However, the physical shedding of the ruthenium from the samples made it impossible to distinguish between the revaporized fraction of ruthenium and the part of the ruthenium that physically fell off from the samples. The explanation is that the oxidative species formed by the air radiolysis induced the corrosion of substrate metals with deposited ruthenium.

6. Summary and conclusions

The work presented in this thesis consists of two parts; the first deals with the transport of ruthenium through a primary circuit of NPP and the second with the containment chemistry of ruthenium in the case of severe nuclear accident.
In the first part it was shown that the air-radiolysis products (NO_2, N_2O, HNO_3) and aerosols (CsI) formed during a severe nuclear accident have a significant effect on the transport of ruthenium through the primary circuit of NPP. These effects were determined at different temperatures (1300 K, 1500 K, and 1700 K). It was shown that even the very low concentrations (50-5 ppmV) of air radiolysis products in a gas stream will affect the chemical composition of transported ruthenium and can decrease or increase the gaseous and aerosol fractions thereof. Additionally, these precursors will affect the absolute amount of transported ruthenium through the primary circuit of the power plant. By means of neutron activation analysis of collected ruthenium samples, these amounts could be quantified. The chemical compositions of the collected aerosol fractions were identified by means of SEM/EDX, XPS and XRD techniques.
Additionally it was shown that there was a strong effect of temperature and air flow (2.5 l/min, 5 l/min) on both the release rates of ruthenium and also the amount and chemical composition of ruthenium transported through the primary circuit of a NPP. It was also shown that the transport of ruthenium does not correspond to the thermodynamic equilibrium calculations, and therefore chemical kinetics will play an important role during a severe nuclear accident.
In the second part of the work the containment chemistry of ruthenium tetroxide was investigated. This part of the work was divided into the three subprojects.
The first subproject focused on the interaction of RuO_4 with the different surface materials (Al, Zn, Cu, epoxy paint) in the containment of a NPP. It was shown that RuO_4 readily reacts with the materials, resulting in the formation of ruthenium-rich deposits. The chemical nature of these deposits was investigated by means of SEM/EDX, XPS and EXAFS techniques. The chemical compositions were proven to be different on the surface ($Ru^{(IV)}O_{(2-y)}OH_y$) and in the whole thickness of deposits ($RuO_2.xH_2O$) in all the materials used in the experiments. Additionally, the distribution ratios of ruthenium between different metals in humid and dry conditions were determined with the use of ^{103}Ru radiotracer and consequent gamma spectrometry measurements. These measurements revealed a high affinity of RuO_4 towards the aluminum surfaces.
The second subproject was focused on the interaction of RuO_4 with the surface materials previously covered by elemental iodine. In this part of the work chemical compositions of both iodine and ruthenium deposits formed on the materials were examined with SEM/EDX and XPS. It was observed that materials for the deposition affected the speciation of the iodine deposits, whereas in the case of ruthenium the chemical speciation remained the same as in the case of non-iodine deposited surfaces. The effect of RuO_4 on the chemical speciation of iodine deposits was shown, together with the ability of RuO_4 to re-vaporize iodine from the deposits in the cases of zinc and aluminum. In the cases of copper and epoxy paint no revaporization of iodine was detected.
The third subproject was performed with the aim of determining the effect of gamma radiation on the ruthenium-deposited materials. It was shown that humidity in the air had a notable effect on the vaporized fractions of ruthenium from the epoxy paint samples and the revaporized fraction increased linearly with the received dose. No revaporization of ruthenium was detected in the dry

air atmosphere. In the cases of the metal samples, strong radiation-induced corrosion was observed, causing a physical flaking off of the ruthenium particles from the samples.

It can be concluded that the chemistry of ruthenium during a severe nuclear accident will be strongly affected by the conditions in both the primary circuit and the containment of a NPP. Other fission products released during an accident, as well as radiolysis products, will have an influence on the behavior of ruthenium during an accident sequence and cannot be neglected in the severe nuclear accident modeling and predictions.

7. Future work

There are several areas that would be interesting to study as a continuation of this work. The first of these is the interaction of ruthenium oxides with air radiolysis products in a more complex matrix. The mixture of the radiolysis-produced gasses at the expected concentrations in an accident can be used to study the impact on the ruthenium transport. Other research topics would be a more focused study on the interaction of ruthenium with iodine compounds at high temperatures to find out if there is a specific interaction between these elements that leads to the formation of ruthenium oxyhalides that could be volatile at the temperatures expected in the containment. Regarding the containment chemistry, the interaction of ruthenium tetroxide with some other iodine compounds, i.e. higher iodine oxides or organic iodides, would be of interest due to the possible contribution to the volatile source term within the containment.

8. Acknowledgements

I would like to thank:

My supervisor Christian Ekberg for the help during my studies, personal support and endless discussions about the Thermodynamics, science that is wrong already in its own name.

Henrik Glänneskog, Joachim Thorn and Mark Foreman my co-supervisors for the helpful meeting and bringing new ideas into my project.

Henrik Ramebäck for the introduction into the gamma spectroscopy as well for the help with uncertainty calculations.

Teemu Kärkelä and Ari Auvinen for the cooperation on the ruthenium transport experiments and showing me the bright side of Finland.

Eric Tam for the help with XPS measurements any time it was needed.

All the people at IMR and NC department for making this group such a good place to work in.

I am thankful to my family and friends, you mean more to me than I ever expressed.

My special thanks goes to Mira for surviving these 5 years with me, which was probably much harder than my studies.

The last but not least Goško is acknowledged for helping me to get this opportunity of making my PhD studies.

Part of this research was carried out at beamline I811, MAX-lab synchrotron radiation source, Lund University, Sweden. Funding for the beamline I811 project was kindly provided by The Swedish Research Council and the “Knut och Alice Wallenbergs Stiftelse”.

NKS (Nordic nuclear safety research) is acknowledged for the partial funding of the ruthenium transfer experiments.

APRI-8 and APRI-9 (Accident Phenomena of Risk Importance) are acknowledged for the funding of this project.

9. Bibliography

1. America's Climate Choices: Panel on Informing Effective, D. and C. Actions Related to Climate, *Informing an Effective Response to Climate Change*. 2010, Washington, DC, USA: National Academies Press.
2. International Energy Agency. *Electricity*. 2016 [cited 2016 21.3.2016]; Available from: http://www.iea.org/topics/electricity/.
3. Qvist, S.A. and B.W. Brook, *Environmental and health impacts of a policy to phase out nuclear power in Sweden.* Energy Policy, 2015. **84**: p. 1-10.
4. World Nuclear Association. *Nuclear Power in the World Today*. 2016; Available from: http://www.world-nuclear.org/information-library/current-and-future-generation/nuclear-power-in-the-world-today.aspx.
5. IAEA, *Nuclear Power Reactors in the World*, in *Reference Data Series No.2*. 2015. p. 79
6. World Nuclear Association. *Nuclear Power in Sweden*. March 2016; Available from: http://www.world-nuclear.org/information-library/country-profiles/countries-o-s/sweden.aspx.
7. Clément, B. and R. Zeyen, *The objectives of the Phébus FP experimental programme and main findings.* Annals of Nuclear Energy, 2013. **61**: p. 4-10.
8. Haste, T., Payot, F., Manenc, C., Clément, B., March, Ph., Simondi-Teisseire, B., Zeyen, R.,, *Phébus FPT3: Overview of main results concerning the behaviour of fission products and structural materials in the containment.* Nuclear Engineering and Design, 2013. **261**: p. 333-345.
9. March, P., Simondi-Teisseire, B.,, *Overview of the facility and experiments performed in Phébus FP.* Annals of Nuclear Energy, 2013. **61**: p. 11-22.
10. Pontillon, Y., Ducros, G.,, *Behaviour of fission products under severe PWR accident conditions: The VERCORS experimental programme—Part 2: Release and transport of fission gases and volatile fission products.* Nuclear Engineering and Design, 2010. **240**(7): p. 1853-1866.
11. Pontillon, Y., Ducros, G.,, *Behaviour of fission products under severe PWR accident conditions. The VERCORS experimental programme—Part 3: Release of low-volatile fission products and actinides.* Nuclear Engineering and Design, 2010. **240**(7): p. 1867-1881.
12. Pontillon, Y., Ducros, G., Malgouyres, P. P.,, *Behaviour of fission products under severe PWR accident conditions VERCORS experimental programme—Part 1: General description of the programme.* Nuclear Engineering and Design, 2010. **240**(7): p. 1843-1852.
13. IAEA, *IAEA Safety Glossary*. 2007
14. Atomic Energy Society of Japan, *The Fukushima Daiichi Nuclear Accident*. 2015, DE: Springer Verlag.
15. Beresford, N.A., Smith, J.,, *Chernobyl: Catastrophe, Consequences and Solutions*. 2005: Springer Berlin Heidelberg.
16. Autorité de Sûreté Nucléaire, *Scales for rating nuclear incidents and accidents and radiation protection events*, in *Annual report 2007*. 2007
17. Petrangeli, G., *Chapter 5 - Severe accidents*, in *Nuclear Safety*. 2006, Butterworth-Heinemann: Oxford. p. 53-64.
18. Tanaka, S.-i., *Accident at the Fukushima Dai-ichi Nuclear Power Stations of TEPCO -Outline & lessons learned.* Proceedings of the Japan Academy, Series B, 2012. **88**(9): p. 471-484.

19. *Nuclear Fuel Behaviour Under Reactivity-initiated Accident (RIA) Conditions*. 2010, Nuclear Energy Agency.NEA/CSNI/R (2010)1,
20. Kortov, V. and Y. Ustyantsev, *Chernobyl accident: Causes, consequences and problems of radiation measurements.* Radiation Measurements, 2013. **55**: p. 12-16.
21. Choppin, G.R., J.O. Liljenzin, J. Rydberg, and C. Ekberg, *Radiochemistry and nuclear chemistry*. Vol. 4;4;. 2013, Killington, Oxford: Academic Press.
22. Nordlund, A., *Introduction to Nuclear Reactors*. 2012, Göteborg: Chalmers Tekniska Högskola.
23. Japan Atomic Energy Agency, *Graph of Fission Product Yields*, J.A.E. Agency, Editor. 2013, Japan Atomic Energy Agency: Tokai-mura, Naka-gun, Ibaraki-ken, 319-1195, Japan
24. Konings, R.J.M., T. Wiss, and O. Benes, *Predicting material release during a nuclear reactor accident.* Nat Mater, 2015. **14**(3): p. 247-252.
25. Sehgal, B.R., *Chapter 1 - Light Water Reactor Safety: A Historical Review*, in *Nuclear Safety in Light Water Reactors*. 2012, Academic Press: Boston. p. 1-88.
26. Soffer, L., Burson, S. B. , Ferrell, C. M. , Lee, R. Y. , Ridgely, J. N. , *Accident Source Terms for Light-Water Nuclear Power Plants*. 1995, U.S. Nuclear Regulatory Commission: Washington, DC.NUREG-1465,
27. Nourbakhsh, H.P., *Estimate of radionuclide release characteristics into containment under severe accident conditions. Final report*, in *Other Information: PBD: Nov 1993*. 1993. p. Medium: ED; Size: 138 p.NUREG/CR--5747; ,
28. *Chapter 5 - Fission Product Release and Transport*, in *Nuclear Safety in Light Water Reactors*, B.R. Sehgal, Editor. 2012, Academic Press: Boston. p. 425-517.
29. Hastings, I.J., C.E.L. Hunt, and J.J. Lipsett, *Release of short-lived fission products from UO2 fuel: Effects of operating conditions.* Journal of Nuclear Materials, 1985. **130**: p. 407-417.
30. Kleykamp, H., *The chemical state of the fission products in oxide fuels.* Journal of Nuclear Materials, 1985. **131**(2): p. 221-246.
31. Ducros, G., Y. Pontillon, and P.P. Malgouyres, *Synthesis of the VERCORS experimental programme: Separate-effect experiments on Fission Product release, in support of the PHEBUS-FP programme.* Annals of Nuclear Energy, 2013. **61**: p. 75-87.
32. Grégoire, A.C. and T. Haste, *Material release from the bundle in Phébus FP.* Annals of Nuclear Energy, 2013. **61**: p. 63-74.
33. Matus, L., Hozer, Z., Toth, B., Ver, N., Kunstar, M., Pinter, A., Osan, J.,, *Oxidation and Release of Ruthenium from White Inclusions*, in *EUR - Scientific and Technical Research Reports*. 2007, European Commission Joint Research Centre
34. Auvinen, A., Davidovich, N., Ducros, G., Dutheillet, Y., Kissane, M.P.,, *On-going Investigation of Ruthenium Release and Transport*, in *The first European Review Meeting on Severe Accident Research (ERMSAR-2005)*. 2005: Aix-en Provence, France
35. Geiger, E., R. Bès, P. Martin, Y. Pontillon, G. Ducros, and P.L. Solari, *Insights on fission products behaviour in nuclear severe accident conditions by X-ray absorption spectroscopy.* Journal of Nuclear Materials, 2016. **471**: p. 25-33.

36. Mariani, R.D., D.L. Porter, T.P. O'Holleran, S.L. Hayes, and J.R. Kennedy, *Lanthanides in metallic nuclear fuels: Their behavior and methods for their control.* Journal of Nuclear Materials, 2011. **419**(1–3): p. 263-271.
37. Hunt, C.E.L., D.S. Cox, and F.C. Iglesias, *Fission-product release during accidents — an accident management perspective.* Nuclear Engineering and Design, 1994. **148**(2): p. 205-216.
38. Cox, D.S., C.E.L. Hunt, R.F. O'Connor, R.D. Barrand, and F.C. Iglesias, *High-temperature oxidation behaviour of UO2 in air and steam A2 - Embury, J.D*, in *High-Temperature Oxidation and Sulphidation Processes*. 1990, Pergamon: Oxford. p. 198-211.
39. Ronneau, C., J. Cara, and A. Rimski-Korsakov, *Oxidation-enhanced emission of ruthenium from nuclear fuel.* Journal of Environmental Radioactivity, 1995. **26**(1): p. 63-70.
40. Barrand, R.D., R.S. Dickson, Z. Liu, and D.D. Semeniuk, *Release of fission products from CANDU fuel in air, steam and argon atmospheres at 1500-1900 deg C: the HCE3 experiment*. 1999, Canada: Canadian Nuclear Society.
41. Miwa, S., S. Yamashita, A. Ishimi, M. Osaka, M. Amaya, K. Tanaka, and F. Nagase, *Research Program for the Evaluation of Fission Product and Actinide Release Behaviour, Focusing on their Chemical Forms.* Energy Procedia, 2015. **71**: p. 168-181.
42. Bream, R.A., Osborne, M.F., , *A Summary of ORNL Fission Product Release Tests With Recommanded Release Rates and Diffusion Coefficients*. 1995, Oak Ridge Laboratory.ORNL/TM 12801, NUREG/CR 6261,
43. Magill, J., Pfennig, G., Galy J. „ *Karlsruher Nuklidkarte 7th edition*. 2006: OPOCE.
44. Eichholz, G.G., *Hazards and control of ruthenium in the nuclear fuel cycle.* Progress in Nuclear Energy, 1978. **2**(1): p. 29-76.
45. Liljenzin, J.O., *Some estimates of the total nuclide inventory in the year 2100 from Swedish nuclear power production*. 1990, Chalmers University of Technology: Göteborg, Sweden
46. A. Auvinen, N.D., G. Ducros, Y. Dutheillet, M. Kissane, L. Matus, A. Rizoiu. *On-going Investigation of Ruthenium Release and Transport*. in *ERMSAR 2005*. 2005. Aix en Provence, France.
47. Johnson, I., C.E. Johnson, C.E. Crouthamel, and C.A. Seils, *Oxygen potential of irradiated urania-plutonia fuel pins.* Journal of Nuclear Materials, 1973. **48**(1): p. 21-34.
48. Sato, I., H. Furuya, K. Idemitsu, T. Arima, K. Yamamoto, and M. Kajitani, *Distribution of molybdenum in FBR fuel irradiated to high burnup.* Journal of Nuclear Materials, 1997. **247**: p. 46-49.
49. Kleykamp, H., *Post-irradiation examinations and composition of the residues from nitric acid dissolution experiments of high-burnup lwr fuel.* Journal of Nuclear Materials, 1990. **171**(2): p. 181-188.
50. Lewis, B.J., R. Dickson, F.C. Iglesias, G. Ducros, and T. Kudo, *Overview of experimental programs on core melt progression and fission product release behaviour.* Journal of Nuclear Materials, 2008. **380**(1–3): p. 126-143.
51. Iglesias, F.C., B.J. Lewis, P.J. Reid, and P. Elder, *Fission product release mechanisms during reactor accident conditions.* Journal of Nuclear Materials, 1999. **270**(1–2): p. 21-38.
52. Jean-Pierre, L., Bernard, A., Ducros, G., Le Marois G., Lhiaubet, G.,, *The HEVA Experimental Program.* Nuclear Technology, 1994. **108**(1): p. 33-34.

53. Powers, D.A., L.N. Kmetyk, and R.C. Schmidt, *A review of the technical issues of air ingression during severe reactor accidents*. 1994, Nuclear Regulatory Commission, Washington, DC (United States). Div. of Systems Research; Sandia National Labs., Albuquerque, NM (United States). p. Medium: X; Size: 81 p.NUREG/CR--6218; SAND--94-0731,
54. Haste, T., F. Payot, and P.D.W. Bottomley, *Transport and deposition in the Phébus FP circuit.* Annals of Nuclear Energy, 2013. **61**: p. 102-121.
55. Ducros, G., P.P. Malgouyres, M. Kissane, D. Boulaud, and M. Durin, *Fission product release under severe accidental conditions: general presentation of the program and synthesis of VERCORS 1–6 results.* Nuclear Engineering and Design, 2001. **208**(2): p. 191-203.
56. Ducros G., P.Y., Malgouyres P., Taylor P., Dutheillet Y. *Ruthenium release at high temperature from irradiated PWR fuel in various oxidising conditions; main findings from the VERCORS program*. in *Conference on Nuclear Energy in New Europe 2005, SARNET-ST-P40*. 2005. Bled, Slovenia.
57. Auvinen, A., G. Brillant, N. Davidovich, R. Dickson, G. Ducros, Y. Dutheillet, P. Giordano, M. Kunstar, T. Kärkelä, M. Mladin, Y. Pontillon, C. Séropian, and N. Vér, *Progress on ruthenium release and transport under air ingress conditions.* Nuclear Engineering and Design, 2008. **238**(12): p. 3418-3428.
58. Nagy, I., Hozer, Z., Matus, L., Pinter, A., Windberg, P., Ver, N., Kunstar, M., Alfoeldy, B., Mueller, K.,, *Oxidation and Release of Ruthenium from Short Fuel Rods above 1500oC*. 2005, European Comission.JRC32373,
59. Vér, N., L. Matus, M. Kunstár, J. Osán, Z. Hózer, and A. Pintér, *Influence of fission products on ruthenium oxidation and transport in air ingress nuclear accidents.* Journal of Nuclear Materials, 2010. **396**(2–3): p. 208-217.
60. Schäfer, H., A. Tebben, and W. Gerhardt, *Zur Chemie der Platinmetalle. V Gleichgewichte mit Ru(f)5 RuO2(f)5 RuO3(g) und RuO4(g).* Zeitschrift für anorganische und allgemeine Chemie, 1963. **321**(1-2): p. 41-55.
61. Giordano, P., A. Auvinen, G. Brillant, J. Colombani, N. Davidovich, R. Dickson, T. Haste, T. Kärkelä, J.S. Lamy, C. Mun, D. Ohai, Y. Pontillon, M. Steinbrück, and N. Vér, *Recent advances in understanding ruthenium behaviour under air-ingress conditions during a PWR severe accident.* Progress in Nuclear Energy, 2010. **52**(1): p. 109-119.
62. Eichler, B., F. Zude, W. Fan, N. Trautmann, and G. Herrmann, *Volatilization and Deposition of Ruthenium Oxides in a Temperature Gradient Tube.* Radiochimica Acta, 1992. **56**(3): p. 133-140.
63. Kärkelä, T., Backman, U., Auvinen, A., Zilliacus, R., Lipponen, M., Kekki, T., Tapper U., Jokiniemi, J., , *Experiments on the behaviour of ruthenium in air ingress accidents - Final report*. 2007, VTT research report - VTT-R-01252-07
64. Backman, U., M. Lipponen, A. Auvinen, U. Tapper, R. Zilliacus, and J.K. Jokiniemi, *On the transport and speciation of ruthenium in high temperature oxidising conditions.* Radiochimica Acta, 2005. **93**(5): p. 297-304.
65. Kärkelä, T., N. Vér, T. Haste, N. Davidovich, J. Pyykönen, and L. Cantrel, *Transport of ruthenium in primary circuit conditions during a severe NPP accident.* Annals of Nuclear Energy, 2014. **74**: p. 173-183.
66. Kärkelä, T., Pyykönen, J., Auvinen, A., Jokiniemi, J., *Analysis of Flow Fields, Temperatures and Ruthenium Transport in the Test Facility*. 2008, VTT

Technical Research Centre of Finland: Espoo, Finland.VTT-R-00947-08, NKS-161,
67. Holm, J., Glänneskog, H., Ekberg, Ch.,, *Deposition of RuO4 on various surfaces in a nuclear reactor containment.* Journal of Nuclear Materials, 2009. **392**: p. 55-62.
68. Mun, C., L. Cantrel, and C. Madic, *Study of RuO4 decomposition in dry and moist air.* Radiochimica Acta, 2007. **95**(11): p. 643-656.
69. Mun, C., L. Cantrel, and C. Madic, *Radiolytic Oxidation of Ruthenium Oxide Deposits.* Nuclear Technology, 2008. **164**(2): p. 245-254.
70. Mun, C., L. Cantrel, and C. Madic, *Oxidation of ruthenium oxide deposits by ozone.* Radiochimica Acta, 2008. **96**(6): p. 375-384.
71. Mun, C., J. Ehrhardt, J. Lambert, and C. Madic, *XPS investigations of ruthenium deposited onto representative inner surfaces of nuclear reactor containment buildings.* Applied Surface Science, 2007. **253**(18): p. 7613-7621.
72. Holm, J., *Investigation of the behaviour of gaseous I2 and RuO4 in different atmospheres*, in *Nuclear Chemistry*. 2009, Chalmers university of technology
73. Mun, C., L. Cantrel, and C. Madic, *Review of literature on ruthenium behavior in nuclear power plant severe accidents.* Nuclear Technology, 2006. **156**(3): p. 332-346.
74. Igarashi, H., K. Kato, and T. Takahashi, *Absorption Behaviour of Gaseous Ruthenium into Water*, in *Radiochimca Acta*. 1992. p. 51.21933405, 10.1524/ract.1992.57.1.51
75. Könönen, N., Rossi, J., Penttilä K.,, *The formation of nitric acid inside a BWR containment after severe accident*. 2012, VTT Technical Research Centre of Finland.VTT-R-01408-12,
76. Busuoli, G., *Radiological Consequences of the Chernobyl Accident for Italy.* Radiation Protection Dosimetry, 1987. **19**(4): p. 247-251.
77. Fry, F.A., R.H. Clarke, and M.C. O'Riordan, *Early estimates of UK radiation doses from the Chernobyl reactor.* Nature, 1986. **321**(6067): p. 193-195.
78. Denschlag H, O., A. Diel, K.H. GlÄSel, R. Heimann, N. Kaffrell, U. Knitz, H. Menke, N. Trautmann, M. Weber, and G. Herrmann, *Fallout in the Mainz Area from the Chernobyl Reactor Accident*, in *Radiochimica Acta*. 1987. p. 163.21933405, 10.1524/ract.1987.41.4.163
79. Shershakov, V.M., S.M. Vakulovski, R.V. Borodin, O.L. Vozzhennikov, G. Ya.l, V.S. Kosykh, K.P. Makhonko, V.B. Chumiciev, A.T. Korsakov, V.P. Martynenko, and A. Godko, *Analysis and prognosis of radiation exposure following the accident at the Siberian chemical combine Tomsk-7.* Radiation Protection Dosimetry, 1995. **59**(2): p. 93-126.
80. Toivonen, H., R. Pollanen, A. Leppanen, S. Klemola, J. Lahtinen, K. Servomaa, A.L. Savolainen, and I. Valkama, *A nuclear incident at a power plant in Sosnovyy Bor, Russia.* Health Physics, 1992. **63**(5): p. 571-573.
81. Schwantes, J.M., Orton, C.R., Clark, R.A.,, *Analysis of a Nuclear Accident: Fission and Activation Product Releases from the Fukushima Daiichi Nuclear Facility as Remote Indicators of Source Identification, Extent of Release and State of Damaged Spent Nuclear Fuel*. 2012, Pacific Northwest National Laboratory: Richland, Washington, USA.PNNL-20912,
82. Walther, C. and D.K. Gupta, *Radionuclides in the Environment - Influence of chemical speciation and plant uptake on radionuclide migration*. 2015, Switzerland: Springer International Publishing Switzerland.

83. *25 - Iron, Ruthenium and Osmium A2 - GREENWOOD, N.N*, in *Chemistry of the Elements (Second Edition)*, A. Earnshaw, Editor. 1997, Butterworth-Heinemann: Oxford. p. 1070-1112.
84. Cotton, F.A., Wilkinson, G.,, *Advanced inorganic chemistry*. 4th edition ed. 1980: Wiley.
85. Lewis, S., Richard J. and N.I. Sax, *Sax's dangerous properties of industrial materials: Vol. 2 : [General chemicals: A-G]*. 2000, New York: Wiley.
86. *Strålsäkerhetsmyndighetens föreskrifter om laboratorieverksamhet med radioaktiva ämnen i form av öppna strålkällor*, in *Strålsäkerhetsmyndighetens författningssamling*, J. Strandman, Editor. 2008, Strål Säkerhets Myndigheten.SSMFS 2008:28,
87. Sandalls, F.J., M.G. Segal, and N. Victorova, *Hot particles from Chernobyl: A review.* Journal of Environmental Radioactivity, 1993. **18**(1): p. 5-22.
88. Kashparov, V.A., Y.A. Ivanov, S.I. Zvarisch, V.P. Protsak, Y.V. Khomutinin, A.D. Kurepin, and E.M. Pazukhin, *Formation of hot particles during the Chernobyl nuclear power plant accident.* Nuclear Technology, 1996. **114**(2): p. 246-253.
89. Pöllänen, R., I. Valkama, and H. Toivonen, *Transport of radioactive particles from the chernobyl accident.* Atmospheric Environment, 1997. **31**(21): p. 3575-3590.
90. Pöllänen, P., *Highly Radioactive Ruthenium Particles Released from the Chernobyl Accident: Particle Characteristics and Radiological Hazard.* Radiation Protection Dosimetry, 1997. **71**(1): p. 23-32.
91. *12 - Low Oxidation States*, in *Topics in Inorganic and General Chemistry*, A.S. Elaine and R.S. Kenneth, Editors. 1984, Pergamon. p. 975-976.
92. Miradji, F., S. Souvi, L. Cantrel, F. Louis, and V. Vallet, *Thermodynamic Properties of Gaseous Ruthenium Species.* The Journal of Physical Chemistry A, 2015. **119**(20): p. 4961-4971.
93. Miradji, F., F. Virot, S. Souvi, L. Cantrel, F. Louis, and V. Vallet, *Thermochemistry of Ruthenium Oxyhydroxide Species and Their Impact on Volatile Speciations in Severe Nuclear Accident Conditions.* The Journal of Physical Chemistry A, 2016. **120**(4): p. 606-614.
94. Di Lemma, F.G., J.Y. Colle, O. Beneš, and R.J.M. Konings, *A separate effect study of the influence of metallic fission products on CsI radioactive release from nuclear fuel.* Journal of Nuclear Materials, 2015. **465**: p. 499-508.
95. Garisto, F., *Thermodynamic behaviour of ruthenium at high temperatures*. 1988, Atomic Energy of Canada limited, Whiteshell Nuclear Research Establishment: Pinawa, Manitoba.AECL-9552,
96. Ortner, M.H., *INFRARED SPECTRUM AND THERMODYNAMIC PROPERTIES OF RUTHENIUM TETROXIDE.* Journal Name: Journal of Chemical Physics (U.S.); Journal Volume: Vol: 34; Other Information: Orig. Receipt Date: 31-DEC-61, 1961: p. Medium: X; Size: Pages: 556-8.
97. Rard, J.A., *Chemistry and thermodynamics of ruthenium and some of its inorganic compounds and aqueous species.* Chemical Reviews, 1985. **85**(1): p. 1-39.
98. Norman, J.H., H.G. Staley, and W.E. Bell, *Mass Spectrometric Study of the Noble Metal Oxides*, in *Mass Spectrometry in Inorganic Chemistry*. 1968, AMERICAN CHEMICAL SOCIETY. p. 101-114.
99. Bale, C., P. Chartrand, S.A. Degterov, G. Eriksson, K. Hack, R. Ben Mahfoud, J. Melancon, A.D. Pelton, and S. Petersen, *FactSage thermochemical*

software and databases. Calphad-Computer Coupling of Phase Diagrams and Thermochemistry, 2002. **26**(2): p. 189-228.
100. Bell, W.E. and M. Tagami, *HIGH-TEMPERATURE CHEMISTRY OF THE RUTHENIUM—OXYGEN SYSTEM1.* The Journal of Physical Chemistry, 1963. **67**(11): p. 2432-2436.
101. Hertel, E., *Crystal structures, von Ralph W. G. Wyckoff. Interscience Publishers, Inc., New York, 1951. Vol. II. 253 S., 74 Abb., $ 10.\'96*.
102. Cotton, F.A. and J.T. Mague, *The Crystal and Molecular Structure of Tetragonal Ruthenium Dioxide.* Inorganic Chemistry, 1966. **5**(2): p. 317-318.
103. Backman, U., Lipponen, M., Auvinen, A., Jokiniemi, J., Zilliacus, R.,, *Ruthenium Behaviour in Severe Nuclear Accident Conditions - Final Report*, in *VTT research report PRO3/P27/04*. 2004.VTT research report PRO3/P27/04,
104. Schäfer, H., G. Schneidereit, and W. Gerhardt, *Zur Chemie der Platinmetalle. RuO2 Chemischer Transport, Eigenschaften, thermischer Zerfall.* Zeitschrift für anorganische und allgemeine Chemie, 1963. **319**(5-6): p. 327-336.
105. Kim, K.S. and N. Winograd, *X-Ray Photoelectron Spectroscopic Studies of Ruthenium-Oxygen Surfaces.* Journal of Catalysis, 1974. **35**(1): p. 66-72.
106. Zimmerman, G.L., S.J. Riviello, T.A. Glauser, and J.G. Kay, *Photochemical decomposition of ruthenium tetroxide.* The Journal of Physical Chemistry, 1990. **94**(6): p. 2399-2404.
107. Koda, Y., *Boiling points and ideal solutions of ruthenium and osmium tetraoxides.* Journal of the Chemical Society, Chemical Communications, 1986(17): p. 1347-1348.
108. *3 - Ruthenium(VIII)*, in *Topics in Inorganic and General Chemistry*, A.S. Elaine and R.S. Kenneth, Editors. 1984, Pergamon. p. 43-55.
109. Runkle, G.E. and M.B. Snipes, *System for Nose-Only Inhalation Exposures of Small Animals to (Ruo4)-Ru-106.* Journal of Aerosol Science, 1979. **10**(5): p. 431-435.
110. Remy, H., *Aus der Chemie des Ruthens.* Angewandte Chemie, 1926. **39**(36): p. 1061-1065.
111. Weigel, F., *Chemistry in Nuclear Technology. Von S. Peterson und R. G. Wymer. Addison-Wesley Series in Nuclear Science and Engineering. Herausgeg. v. H. Goldstein. Pergamon Press, Oxford-London-Paris-Frankfurt 1963. 1. Aufl., X, 374 S., zahlr. Abb. u. Tab., geb. £ 4.14.0d.* Angewandte Chemie, 1964. **76**(16): p. 727-727.
112. Connick, R.E. and C.R. Hurley, *Chemistry of Ru(VI), -(VII) and -(VIII). Reactions, Oxidation Potentials and Spectra.* Journal of the American Chemical Society, 1952. **74**(20): p. 5012-5015.
113. Parkhurst, D.L.a., *Description of input and examples for PHREEQC version 3--a computer program for speciation, batch-reaction, one-dimensional transport, and inverse geochemical calculations*. 2013: Reston, Virginia : U.S. Department of the Interior, U.S. Geological Survey, 2013.
114. Tietze, S., *Formation, partitioning and interactions of organic iodides under severe nuclear accident conditions*. 2012, Chalmers University of Technology
115. Holm, J., H. Glänneskog, and C. Ekberg, *Deposition of RuO4 on various surfaces in a nuclear reactor containment.* Journal of Nuclear Materials, 2009. **392**(1): p. 55-62.
116. Glänneskog, H., *Personal Communications*. 2016: Göteborg, Sweden

117. Glänneskog, H., *Interactions of I2 and CH3I with reactive metals under BWR severe-accident conditions.* Nuclear Engineering and Design, 2004. **227**(3): p. 323-329.
118. Sakurai, T., A. Takahashi, and G. Fujisawa, *Interaction of Ruthenium Tetroxide with Stainless-Steel.* Journal of Nuclear Science and Technology, 1983. **20**(1): p. 81-83.
119. Ortins de Bettencourt, A. and A. Jouan, *VOLATILITY OF RUTHENIUM DURING VITRIFICATION OPERATIONS ON FISSION PRODUCTS. PART II. FIXATION ON A STEEL TUBE. DECOMPOSITION OF THE PEROXIDE*, in *Other Information: UNCL. Orig. Receipt Date: 31-DEC-69*. 1969. p. Medium: X; Size: Pages: 54.CEA-R--3663(2) FranceTue Feb 05 23:21:41 EST 2008Dep.DTIE; NSA-23-024140French,
120. D.A. Powers, M.T.L., R.O. Gauntt, R.Y. Lee, M. Salay, *Accident source terms for light-water nuclear power plants using high-burnup or MOX fuel*. 2011, U.S. Nuclear Regulatory Commission: Washington, DC. p. Medium: ED; Size: 60 p.SAND2011-0128; ,
121. Charlot, G., *POTENTIELS D'OXYDO-RÉDUCTION*, in *Selected Constants Oxydo-Reduction Potentials*, G. Charlot, Editor. 1958, Pergamon. p. 4-35.
122. Kajan, I., S. Tietze, and C. Ekberg, *Interaction of ruthenium tetroxide with iodine-covered surfaces of materials in nuclear reactor containment building.* Journal of Nuclear Science and Technology, 2016: p. 1-10.
123. *HSC Chemistry for Windows, version 5.11.* . 2002, Outokumpu Research Oy; Pori, : Finland
124. Shah, J. and E.C. Maxie, *Gamma-ray radiosynthesis of ozone from air.* The International Journal of Applied Radiation and Isotopes, 1966. **17**(3): p. 155-159.
125. Buck, E.C.W., R.S., *Radiolysis process modeling results for scenarios*. 2012, Pacific Northest National Laboratory
126. Kanda, Y., T. Momose, and M. Taira, *Characterization of radiolytic products from air at a high-energy electron-positron storage ring.* Radiation Physics and Chemistry, 1996. **48**(1): p. 49-54.
127. Bosland, L., F. Funke, G. Langrock, and N. Girault, *PARIS project: Radiolytic oxidation of molecular iodine in containment during a nuclear reactor severe accident: Part 2. Formation and destruction of iodine oxides compounds under irradiation – Experimental results modelling.* Nuclear Engineering and Design, 2011. **241**(9): p. 4026-4044.
128. Kajan, I., Kärkelä, T., Tapper, U., Johansson, L-S., Gouëllo, M., Ramebäck, H., Holmgren, S., Auvinen, A., Ekberg, A.,, *Impact of Ag and NOx compounds on the transport of ruthenium in the primary circuit of nuclear power plant in a severe accident.* Submited to: Annals of Nuclear Energy, 2016.
129. Backman, U., Lipponen, M., Auvinen, A., Jokiniemi, J., Zilliacus, R., *Ruthenium Behaviour in Severe Nuclear Accident Conditions*, in *NKS report*. 200487-7893-159-2
130. Tietze, S., M.R.S. Foreman, and C. Ekberg, *Synthesis of I-131 labelled iodine species relevant during severe nuclear accidents in light water reactors.* Radiochimica Acta, 2013. **101**(10): p. 675-680.
131. Krtil, J. and J. Mencl, Radiochem. Radioanal lett., 1971. **7**: p. 175-180.
132. Kajan, I., H. Lasseson, I. Persson, and C. Ekberg, *Interaction of ruthenium tetroxide with surfaces of nuclear reactor containment building.* Journal of Nuclear Science and Technology, 2016. **53**(9): p. 1397-1408.

133. Holm, N.W. and R.J. Berry, *Manual on Radiation Dosimetry*. 1970: M. Dekker.
134. A. Thompson, D.A., E. Gullikson, M. Howells,K-J. Kim, J. Kirz, J. Kortright, I. Lindau, Y. Liu, P. Pianetta, A. Robinson, J. Scofield, J. Underwood, G. Williams, H. Winick, *X-ray data booklet*. 2009: Lawrence Berkley National Laboratory.
135. (accessed July 2015)]; Available from: http://www.canberra.com/products/detectors/pips-detectors.asp
136. G. N. George, I.F.P., *EXAFSPAK - A suite of Computer Programs for Analysis of X-ray absorption spectra, Stanford Synchrotron Radiation Laboratory*. Stanford, CA
137. Sayers, D.E.B., B. A. I, , *X-Ray Absorption Principles, Applications and Techniques of EXAFS, SEXAFS and XANES*, ed. D.C.K.a.R. Prins. 1988, New York: Wiley-Interscience.
138. Zabinsky, S., J. Rehr, A. Ankudinov, R. Albers, and M. Eller, *Multiple-scattering calculations of X-ray-absorption spectra.* Physical Review B, 1995. **52**(4): p. 2995.
139. *JOINT COMMITTEE ON POWDER DIFFRACTION STANDARDS.* Analytical Chemistry, 1970. **42**(11): p. 81A-81A.
140. Erdtmann, G., *Neutron Activation Tables*. KErnchemie in Einzeldarstellungen, ed. K.H. Lieser. Vol. 6. 1976, New York: Verlag Chemie.
141. Metrology, B.J.C.f.G.i., *JCGM 100:2008, Evaluation of measurement data – Guide to the expression of uncertainty in measurement JCGM 100:2008 (GUM 1995 with minor corrections).* . 2008: Paris
142. Polanyi, J.C., *Erratum: Isotopic Reaction Rates Between Methyl and Hydrogen.* The Journal of Chemical Physics, 1956. **24**(2): p. 493-493.
143. Huffman, R.E. and N. Davidson, *Shock Waves in Chemical Kinetics: The Thermal Decomposition of NO21a.* Journal of the American Chemical Society, 1959. **81**(10): p. 2311-2316.
144. Ellis, W.R. and R.C. Murray, *The thermal decomposition of anhydrous nitric acid vapour.* Journal of Applied Chemistry, 1953. **3**(7): p. 318-322.
145. Harrison, H., H.S. Johnston, and E.R. Hardwick, *Kinetics of the Thermal Decomposition of Nitric Acid Vapor. IV. A Shock Tube Study Between 800-1200°K.* Journal of the American Chemical Society, 1962. **84**(13): p. 2478-2482.
146. *5 - Ruthenium(VI)*, in *Topics in Inorganic and General Chemistry*, A.S. Elaine and R.S. Kenneth, Editors. 1984, Pergamon. p. 63-75.
147. *4 - Ruthenium(VII)*, in *Topics in Inorganic and General Chemistry*, A.S. Elaine and R.S. Kenneth, Editors. 1984, Pergamon. p. 57-61.
148. Kärkelä, T., N. Vér, T. Haste, N. Davidovich, J. Pyykönen, and L. Cantrel, *Transport of ruthenium in primary circuit conditions during a severe NPP accident.* Annals of Nuclear Energy, 2014. **74**(0): p. 173-183.
149. Kajan, I., H. Lasseson, I. Persson, and C. Ekberg, *Interaction of ruthenium tetroxide with surfaces of nuclear reactor containment building.* Journal of Nuclear Science and Technology, 2016: p. 1-12.
150. Ohyoshi, A., F. Götzfried, and W. Beck, *Polynuclear carbonyl complexes of ruthenium and osmium with methylthiolate and bromine bridging ligands.* Chemistry Letters, 1980. **9**(12): p. 1537-1540.

151. Zhou, X.L., F. Solymosi, P.M. Blass, K.C. Cannon, and J.M. White, *Interactions of methyl halides (Cl, Br and I) with Ag(111).* Surface Science, 1989. **219**(1): p. 294-316.
152. Solymosi, F. and I. Kovács, *Carbon-carbon coupling of methylene groups: thermal and photo-induced dissociation of CH2I2 on Pd(100) surface.* Surface Science, 1993. **296**(2): p. 171-185.
153. Zhou, X.-L. and J.M. White, *Thermal decomposition of C2H5I on Ag(111).* Catalysis Letters, 1989. **2**(6): p. 375-384.
154. Wagner, C.D., W.M. Riggs, L.E. Davis, J.F. Moudler, and G.E. Muilenberg, *Handbook of X-ray photoelectron spectroscopy*. 1979: Perkin Elmer.
155. Sherwood, P., M., A., , J. Chem. Soc. Faraday Trans. 2, 1976. **72**(II).
156. Dillard, J.G., H. Moers, H. Klewe-Nebenius, G. Kirch, G. Pfennig, and H.J. Ache, *X-ray and electron induced Auger processes for I2 adsorption on uranium.* Spectrochimica Acta Part B: Atomic Spectroscopy, 1984. **39**(12): p. 1533-1536.
157. Sherwood, P.M.A., *X-ray photoelectron spectroscopic studies of some iodine compounds.* Journal of the Chemical Society, Faraday Transactions 2: Molecular and Chemical Physics, 1976. **72**(0): p. 1805-1820.
158. Vasquez, R.P., *CuI by XPS.* Surface Science Spectra, 1993. **2**(2): p. 149-154.
159. Morgan, W.E., J.R. Van Wazer, and W.J. Stec, *Inner-orbital photoelectron spectroscopy of the alkali metal halides, perchlorates, phosphates, and pyrophosphates.* Journal of the American Chemical Society, 1973. **95**(3): p. 751-755.
160. Campbell, C.T. and B.E. Koel, *A model study of alkali promotion of water-gas shift catalysts: Cs/Cu(111).* Surface Science, 1987. **186**(3): p. 393-411.
161. Yang, S.J. and C.W. Bates, *The role of cesium suboxides in low‐work‐function surface layers studied by x‐ray photoelectron spectroscopy: Ag‐O‐Cs.* Applied Physics Letters, 1980. **36**(8): p. 675-677.
162. Haber, J., J. Stoch, and L. Ungier, *X-ray photoelectron spectra of oxygen in oxides of Co, Ni, Fe and Zn.* Journal of Electron Spectroscopy and Related Phenomena, 1976. **9**(5): p. 459-467.
163. Wagner, C.D., D.A. Zatko, and R.H. Raymond, *Use of the oxygen KLL Auger lines in identification of surface chemical states by electron spectroscopy for chemical analysis.* Analytical Chemistry, 1980. **52**(9): p. 1445-1451.
164. Fletcher, J.M., I.L. Jenkins, F.M. Lever, F.S. Martin, A.R. Powell, and R. Todd, *Nitrato and nitro complexes of nitrosylruthenium.* Journal of Inorganic and Nuclear Chemistry, 1955. **1**(6): p. 378-401.
165. Sasahira, A. and F. Kawamura, *Formation Rate of Ruthenium Tetroxide during Nitric Acid Distillation.* Journal of Nuclear Science and Technology, 1988. **25**(7): p. 603-606.
166. Mun C., C.L., Madic C.,. *Study of the Ruthenium Fission-Product Behaviour in the Containment of a Nuclear Reactor, in Case of a Severe Accident Occurring in Oxidizing Conditions*. in *Nuclear Energy for New Europe*. 2005. Bled, Slovenia.
167. Abe, T., S. Inoue, and K. Watanabe, *XRD and electrochemical measurements of RuO2 powder treated by using a mechanical grinding method.* Journal of Alloys and Compounds, 2003. **358**(1–2): p. 177-181.
168. Petrović, Ž., M. Ristić, M. Marciuš, B. Sepiol, H. Peterlik, M. Ivanda, and S. Musić, *Formation of RuO2 nanoparticles by thermal decomposition of Ru(NO)(NO3)3.* Ceramics International, 2015. **41**(6): p. 7811-7815.

169. Olefjord, I. and A. Nylund, *Surface analysis of oxidized aluminium. 2. Oxidation of aluminium in dry and humid atmosphere studied by ESCA, SEM, SAM and EDX.* Surface and Interface Analysis, 1994. **21**(5): p. 290-297.
170. Boehm, H.P., *Acidic and basic properties of hydroxylated metal oxide surfaces.* Discussions of the Faraday Society, 1971. **52**(0): p. 264-275.
171. Kasap, S.O., P. Capper, and SpringerLink, *Springer handbook of electronic and photonic materials*. 2006, New York: Springer.
172. Pollack, G.P. and D. Trivich, *Photoelectric properties of cuprous oxide.* Journal of Applied Physics, 1975. **46**(1): p. 163-172.
173. Bard, A.J., R. Parsons, J. Jordan, P. International Union of, and C. Applied, *Standard potentials in aqueous solution*. 1985, New York: M. Dekker.
174. Latimer, W.M., *Oxidation Potentials*. 1952: Prentice-Hall.
175. McKeown, D.A., P.L. Hagans, L.P.L. Carette, A.E. Russell, K.E. Swider, and D.R. Rolison, *Structure of Hydrous Ruthenium Oxides: Implications for Charge Storage.* The Journal of Physical Chemistry B, 1999. **103**(23): p. 4825-4832.
176. Mo, Y., M.R. Antonio, and D.A. Scherson, *In Situ Ru K-Edge X-Ray Absorption Fine Structure Studies of Electroprecipitated Ruthenium Dioxide Films with Relevance to Supercapacitor Applications.* The Journal of Physical Chemistry B, 2000. **104**(42): p. 9777-9779.
177. Haynes, W.M., *CRC Handbook of Chemistry and Physics, 93rd Edition*. 2012: Taylor & Francis.
178. Wagenknecht, F. and R. Juza, *SECTION 20 - Zinc, Cadmium, Mercury A2 - BRAUER, GEORG*, in *Handbook of Preparative Inorganic Chemistry (Second Edition)*. 1965, Academic Press. p. 1067-1124.
179. Lin, C.-C., *Volatility of iodine in dilute aqueous solutions.* Journal of Inorganic and Nuclear Chemistry, 1981. **43**(12): p. 3229-3238.
180. Brown, M.A., P.D. Ashby, M.J. Krisch, Z. Liu, B.S. Mun, R.G. Green, J.B. Giorgi, and J.C. Hemminger, *Interfacial Dushman-like Chemistry in Hydrated KIO3 Layers Grown on KI.* The Journal of Physical Chemistry C, 2010. **114**(33): p. 14093-14100.
181. Boman, C.E., Acta Chem. Scand., 1970. **24**: p. 116-122.
182. Takeda, T., Nagata, M., Kobayashi, H., Kanno, R., Kawamoto, Y., Takano, M., Kamiyama, T., Izumi, F., Sleight, and A. W., *High-pressure synthesis, crystal structure, and metal-semiconductor transitions in the Tl[2]Ru[2]O[7-8] pyrochlore*. Vol. 140. 1998, Amsterdam, PAYS-BAS: Elsevier.
183. Bolzan, A.A., C. Fong, B.J. Kennedy, and C.J. Howard, *Structural Studies of Rutile-Type Metal Dioxides.* Acta Crystallographica Section B, 1997. **53**(3): p. 373-380.
184. Haines, J., Leger, J. M., Schulte, O., Hull, and S., *Neutron diffraction study of the ambient-pressure, rutile-type and the high-pressure, CaCl[2]-Type phases of ruthenium dioxide*. Vol. 53. 1997, Oxford, ROYAUME-UNI: Blackwell.
185. Davidson, I.J. and J.E. Greedan, *Neutron and X-ray powder diffraction study of LixRuO2 and LixIrO2: The crystal structure of Li0.9RuO2.* Journal of Solid State Chemistry, 1984. **51**(1): p. 104-117.
186. Foo, M.L., Q. Huang, J.W. Lynn, W.-L. Lee, T. Klimczuk, I.S. Hagemann, N.P. Ong, and R.J. Cava, *Synthesis, structure and physical properties of Ru ferrites: BaMRu5O11 (M=Li and Cu) and BaM′2Ru4O11 (M′=Mn, Fe and Co).* Journal of Solid State Chemistry, 2006. **179**(2): p. 563-572.

187. Tse, J.S., D.D. Klug, K. Uehara, Z.Q. Li, J. Haines, and J.M. Léger, *Elastic properties of potential superhard phases of RuO2.* Physical Review B, 2000. **61**(15): p. 10029-10034.
188. Mehtougui, N., D. Rached, R. Khenata, H. Rached, M. Rabah, and S. Bin-Omran, *Structural, electronic and mechanical properties of RuO2 from first-principles calculations.* Materials Science in Semiconductor Processing, 2012. **15**(4): p. 331-339.
189. Rao, K.V.K. and L. Iyengar, *X-ray studies on the thermal expansion of ruthenium dioxide.* Acta Crystallographica Section A, 1969. **25**(2): p. 302-303.
190. Goldschmidt, V.M., Barth, T., Holmsen, D., Lunde, G., Zachariasen, W.,, *Skrifter utgitt av det Norske Videnskaps-Akademi i Oslo.* Matematisk-Naturvidenskapelig Klasse, 1926: p. 5-21.
191. Haines, J., J.M. Leger, M.W. Schmidt, J.P. Petitet, A.S. Pereira, J.A.H. Da Jornada, and S. Hull, *Structural characterisation of the pa3-type, high pressure phase of ruthenium dioxide.* Journal of Physics and Chemistry of Solids, 1998. **59**(2): p. 239-243.

Appendix A

Table A1. *Operating parameters of the Thermo Scientific™ Element 2 apparatus.*

	Parameters	
Instrument parameters	Value	Unit
Sample entrance		
Peristaltic pump speed	11	rpm
Nebulization		
Nebulizer	Meinhard (quartz)	
Nebulizer gas	Argon	
Nebulizer gas flow	1.097	l/min
Plasma		
RF power	1300	W
Plasma gas flow	16.38	l/min
Auxiliary gas flow	0.95	l/min
Interface		
Extraction	-2000	V
Focus	-1082	V
Acquisition parameters		
Scanning mode	Peak hopping	
Take-up time	65	s
Wash time	60	s
Settling time (Iodine)	0.016	s
Settling time (Rhodium)	0.300	s
Sample time	0.0100	s
Runs	3	
Passes	4	
Replicates (samples per peak)	10	
Integration mode	Average	

Table A2. *Contents of CLMS-2 SPEX CertiPrep Catalog Number*

	Description
CLMS-2	10 µg/ml: Ag, Al, As, Ba, Be, Bi, Ca, Cd, Co, Cr, Cs, Cu, Fe, Ga, Hg*, In, K, Li, Mg, Mn, Na, Ni, Pb, Rb Se, Sr, Tl, U, V, and Zn in 5% HNO_3. * Hg supplied as a separate solution.

Appendix B

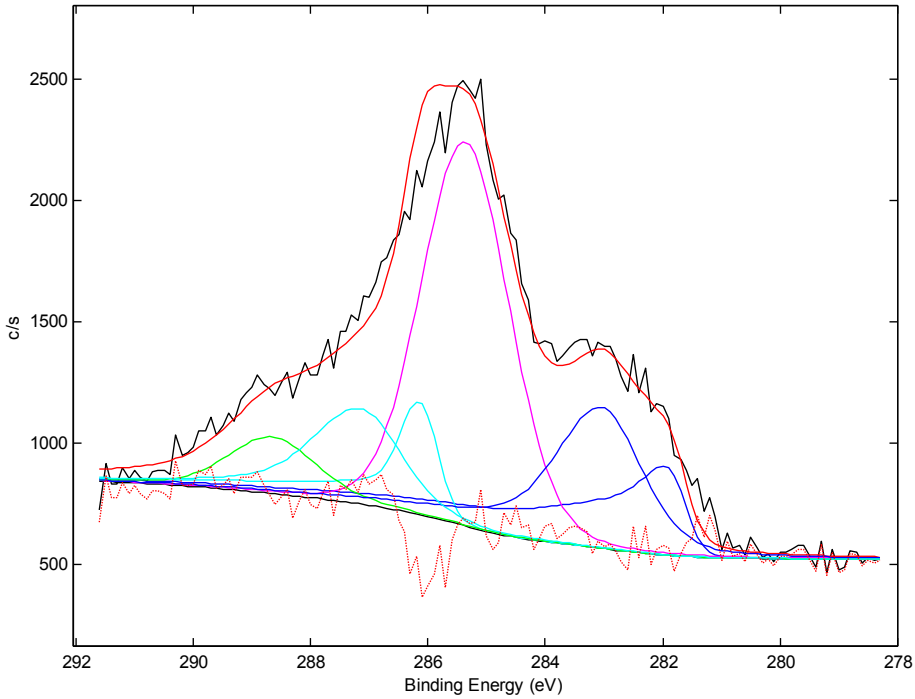

Figure B1. *XPS spectrum of ruthenium in aerosols collected from ruthenium transport experiments with CsI injection at a temperature of 1300 K.*

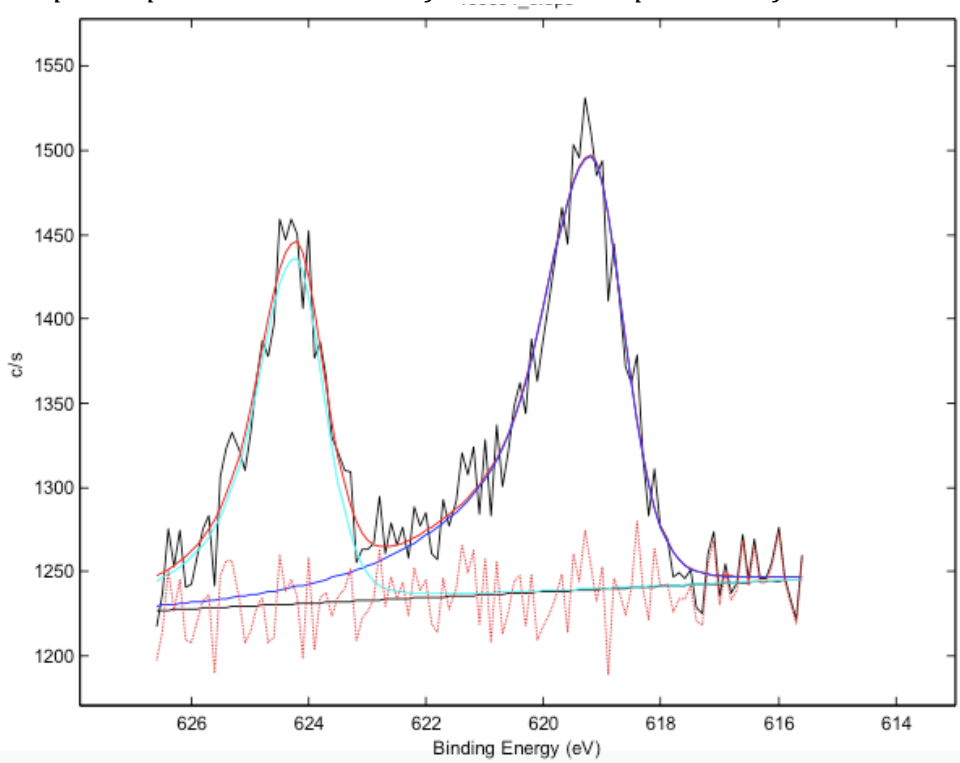

Figure B2. *XPS spectrum of iodine in aerosols collected from ruthenium transport experiments with CsI injection at a temperature of 1300 K.*

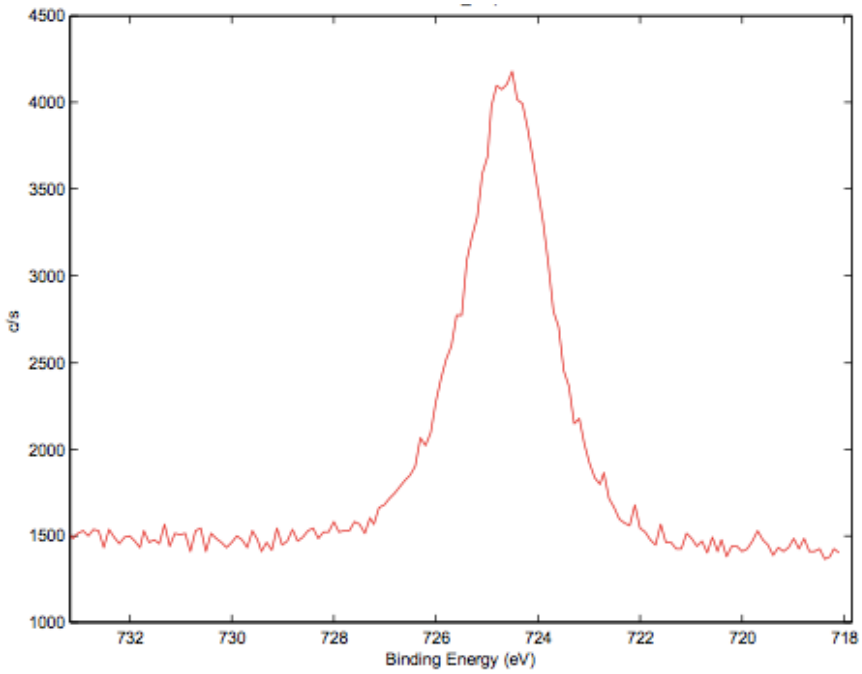

Figure B3. *XPS spectrum of cesium in aerosols collected from ruthenium transport experiments with CsI injection at a temperature of 1300 K.*

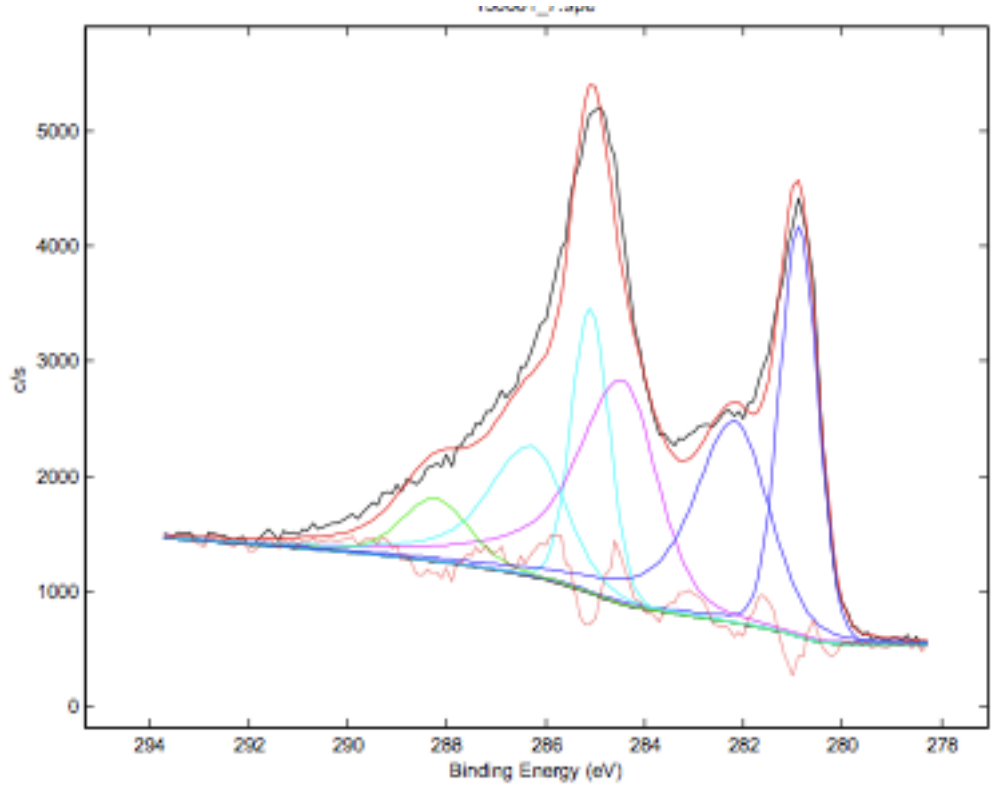

Figure B4. *XPS spectrum of ruthenium in aerosols collected from ruthenium transport experiments with CsI injection at a temperature of 1500 K.*

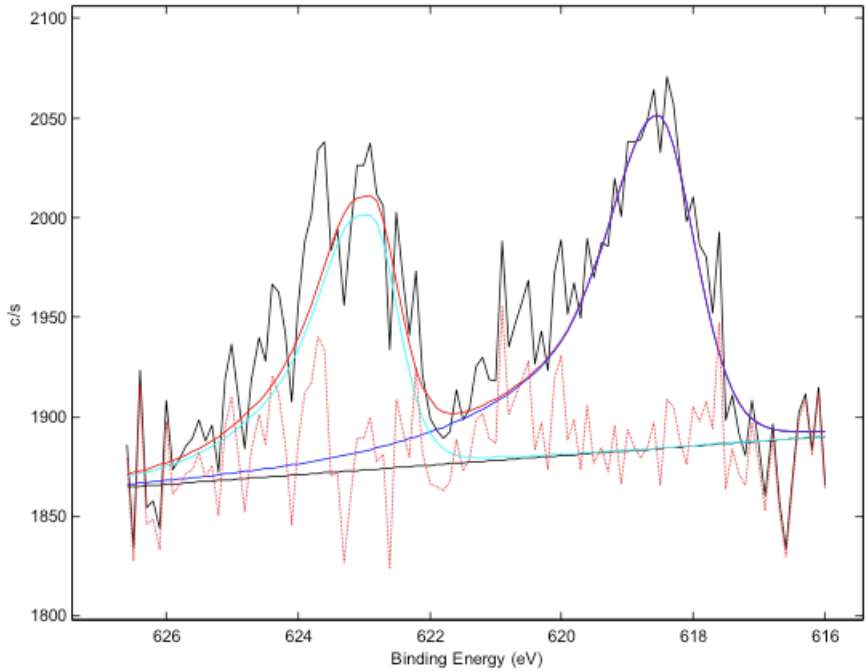

Figure B5. *XPS spectrum of iodine in aerosols collected from ruthenium transport experiments with CsI injection at a temperature of 1500 K.*

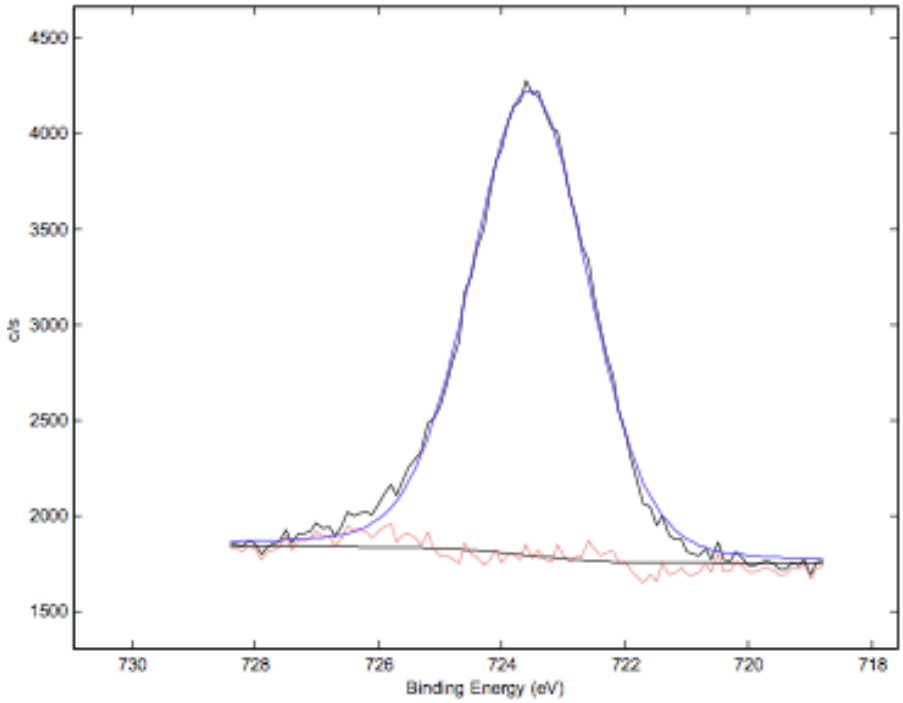

Figure B6. *XPS spectrum of cesium in aerosols collected from ruthenium transport experiments with CsI injection at a temperature of 1500 K.*

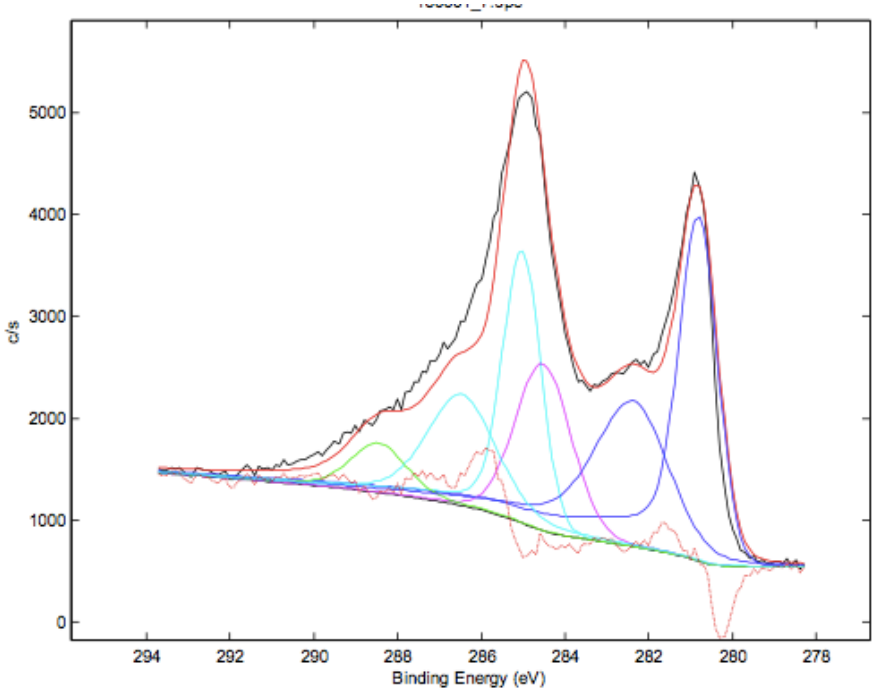

Figure B7. *XPS spectrum of ruthenium in aerosols collected from ruthenium transport experiments with CsI injection at a temperature of 1700 K.*

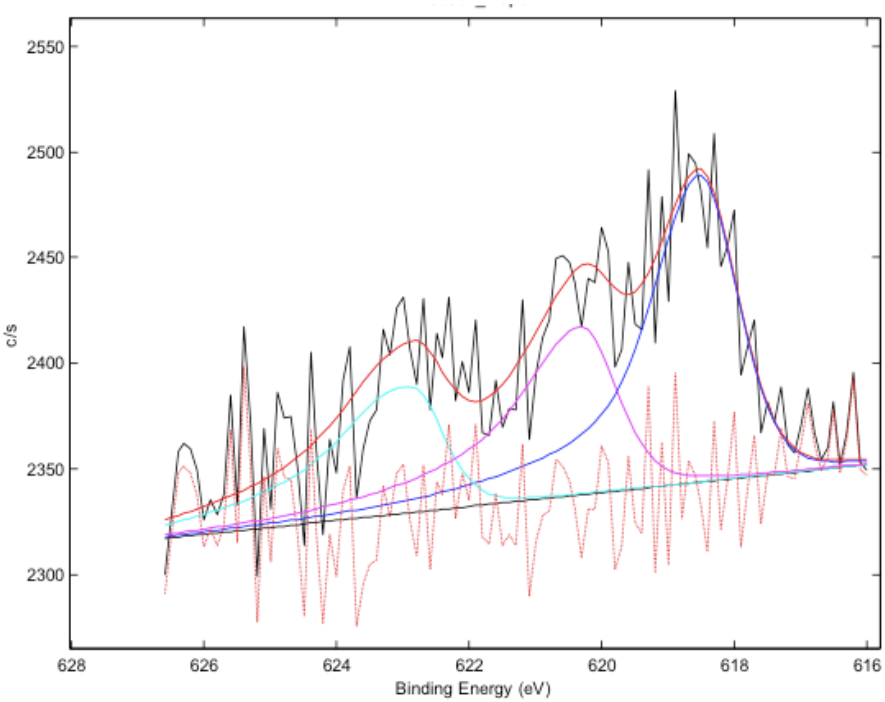

Figure B8. *XPS spectrum of iodine in aerosols collected from ruthenium transport experiments with CsI injection at a temperature of 1700 K.*

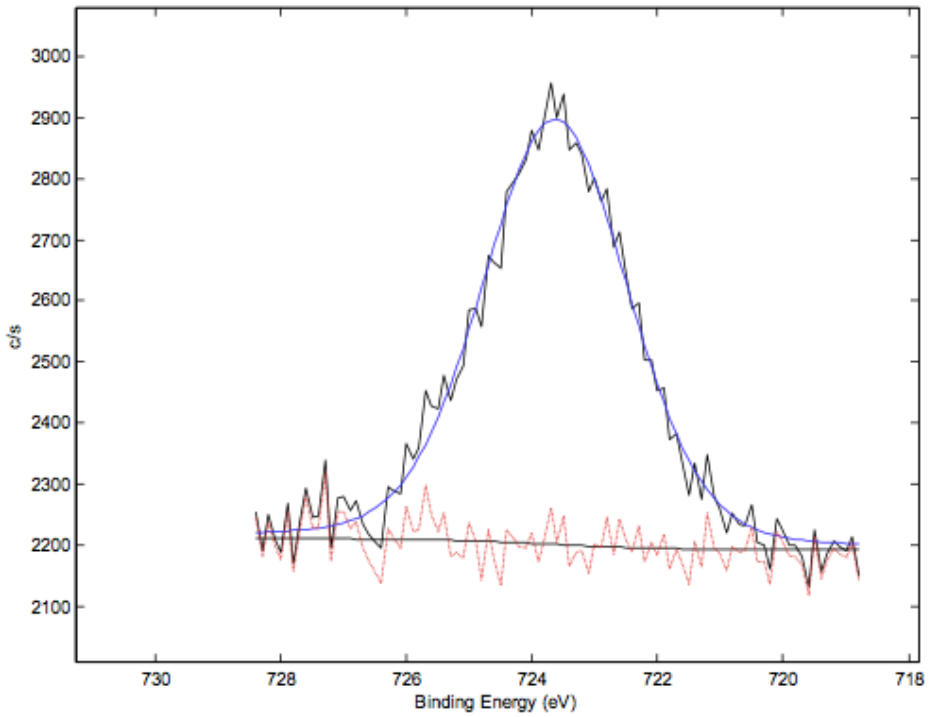

Figure B9. *XPS spectrum of cesium in aerosols collected from ruthenium transport experiments with CsI injection at a temperature of 1700 K.*

Appendix C

Table 1C. Reported structures of solid ruthenium(IV) oxide. Ruthenium(IV) oxide, RuO_2, crystallizes in four different space groups depending on the conditions. A summary of the reported structures of solid RuO_2 is shown below.

d(Ru-O)/Å	*N*	*d*(Ru-O)/Å	*N*	*d*(Ru-O)/Å	*N*	*d*(Ru···Ru)/Å	*N*	*d*(Ru···Ru)/Å	*N*	Space group	Reference
1.970+1.984	2+4	3.407	4	3.664	4	3.107	2	3.536	8	$P4_2/mnm$	[181]
1.918+1.999	2+4	3.416	4	3.651	4	3.107	2	3.535	8	$P4_2/mnm$	[102]
1.962+1.970	2+4	3.398	4	3.673	4	3.105	2	3.534	8	$P4_2/mnm$	[182]
1.942+1.986	2+4	3.412	4	3.662	4	3.105	2	3.538	8	$P4_2/mnm$	[183]
1.942+1.985	2+4	3.400	4	3.644	4	3.093	2	3.513	8	$P4_2/mnm$	[184]
1.938+1.986	2+4	3.410	4	3.660	4	3.105	2	3.536	8	$P4_2/mnm$	[185]
1.928+1.990	2+4	3.413	4	3.650	4	3.099	2	3.534	8	$P4_2/mnm$	[186]
1.935+1.975	2+4	3.394	4	3.647	4	3.092	2	3.521	8	$P4_2/mnm$	[187]
1.929+1.964	2+4	3.400	4	3.636	4	3.075	2	3.523	8	$P4_2/mnm$	[188]
1.962+1.971	2+4	3.375	4	3.627	4	3.075	2	3.502	8	$P4_2/mnm$	[189]
1.971+1.975	2+4	3.414	4	3.682	4	3.111	2	3.548	8	$P4_2/mnm$	[190]
1.989	6	2.955	2	3.314	6			3.436	12	Pa3	[191]
1.963	6	2.926	2	3.260	6			3.388	12	Pa3	[187]
1.999	6	2.963	2	3.337	6			3.454	12	Pa3	[187]
1.980	6	2.941	2	3.299	6			3.420	12	Pa3	[188]
1.927+1.975	2+4	3.385	4*			3.093	2	3.513	8	Pnmn	[184]
2.054	8	3.933	24					3.354	12	Fm-3m	[187]
2.097	8	4.015	24					3.424	12	Fm-3m	[187]